Thesis for the Degree of Doctor of Philosophy

Effect of Phase Separated Sericin on the Gelation Behavior of Silk Fibroin

상분리된 세리신이 실크 피브로인의 겔화에 미치는 영향

February 2016

by

Hyo Won Kwak

Department of Biosystems & Biomaterials Science and Engineering

Seoul National University

Effect of Phase Separated Sericin on the Gelation Behavior of Silk Fibroin

상분리된 세리신이 실크 피브로인의 겔화에 미치는 영향

지도교수 이기훈

이 논문을 농학박사 학위논문으로 제출함
2015 년 12월

서울대학교 대학원
바이오시스템·소재학부
바이오소재공학전공
곽 효 원

곽효원의 박사 학위논문을 인준함
2016 년 2월

위 원 장 현 진 호 (인)

부위원장 이 기 훈 (인)

위 원 김 태 일 (인)

위 원 기 창 석 (인)

위 원 진 형 준 (인)

Abstract

The silk spinning process offers several advantages over the synthetic fiber spinning process. However, the mechanism of silk spinning has not been clearly elucidated. Silk consists of two proteins—silk fibroin (SF) and silk sericin (SS). Most studies have focused on the silk spinning mechanism based on the self-assembly of SF. However, the role of SS should not be ignored, because SS accounts for 25% of the total silk protein and surrounds the SF in the middle silk gland, maintaining the phase separation between them. Thus, the primary aim of this study was to investigate the effect of phase-separated SS on the conformational transition of SF. In addition, the metal ion partition between SF and SS was also investigated. Finally, the effects of metal ion diffusion between the phase-separated SF and SS on the gelation kinetics of SF were examined.

For the study, an SF hydrogel was prepared in the presence of phase-separated SS over an SF solution. The gelation time of SF increased as the concentration of SS in the upper layer increased. The increased gelation time resulted in slow β-sheet formation in the SF solution in the presence of the SS layer. Moreover, the SF hydrogels prepared with 0.5% and 1.0% SS in the upper layer showed the typical X-ray diffraction pattern of Silk I. Thus, SS not

only prevents the premature β-sheet formation of SF, but also induces a Silk I hydrogel structure in the SF, even in the phase-separated state.

In the ion diffusion experiment, most metal ions showed a higher affinity for SF, except for the Na^+ ion. The amount of diffused metal ions and the presence of phase-separated SS affected the gelation kinetics of SF. Most ions that diffused into the SF solution increased the gelation time of the SF solution. Among these, Ca^{2+} had the strongest delaying effect. The presence of phase-separated SS further increased the gelation time. However, Cu^{2+} shortened the gelation time.

Keyword : : Silk fibroin, silk sericin, Silk I structure, gelation, metal ion, diffusion

Student Number : 2010-21192

Contents

List of Figures

List of Tables

1. Introduction

Silk fiber, a legendary material, is produced by some arthropods (silkworms, spiders, scorpions, mites, etc.) and is the most highly prized natural fiber [1]. This material has been used in the textile industry for a long time because of its excellent mechanical properties. In addition, because of its biocompatibility, it has recently attracted great interest as a biomaterial for tissue engineering, drug delivery, and high technology interfaces [2–4]. Among various silk fibers, *Bombyx mori* silk fiber has been widely used due to its broad domestication area and generality [5]. The fiber secreted by *Bombyx mori* is a continuous strand composed of two proteins, namely, fibroin and sericin, with very different characteristics. Fibroin constitutes 75% of the fiber strand weight and functions as a structural component. It is composed of two polypeptide subunits of 370 and 25 kDa, which are covalently linked by disulfide bonds. Sericin is a minor silk protein that glues the two fibroin threads together in order to create the compact and closed structure of the cocoon [6].

The process of spinning silk fibers is environmentally friendly, and it has various advantages over synthetic fiber spinning. Silk spinning uses water as a solvent and spinning of the fibers occurs at ambient temperatures. In contrast, spinning of commercial synthetic fibers often requires organic solvents and temperature elevation [7]. However, the mechanism of silk fiber spinning has not been

fully elucidated. Understanding of silk spinning process will provide not only basic scientific insight, but also technical information for the manufacture of synthetic fibers.

The spinning of silk is a type of dry spinning, with the solution state of silk gland protein converted into solid-state silk fibers in ambient air condition. The silk glands in the silkworm larvae are a pair of tubes. Silk fibroin and sericin are synthesized in the posterior and middle silk glands of the silkworms, respectively, and then transit into the anterior glands. During the silk spinning process, silk dope solution undergoes to some changes in its composition and physical state. First, the concentration of fibroin increases. Fibroin is synthesized in the posterior division (12%, w/v), and is transferred to the middle division (25%, w/v), followed by dehydration in the anterior division (30%, w/v). In this process, a conformational transition from random coil or Silk I structure to β-sheet rich Silk II structure is accompanied by a gel-sol conversion. The pH of the silk glands decreases gradually during the spinning process. In the posterior silk gland, a decrease in pH was observed from pH 8.2 to 7.2. In the middle silk gland, the pH of the dope solution is maintained at a neutral pH of 7. At beginning of the anterior silk gland, a gradient decrease of pH was observed from pH 6.8 to 6.2 [8]. Various metal elements, including Na^+, K^+, and Cu^{2+} increase from the posterior division to the anterior division, with the exception of Ca^{2+}, which decreases significantly in the anterior division [9].

Among various hypotheses of silk spinning mechanisms, the most well established is the micellar self-assembly model based on the primary structure of fibroin. Jin & Kaplan [10] blended fibroin with poly ethylene oxide (PEO) and observed micelle structures of fibroin. Fibroin molecules have alternating repeated hydrophobic sequences (GAGAGS and GAGAGY) and non-repeated hydrophilic sequences. This amphiphilic structure of fibroin allows it to assemble into micelle structures. Due to this micelle structure of fibroin, hydrophobic regions of fibroin are buried inside the micelles. This micelle structure will therefore prevent β-sheet formation and its related aggregation, even though there is a high concentration of fibroin in silk glands.

We have a lot of information on silk gland and spinning process, but we still cannot fabricate silk protein fibers with similar strength as natural silk fibers. This means that we do not fully understand the silk spinning process. As mentioned above, silk protein consists of fibroin and sericin. So far, most research on silk spinning mechanisms has focused on the self-assembly of fibroin itself. There has been relatively little study on the role of sericin, which accounts for 25% of the total silk protein. For example, in order to change the metal ion concentration, metal transfer between fibroin and sericin is required. However, the change in metal concentration in fibroin cannot be explained without the sericin layer that surrounds the fibroin. However, there are no studies on metal ion diffusion behavior between these silk proteins. Recently, there have

been a few reports on the role of silk sericin in the process of spinning silk fibers. Lee [11] observed micelle structures in a blended film of fibroin and sericin. He speculated that the hydrogen bonds between fibroin and sericin retard the β−sheet crystallization of fibroin even though the two silk proteins are phase separated. However, Lee investigated film form of silk proteins, which is different from the sol state of the natural silk gland dope solution. For this reason, it is necessary to examine the interaction between fibroin and sericin in the liquid state.

In this study, the interaction between the liquid state of fibroin and sericin was investigated. The effect of sericin on the gelation of fibroin was determined in a macro phase separation state. The effects of sericin concentration on gelation and β−sheet conformational transition kinetics were also studied. The secondary and crystal structures of fibroin during gelation with phase−separated sericin were studied using Fourier transform infrared spectroscopy (FTIR) and X−ray powder diffraction (XRD).

Ion diffusion behavior between fibroin and sericin was investigated in phase separation, which is similar to the structure of natural silk glands. In order to study ion diffusion between silk proteins, an ion−coupled plasmon atomic emission spectrometer (ICP−AES) was used to calculate the amount of diffused metal ions. Additionally, the effects of metal ion diffusion on the gelation kinetics of fibroin were investigated.

2. Literature survey

2.1. Silk protein

2.1.1 Silk fibroin (SF)

Silk proteins that are spun into fibers by silkworms and spiders in mild environments, including ambient and aqueous conditions, have long been used in the textile, industrial, and biomedical fields because of their excellent mechanical properties [12-15]. There are various sources of silk fibers, but most silk is obtained from the cocoon silk produced by *Bombyx mori*, because of its widespread domestication. Silk fiber secreted by *Bombyx mori* contains two types of proteins, namely, silk fibroin (SF) and silk sericin (SS). SF, the 'core' protein, accounts for about 70-75% of the total cocoon and is a hydrophobic protein secreted from the posterior part of the silk gland [16]. SF is a heterodimeric protein that consists of a heavy chain (H-chain) and a light chain (L-chain) linked by disulfide bonding between cysteine residues [17-20]. The molecular weights of the H-chain and L-chain are approximately 390 and 25 kDa, respectively [21,22]. Analysis of the amino acid composition of SF shows that it mainly contains glycine (G), alanine (A), and serine (S) [23]. The results of a sequence analysis of the SF heavy chain, indicates that it has 12 repetitive and 11 non-repetitive regions that alternate [24,25]. The repetitive regions tend to form the crystalline regions, while the

non-repetitive regions may form the amorphous regions. Highly repetitive regions begin with the amino acid sequence GAGAGS (generally repeated 15 times), end with GAAS, and form β-sheet structures in the spun fibers, which are responsible for their mechanical properties [26]. In addition, the non-repeated region is made of hydrophilic amino acids, which are located between the hydrophobic repeated sequences (Figure 1.). Therefore, the SF molecule exhibits amphiphilic properties [27,28]. SF can be extracted from silk cocoons in a process called degumming, which removes SS from SF.

2.1.2. Silk sericin (SS)

SS is a group of polypeptides that make up 25–30% of the total silk protein weight [29,30]. SS is synthesized and secreted in the middle gland of the silkworm and forms a phase-separated sticky layer that surrounds the SF. SS is a glue-like protein that serves not only as a cover for the SF filament, but also as an adhesive to bind the two SF filaments together. Five SS polypeptides, s-1, s-2, s-3, s-4, and s-5, have been reported from different sections of the middle gland of *Bombyx mori*, among which s-1, s-2, and s-3 are the major components [31]. These major fractions of SS have been isolated from cocoons, and they have molecular weights of 400, 250, and 150 kDa, respectively. These proteins also correspond to the SS secreted in the middle, anterior, and posterior

parts of the middle gland, respectively [32]. SS is composed of 18 amino acids with polar amino acids that have hydroxyl and carboxyl groups. SS is water soluble and hydrophilic, due to the high content of serine and aspartic acid, which represent approximately 33.4% and 16.7% of the amino acid content of SS, respectively [33,34] Although most of the SS protein is soluble in hot water or alkaline aqueous solutions, SS can be easily removed in a process known as 'degumming' and isolated as a pure product if needed. Depending on the extraction methods, the reported molecular weights of SS have ranged from 10 kDa to over 400 kDa [35-37].

2.2. Mechanism of silk spinning process

2.2.1. Crystalline structure of SF

The crystalline structure of *Bombyx mori* silk SF is divided into Silk I, II, and III structures. Among these, Silk III is a new silk structure that was first observed at the air-water interface and later at organic-water interfaces [38].

The two most commonly recognized crystalline structures are called Silk I and II. During the spinning process, silk protein in the *Bombyx mori* silkworm exists primarily as either Silk I or random coil forms in the silk glands and then undergoes a conformational transition to the ß-sheet conformation dominated Silk II crystalline form [39].

Silk I crystalline structure is a metastable structure in the glands of silkworms before the spinning process. These crystalline structures of SF have been characterized in details by X-ray diffraction, electron diffraction, and infrared and solid-state nuclear magnetic resonance (NMR) spectroscopic techniques [40-44]. Suzuki et al. determined the liquid silk structure before spinning at the atomic level using solution NMR. The structure of native silk gland was determined and compared with that of synthetic motifs, especially between repeated sequences with (GAGAGX)n (X = S, Y, V) and GAASGA motifs in the *Bombyx mori* SF. They proposed a type II β-turn structure for liquid silk, which is close to the structure determined from solid state NMR for the motif, (GAGXGA)n, while the motif GAASGA is disordered in its conformation and probably forms a flexible segment.

Silk II gives rise to the crystalline structure of SF in native silk fibers, with anti-parallel β-sheets crystallized in hydrophobic regions. Marsh et al. [45] were the first to propose an anti-parallel β-sheet model, based on a fiber diffraction study of native *Bombyx mori* silk fiber. Takahashi et al. [46] reported a more detailed X-ray fiber diffraction analysis of *Bombyx mori* SF based on 35 quantified intensities and proposed that two anti-polar anti-parallel β-sheet structures were stacked in different orientations, occupying the crystal site at a ratio of 1:2. Even though the local protein conformation is still the β-sheet, the refined Silk II model accounts for the stacking of the β-sheet planes in two different

arrangements.

Crystalline and secondary structures of SF have been identified by X-ray diffraction. [47-49]. Silk I has random coils with some β-turn structures (type II β-turn), and Silk II has anti-parallel β-pleated sheet structures. The corresponding d spacing for Silk I and II are as follows (in nm): 0.98 nm, 0.48 nm, and 0.43 nm in Silk II, and 0.74 nm, 0.56 nm, 0.44 nm, 0.41 nm, 0.36 nm, 0.32 nm, and 0.28 nm in Silk I structures, respectively. From these d spacing peaks, the typical peak occurs at 0.74 nm in a typical Silk I crystalline structure region of scattering space, which is separated from peaks found in the Silk II structure. Therefore, a peak near 0.75 nm is strong evidence for a Silk I structure [50].

2.2.2. Self-assembly of SF

Silk protein fibers produced by some arthropods (silkworms, spiders, scorpions, mites, etc.) play variety roles, such as structural support, protective shelter, foraging, and reproduction. Silk protein fibers possess extraordinary mechanical properties compared to other natural protein fibers. In order to explain the superior mechanical properties of silk fiber, the self-assembly process of the silk proteins in its spinning process must be understood.

From previous studies related to the structural changes in or self-assembly of the silk protein, it is clear that silk protein

experiences conformational transitions from the water-soluble Silk I-like conformation to water-insoluble crystalline β-sheet Silk II conformation [51-53]. The secondary structures of SF in aqueous solution in the middle gland are gradually transformed from random coils to a β-sheet conformation [54]. The anterior part of the middle gland shows birefringence, indicating the formation of liquid crystal structures. This structural change in the silk protein is known to take place along with the flow of silk protein in the silk gland. However, these changes are not fully understood.

Inoue et al. observed the morphological structure of SF from *Samia cynthia ricini* using Atomic force microscopy (AFM) and proposed the textile fabric-like protofilament aggregation mechanism [55]. The α-helical SF molecules self-assemble to highly ordered nano-fabric structures (Figure 1). As a result, a rigid rod-like structure forms aggregates by end-to-end electrostatic interactions. However, this hypothesis did not include the conformational transition of SF molecules from an α-helical to a β-sheet structure, which is the main secondary structure of *Samia cynthia ricini* fibers [56].

Li et al. [57] investigated the conformational transition from random coils to β-sheets and the β-sheet aggregation of *Bombyx mori* SF by circular dichroism (CD) spectroscopy and concluded that this conformational transition is mediated by a nucleation-dependent aggregation process. They proposed a two-step aggregation mechanism: First, a nucleation step that is

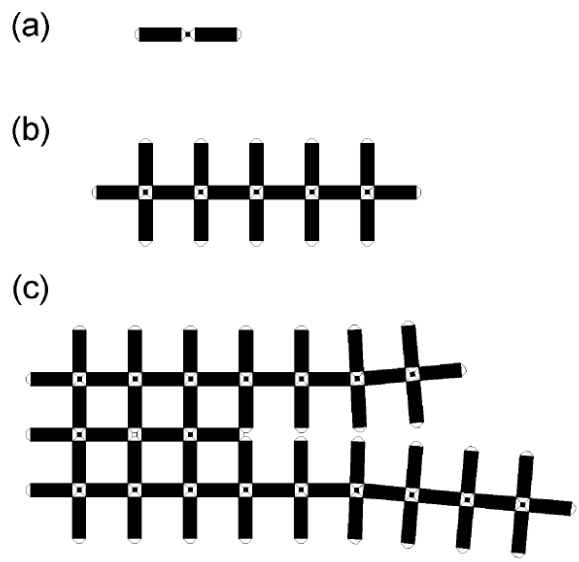

Figure 1. Schematic of the textile fabric-like protofilament aggregation mechanism [55].

rate-limiting and that involves the conversion of soluble random coils to insoluble β-sheets. This formation of ordered β-sheet aggregates, called a nucleus or seed, is thermodynamically unfavorable. Once nuclei are formed, the aggregation step is followed by further growth of the β-sheet unit is thermodynamically favorable, resulting in the rapid extension of β-sheet aggregations.

Gong et al. [58] promoted the in vitro assembly of *Bombyx mori* SF in solution by providing a certain microenvironment and observed SF protofibrils with an average width of about 5.5 nm. In addition, they measured the height of protofibrils by AFM, which showed an average height of 1.3 nm, indicating that the silk nanofibrils are in a tape-like shape rather than cylindrical. From 2D wide-angle X-ray diffraction (WAXD), the crystal structure of silk nanofibrils was found to be partially oriented in a cross β-sheet structure. Alternating β-strands and disordered loops or turns will form a laminated β-sheet, and the stacking of two such β-sheets forms a tape-like structure (Figure 2). They suggested that the repetitive sequence of SF forms one strand, and the turn-pair and tyrosine-rich sequences such GAGAGY form the extended disordered structures. Furthermore, applying simple shear force, the direction of β-strands could be oriented parallel to the fibril axis. This shear force commonly exists in the natural silk spinning process and has a vital role in the orientation of molecules in silk fibers. The most credible hypothesis among many is the micelle- mediated

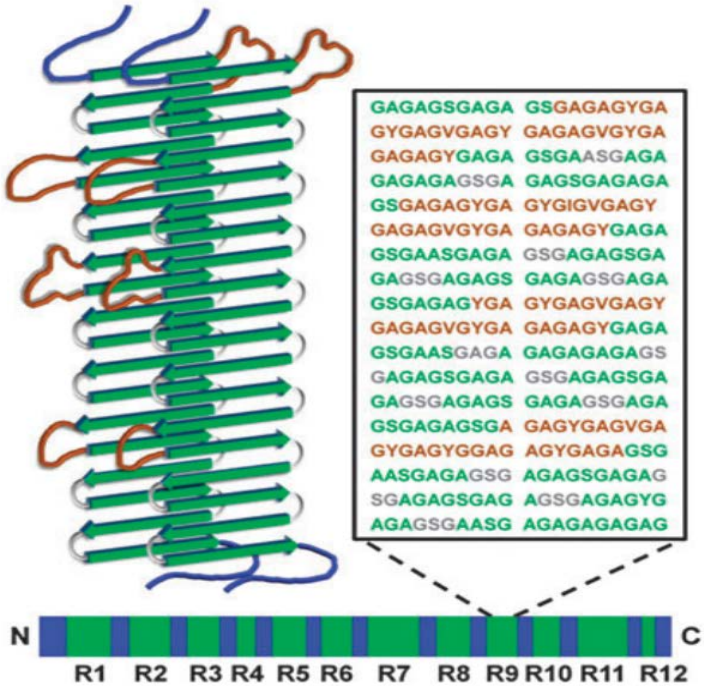

Figure 2. Structural model of the molecular arrangement of cross β-fibrils in silk fibroin [58].

nanofiber formation mechanism (Figure 3). Jin and Kaplan [10] found spherical micelle structures of SF in PEO/SF blend films. These micelle structures assembled because of the unique amino acid sequence of SF, with the repeated hydrophobic blocks (GAGAGS) between hydrophilic amino acid blocks (non-repetitive) and the polar N-terminus and C-terminus present at the ends of the molecules. Due to the repetition of these hydrophobic-hydrophilic amino acid sequences, SF can form a micelle structure to increase solubility and conformational stability in water in a high polymer concentration. These micelle structures are attracted to one another to form of globular microsphere, and with the elongation and alignment of globules that occur with physical shear force, the fibrillar structures finally resemble filament-like structures. Herein, a synthetic hydrophilic polymer, PEO, is used for the replacement of SS protein that surrounds SF.

2.2.3. Silk gland composition and the role of the silk gland at each stage in the silk spinning process

The *Bombyx mori* silkworm is known to spin silk fibers with outstanding mechanical properties. This silk spinning process has three advantages. First, it uses water as a solvent; second, the spinning process is performed at room temperature and pressure; and, third, silk fibers form without a specific coagulation bath. To understand the spinning mechanism of natural silk fibers,

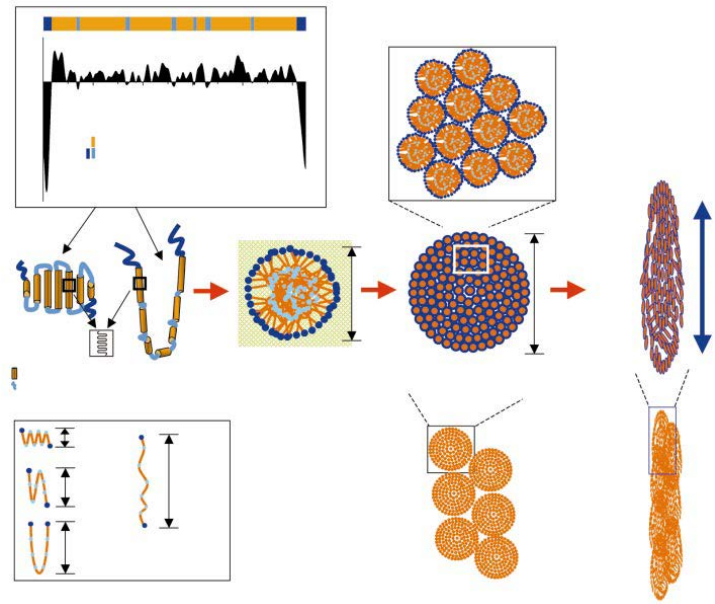

Figure 3. Schematic of the micellar self-assembly mechanism [10].

investigations on the in vivo spinning process of silkworms is very important.

The silkworm gland has a unique and specialized secretory system. Silk glands of Bombyx mori silkworm are paired and are located on each side of larvae [59, 60]. Generally, silk glands are divided into three parts, the posterior (P), middle (M), and anterior (A) divisions. The middle part of the silk gland is again divided into three divisions (Figure 4), the posterior (MP), middle (MM), and anterior (MA) divisions of the middle part of silk gland [61, 12]. The different parts of the silk gland have their characteristic properties and roles in the spinning process [62]. In the posterior part, SF is synthesized and secreted into the lumen of the silk gland. The S-shaped middle part of silk gland acts as a large reservoir, receiving the SF from the posterior part. At the same time, SS is synthesized and secreted in this part. During spinning, SF and SS migrate without mixing into the anterior parts. Here, a gel-sol transition occurs upon migration from the middle division to the anterior division. In the anterior division, dehydration and concentration processes occur, and, finally, the liquid crystalline sol state of silk protein will be spun into fiber [63, 64]. During this process, silk proteins are exposed to various environments. Previous studies have shown that water contents, pH, metal ion concentration, and shear and elongational stress vary in the silk gland. From the posterior to anterior division, the concentration of SF increases, the pH of the silk solution decreases, and the

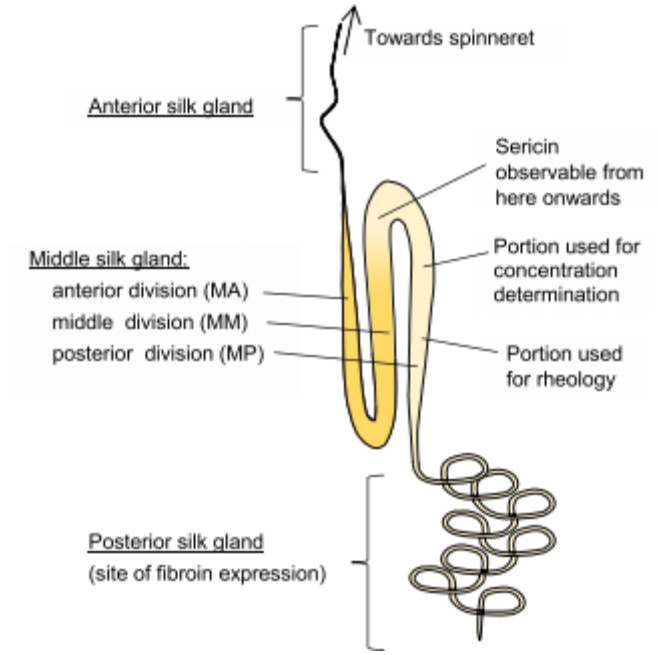

Figure 4. Silk gland composition and its role of silk gland at each stage in silk spinning process [12].

concentration of most of metal ions increases.

2.3. Effects of interaction between SF and SS on the process of spinning silk fiber

In the silk spinning process, the pH of the silk solution, ionic strength, and water contents all have very important roles. However, studies on the silk spinning process have all been carried out with SF alone. When the *Bombyx mori* silk fibers are viewed under a microscope, one strand of SS is seen wrapped and glued around two strands of SF. Therefore, a change in physiological composition of SF must take place when substances move out or in through the SS layer. In the movement of physiological substances, with the SS layer containing various functional groups, it is difficult to imagine that the SS does not have any role in the silk spinning process. Even though SS accounts for one quarter of the total silk fiber, its role has not yet been determined, although some minor functions have been suggested.

Recently, the effect of SS on the mechanical properties of regenerated silk fibers has been revealed. Ki et al. [65] investigated the effect of residual SS on the mechanical properties of regenerated silk fibers. The regenerated silk protein containing residual SS was obtained by control the degumming process. The properties of formic acid redissolved in regenerated silk dope

solution and fiber formation characteristics of wet spun silk filament were investigated. The tenacity of regenerated silk filaments containing 10–20% of SS was 50% higher than the filaments without SS. Furthermore, in the regenerated aqueous SF solution under shearing conditions, SS accelerated the formation of silk protein aggregates. Additionally, the rate of formation rate and amount of precipitated aggregates were enhanced when a certain amount of SS was in the solution. The main secondary structures of the resulting precipitate were β-sheets, indicating that a proper amount of SS combined with shearing forces could induce a transition in silk conformation [66].

Hang et al. [67] mimicked the core-shell structure of the natural silkworm silk to produce electrospun silk nanofibers. The average breaking strength and breaking energy of a coaxial SF/SS fiber mat were greater than those of electrospun pure SF fibers. The coaxial SF/SS fiber had more β-sheet (and related intermediate) structures and better thermo-stability. The hydrophilic amino acid side chains of SS affected the dehydrating process of SF molecules and induced the β-sheet conformational transition.

Lee [11] investigated that the micelle structure of SF with a phase-separated morphology in a prepared SF and SS blended film. Interestingly, the crystallization process of SF was affected by SS. The thermal and structural analysis of the SF and SS blend films revealed that a delay in crystallization of SF occurred when SS was located around the SF micelle. This tendency was also found in high

molecular weight SS, which is similar to actual SS, even though the SS layer is located in macroscopic phase separation conditions [68].

2.4 Metal ion concentrations in the silkworms and their effects

Metal ions are known to influence the conformational transition in silk-like proteins, such as prion proteins (PrP) and amyloid β-peptides, associated with fatal neurodegenerative disease and Alzheimer's disease, respectively [69, 70]. These proteins undergo a transition from a helical conformation to β-sheet structures, and this is greatly affected by the presence and concentration of metal ion species. Therefore, SF, which has a similar structural transition, the investigation of metallic ions in the silk gland is very important. However, there are only a few studies on this subject. Zhou et al. [71] analyzed the metal elements in silk glands and silk fibers of *Bombyx mori* silkworms by proton induced X-ray emission (PIXE), inductively coupled plasma mass spectroscopy (ICP-MS), and atomic adsorption spectroscopy (AAS). Various metals, including the alkali metals (Na^+, K^+), alkali earth metals (Mg^{2+}, Ca^{2+}), and transition metals (Zn^{2+}, Cu^{2+}, Fe^{3+}), were found in both silk glands and produced silk fibers. Since cocoon silk, forced drawn silk and degummed silk have different concentrations of these various metal species, these differences

might relate to the spinning process of the *Bombyx mori* silkworm. For detailed studies on the effects of metal ions on the secretory pathway of *Bombyx mori*, a change in six major metallic ions (Na^+, K^+, Ca^{2+}, Cu^{2+}, Mg^{2+}, Zn^{2+}) in each part of the middle of the silk gland were investigated. K^+ and Ca^{2+} were the most abundant metal ions in all parts of the silk gland (several mg of metal ions per gram of silk protein). The change in concentration of the ions concentration, with the exception of Ca^{2+}, tended to increase from the posterior part to anterior part.

Ochi et al. [72] proposed that SF molecules from silk glands consisted of elementary units (EU) and that their interactions resulted in different behaviors according to their concentrations. In the dilute region, SF molecules show a network structure with little elasticity, mainly due to ionic bonding between COO^- ions of the SF molecules and divalent metal ions such as Ca^{2+} or Mg^{2+}. These network structures showed increasing viscoelastic properties as the metal ion concentrations increased, and are helpful in the storage role of middle gland. At a concentration of 27.5 wt%, which is equal to that of the middle gland, the network structure is homogeneous and more stable in varying temperatures.

Only a few research groups have investigated the effect of ion species on the mechanical properties of silk fibers. Recently, Xia et al.[73] investigated the effect of Na^+, K^+, and Ca^{2+} on the mechanical properties of silk fibers by over-expressing ion-transporting proteins in the spinning ducts of silkworms. The

reduction in Na^+ and K^+ disrupted the ordered structures and maintained the random coil structures, which made the cocoon fiber more brittle and weaker than the silk fibers that had not been genetically modified. Whereas Ca^{2+} induced silk fibers with more α−helical and β−sheet structures that stabilized the ordered structures of silk fibers and produced fibers with higher breaking strength and tenacity. This suggests that, in the silk spinning process, metal ion species and concentrations have a great impact on the mechanical properties of silk fibers and the silk spinning process.

3. Materials and methods

3.1. Materials

Bombyx mori silkworm and its cocoons were kindly provided by National Academy of Agricultural Science. Lithium chloride (LiCl), formic acid, sodium carbonate (Na_2CO_3), sodium oleate, calcium chloride ($CaCl_2$) and sodium chloride (NaCl) purchased from Sigma Aldrich (USA). Methanol and ethanol (EtOH) were purchased from Samchun (Korea) and dimethyl sulfoxide (DMSO) was purchased from Acros (USA). Other reagents were purchased from Sigma Aldrich (USA).

3.2. Preparation of regenerated aqueous SF and SS solution

The silk cocoons were degummed twice with 0.2% (w/v) sodium carbonate and 0.3% (w/v) Marseille soap solution at 100 ℃ for 30 min, and then rinsed with distilled water to remove residual SS. Following this, the SF was dried in an oven at 50 ℃.

To obtained the high molecular weight SS which is prevented from the molecular degradation, urea-mercaptoethanol extraction method used. The cocoon pieces were immersed in a 5% (v/v) 2-

mercaptoethanol in 8 M urea solution and were heated at 80 ℃ for 10 min. After the extraction, the solutions were filtered through a nonwoven filter to remove the remaining cocoon pieces. Extracted SS solution lyophilized and stored in desiccator before the use.

For the preparation of aqueous regenerated SF and SS solution, extracted SF and SS dissolved in a 9.3 M LiBr solution at 50 ℃ for 4 h. The solution was then dialyzed in distilled water with a cellulose membrane (molecular weight cut off = 6000–8000, Spectrum Laboratories, Inc.) for two days. The final SF and SS concentration was adjusted 4%, 1% (w/v) with distilled water respectively.

3.3. Gelation experiment of SF

3.3.1. Gelation kinetics of SF with phase separated SS

To monitor the gelation of SF with phase separated SS, 10 ml of aqueous SF solution added to the 20 ml vial. Then, 5 ml of distilled water and aqueous SS (0, 0.25, 0.50 and 1.00%, w/v) with 100 ppm of rhodamine B dye was added to the above SF solution. In order to maintain the interface between the two solutions, SS was added carefully using a syringe pump (KD Scientific, USA). The phase separation SF and SS was observed using digital camera by taking

photos when gelation was occurred at each SF solution.

Gelation time was investigated in covered 24-well plate and incubated in micro-plate reader which is available to control the temperature at 50 ℃. First, 2.0 mL of aqueous SF was added to each well. Then, 1.0 mL of distilled water or aqueous SS with various concentrations (0, 0.25, 0.50, and 1.00%, w/v) were added the above the SF solution (Figure 5). To determine the gelation time, turbidity changes at 550 nm were monitored with a Microplate Reader (Synergy H1, Biotek, USA). SF gelation occurs with a heterogeneous microstructure leads to an increase the degree of light scattering which is possible to know the increase of the absorbance. Gelation time of SF was defined as the time from the beginning of incubation to the point when the plateau of optical density was reached [86]

3.3.2 β-sheet transition kinetics of SF with phase separated SS

A fluorescence spectrum (FLS) was recorded using a microplate reader. For fluorescence measurement, 20 μM of thioflavin T (ThT) was added to the SF (4%, w/v) solution. For the effective monitoring of fluorescence signal, the gelation process was conducted using black plate (Vision plate 24, 4titude, England). The excitation wavelength was set at 420nm and the emission spectrum

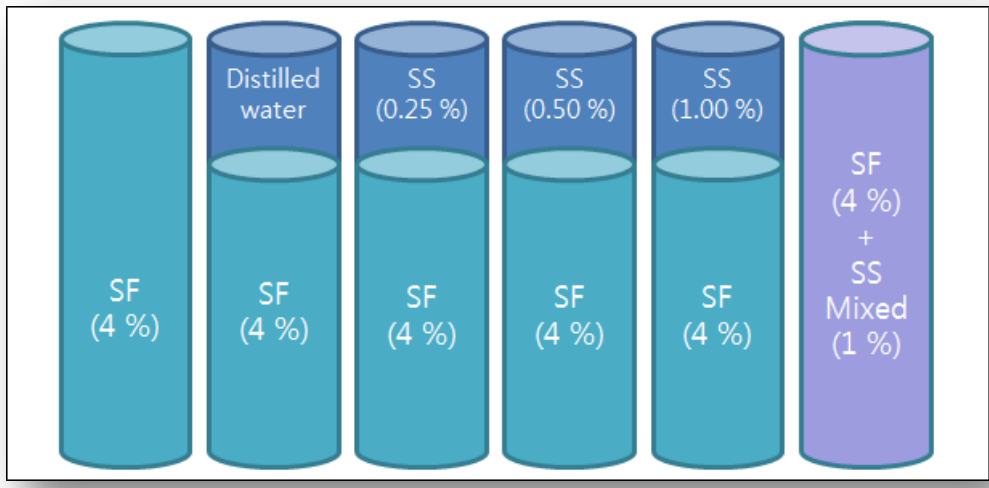

Figure 5. Typical experimental setup for the observation of gelation time of SF in a phase separated system.

was taken from 480 nm. Time interval for the gelation kinetics was 1 h. Relative gelation kinetics was obtained by following as:

$$\textit{ß-sheet transition kinetics (\%)} = \frac{Intensity_{SF_t} - Intensity_{SF_s}}{Intensity_{SF_g} - Intensity_{SF_s}} \times 100$$

$Intensity_{SFg}$ = Fluorescence intensity of SF when gelation completed

$Intensity_{SFs}$ = Fluorescence intensity of SF solution at $time_0$

$Intenstity_{SFt}$ = Fluorescence intensity of SF solution at $time_t$

3.4. Characterization of SF solution and hydrogel

3.4.1. Fourier-transform infrared (FTIR) spectroscopy

Prepared SF solution and hydrogel were lyophilized for characterization of SF structure. Lyophilized silk sponges were prepared into pellet (diameter < 13 mm) using pellet press (The PIKE Technologies, USA). FTIR absorption spectra of SF sponge at the wavenumber range of 1600-1700 cm^{-1} was determined with a Fourier Transform Infrared Instrument (FTIR Nicolet iS5, Thermo Scientific, USA). For each measurement, scanning was repeated 128 times with a resolution of 4 cm^{-1}. The quantitative analysis on the structural characteristics of SF hydrogel was carried out at the amide I band between 1600-1700 cm^{-1} through the multi-peak fitting method. Prior to fitting amide I band, the baseline correction with a straight line between 1600-1700 cm^{-1} and the nine-point multi-peak Gaussian fitting of FTIR spectra were performed by

Origin software. The relative area of the overlapped single bands are used for estimating the proportion of secondary structures such as random coil, α-helices, β-sheet and turns. The single bands of SF hydrogel were assigned to the corresponding secondary structures according to previous studies [74,75]:

1605–1615 cm^{-1}; aggregated strands, 1616–1637 cm^{-1}; β-sheet, 1638–1655 cm^{-1}; random coil, 1656–1662 cm^{-1}; α-helices, 1663–1695 cm^{-1}; turns. The crystallinity index of a SF hydrogel was calculated as the intensity ratio of the 1645 and 1620 cm^{-1} absorptions of the amide-I band which corresponded to the β-sheet and random coil conformation, using Eq [76, 77].

$$Crystallinity\ index\ (\%) = \frac{A_{1620cm^{-1}}}{A_{1620cm^{-1}} + A_{1645cm^{-1}}} \times 100$$

$A_{1620\ cm^{-1}}$, Absorbance at 1620 cm^{-1}

$A_{1645\ cm^{-1}}$, Absorbance at 1645 cm^{-1}

3.4.2. X-ray diffraction (XRD)

Subsequently, X-ray diffraction (XRD) was performed using an X-ray diffractometer (D8 DISCOVER, Bruker, USA) with CuKa radiation. Irradiation conditions were 40 kV and 40 mA. XRD patterns were recorded at a speed of 2° /min at 40 kV and 35 mA in the region of 2θ from 5° to 40° .

3.4.3. Mechanical tests

To investigate the mechanical property of SF hydrogel, uniaxial compression experiment was performed. Cylindrical hydrogel with flat and parallel surfaces with 15 mm diameter and 10 mm height were prepared and were allowed to swell in distilled water for 24 h before the test. The samples were mounted at the base and compression tests of hydrogels were performed on an Universal Testing Machine (Lloyd Instruments, Ltd., UK) equipped with a 0.5 kN load cell at room temperature. A cross head speed was 10 mm/min. All data were collected for quadrupled samples.

3.4.4. Dissolution and enzymatic degradation test

Lyophilized SF hydrogel samples of 15 mg (±1 mg) with incubated at 37 ℃ in phosphate-buffered saline (PBS) solution containing α-chymotrypsin from human pancreasin 1.5 ml eppendorf tubes. Degradation studies were performed with 1 U/ml α-chymotrypsin in phosphate buffered saline (PBS). After one day incubation period, SF residues were centrifuged at 10,000 rpm for 10 minutes and wash twice with distilled water. After rinsing, SF residues were centrifuged again at 10,000 rpm for 10 minutes to collect the silk residues. The SF residues were dried overnight in a hood and the mass were determined using an analytical balance. Four samples from each group were taken at each time point to get

statistically significant data (N= 4). Samples incubated in PBS at 37 ℃ without enzymes to investigate the dissolution properties of SF.

3.5. Preparation of Bombyx mori Silk Gland Samples

Whole silk glands were dissected from mature fifth instar *Bombyx mori* silkworms approximately 12 h before commencement of spinning. The silkworms were immersed in diethyl ether for 1 min for anesthesia. The epithelium was not removed from the gland to reduce the risk of loss of metallic ions from the luminal contents. The gland was briefly rinsed with distilled water to remove hemolymph, and then was blotted with tissue paper. The silk gland is divided into three divisions: posterior (P) division, middle (M) division, and anterior (A) division. In these parts of silk gland we choose the middle division of silk gland for the investigation of metal ion contents because of its lager volume and mass. The metal ion content in the silk gland and cocoon fiber was measured as follows. An equal amount of protein in the silk gland and cocoon fiber was dissolved in 50% (v/v) HNO_3 solution. The resulting solution was diluted with a known volume of distilled water. The measurements were performed with a ICP-Atomic Emission Spectrometer (ICP-AES, Optima-4300 DV, Perkin-Elmer inc, USA) using the following conditions: power, 1350 W; detection mode, pulse counting. All measurements were repeated 5 times and

averaged.

For component analysis of middle division of silk gland, the wide M division is further divided into three divisions, the posterior (MP), the middle (MM) and the anterior (MA). The thin epithelial surface of the glands was removed carefully with forceps. After blotting with filter paper, the whole middle divisions and the separated parts were transferred directly moisture analyzer (MB45, Ohaus, USA). The remaining solid silk protein transferred into methanol for 1 h to carried out the selective β-sheet crystallization. SF molecules converted into β-sheet conformation with very short time while SS molecules maintained the its random coil conformation due to its difference of hydrophilicity. The methanol treated silk protein was degummed with 0.2% (w/v) sodium carbonate and 0.3% (w/v) marseille soap solution at 100 ℃ for 30 min, and then rinsed with distilled water to remove any SS. The remaining solid contents determined as contents of SF. The amount of SS was calculated the difference between total solid contents and contents of SF.

3.6. Ion diffusion behavior between SF and SS

3.6.1 Ion diffusion between SF and SS

To investigate the ion diffusion behavior between SF and SS, experimental condition divided into two circumstances, first is phase separation between SF and distilled water, the second is in

vitro macro phase separation between SF (4%, w/v) and SS solution (1%, w/v). The macro phase separation condition between SF and distilled water was prepared using syringe pump. 20 ml of SF solution (4%, w/v) containing metal ion solutions (4000 μg) added into the 50 ml of conical tube. Then, 20 mL of distilled water or SS solution was added to the above SF solution. In order to maintain the interface between the two solutions, distilled water or sericin solution was added carefully using a syringe pump (KD Scientific, USA), (Figure 6). Phase separated solutions incubated in oven at 25 ℃, and 10 ml of upper layer solution was carefully obtained for the analysis of metal ion diffuse amount. The concentration of metal ions using a ICP-Atomic Emission Spectrometer (ICP-AES, Optima-4300 DV, Perkin-Elmer inc, USA).

3.6.2. Ca^{2+} binding ability of SF and SS

The Ca^{2+} binding abilities of the aqueous SF and SS solutions were examined according to a previously reported method. [78] The formation rate of turbid calcium carbonate precipitates was monitored by the absorption at 570 nm of a solution prepared by adding 1.5 mL of 100 mM $CaCl_2$ solution to a mixture of 1.5 mL of 100 mM $NaHCO_3$ (pH 8.7) and 300 μL of aqueous SF and SS solutions with concentrations of 0.5% and 1.0% (w/v). An ultraviolet/visible spectrophotometer (optizen 2120uv plus, mecasys, USA) was used to test the absorbance at 570 nm of the

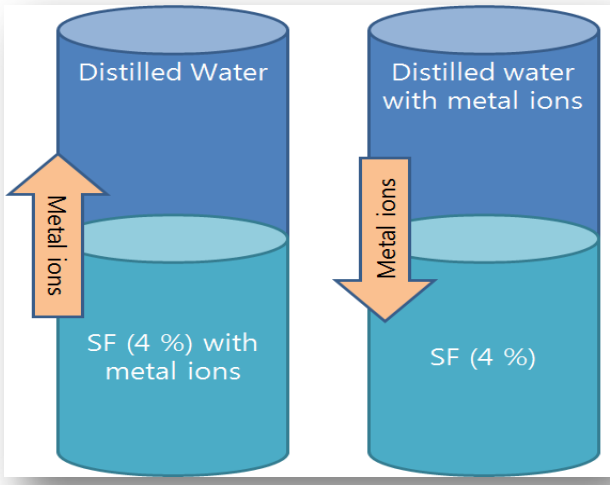

(a)

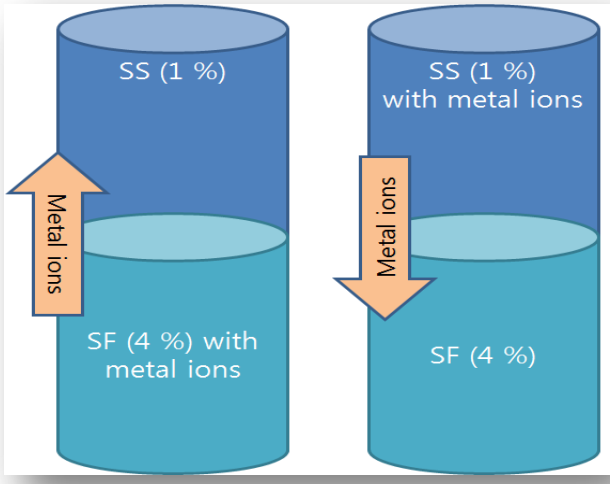

(b)

Figure 6. Initial experimental setup of ion diffusion behavior between SF and distilled water (a), and SF and SS (b).

resultant mixture. The distilled water was used as a control.

3.6.3. Cu^{2+} adsorption capacity of SF and SS

The lyophilized SF and SS was dissolved in 1M lithium chloride (LiCl) / dimethyl sulfoxide (DMSO) solution for 2 h at 50℃ to prepare a dope solution. The dope solution was dropped into alcohol coagulants through a 26G syringe using a syringe pump (KD scientific, USA). Methanol was used as coagulants. The SF and SS beads were left in the coagulant bath for another 1 h. They were then filtered with a nonwoven filter and washed with the same coagulant to remove the residual LiCl and DMSO. To enhance the water stability and mechanical strength of the SF and SS beads, the beads were immersed in a crosslinking reagent. The crosslinking was performed with 2% (v/v) glutaraldehyde (GA) in the same coagulant. The reaction was carried out for 1 h at room temperature. Finally, the SF and SS beads were washed with the same coagulant followed by distilled water to remove the excess GA.

Synthetic aqueous solutions containing Cu^{2+} (100 mg/l) have been prepared by dissolution of copper nitrate in distilled water. Batch adsorption experiments have been carried out by shaking 0.1 g of SF and SS beads with 100 ml of the copper solution of 100 mg/l concentration at 23 ℃. The suspension is agitated at 180 rpm for 1 day. At the end of the adsorption, the SF and SS beads were removed by filtration and a sample of the filtrate is analyzed by

ICP-AES.

The equilibrium adsorption capacity, q_e, was determined using the following equation:

$$q_e = \frac{C_0 - C_e}{M} \times V$$

where C_o and C_e are the initial and the equilibrium concentration of the Cu^{2+} in the testing solution (mg/L), V is the volume of the testing solution (L), and M is the weight of the SF and SS beads (g) respectively.

3.7. Gelation experiment of SF with SS in ion diffusion environment

The gelation experiments of SF were carried out as follows. First, 3 mL of aqueous SF containing various amounts metal ion solutions was added to 4.5 ml disposable cuvettes. Then, 1.0 mL of aqueous SS was added to the above SF solution. In order to maintain the interface between the two solutions, SS was added carefully using a syringe pump. To determine the gelation time, absorbance changes at 550 nm were monitored with UV/Vis Spectrophotometer (Optizen 2120UV plus, Mecasys, USA). SF gelation occurred with a heterogeneous microstructure leads to an increase the degree of light scattering which is possible to know the increase of the

absorbance.

Relative gelation kinetics was obtained by following as

$$Gelation\ kinetics\ (\%) = \frac{Abs_{SF_t} - Abs_{SF_{gS}}}{Abs_{SF_g} - Abs_{SF_{gS}}} \times 100$$

Abs_{SFg} = Absorbance at 550nm of SF when gelation completed

Abs_{SFs} = Absorbance at 550nm of SF at $time_0$

Abs_{SFt} = Absorbance at 550nm of SF at $time_t$

4. Results and discussion

4.1. Retardation effect of SS on the gelation behavior of SF

4.1.1. Macro phase separation between SF and SS

Among various fibrous protein materials, silk protein fiber, especially that produced by silkworms, has unique core-shell structural characteristics. The core protein is SF, which consists of two strands of a single fiber, and the shell protein is SS, which envelops these SF fibers. Although many studies have been reported on the silk spinning process, most of the results emphasize the self-assembly of SF alone without mimicking the natural structure of silk proteins. In order to fully characterize the silk spinning process, interactions between SF and SS should be identified.

Based on the abovementioned literature survey, it is clear that SS can affect the mechanical properties of regenerated silk fibers. However, the stability of an aqueous silk solution has not yet been studied in detail. In the extracted silk gland solution, the concentration of silk solution has varied from 20-30%. The highly concentrated, regenerated aqueous silk solution is in a metastable state, which is easily converted into a β-sheet structure hydrogel. However, the silk gland solution in a silkworm is maintained in a hydrated gel-like state with a Silk I structure, until the silk protein moves to the spinning duct of the silkworm, which occurs during the

spinning process.

To mimic the phase separation structure of silk fibers, we simplified the structure of SF and SS as macro phase separation environment. Oh et al. [68] found that the phase-separated state of SF and SS could be maintained when the SS solution was carefully loaded onto the top of the SF solution without disturbing the interface. Even though the concentration of silk protein in the silk gland is more than 20%, in this study, 4% (w/v) SF solution was used because a regenerated sericin solution of more than 1% (w/v) easily converts into a gel state before the phase-separated gelation experiment is performed. For this reason, 1% (w/v) sericin was selected as the limit for this experiment. Therefore, taking the weight ratio of SF and SS into consideration, 4% (w/v) SF was used in the gelation experiment. Figure 7 shows the phase separation state of SF (4.0%, w/v) and various concentrations of SS (0, 0.25, 0.5, 1.0%, w/v) with the gelation behavior of SF. Upon gelation, SF converted to an opaque white color resulting from the heterogeneous microstructure of the SF gel. This clearly shows that the phase separation state is well maintained until the complete gelation of SF, which is at the bottom of the SS solution. The gelation of SF was delayed as the concentration of phase-separated sericin was increased.

Nisal et. al [79]. investigated the partition coefficients of commercially available dyes and determined the preferential association of dyes with either SS or SF protein in the silkworm gland and in the cocoon fibers. In addition, the diffusion behavior of various

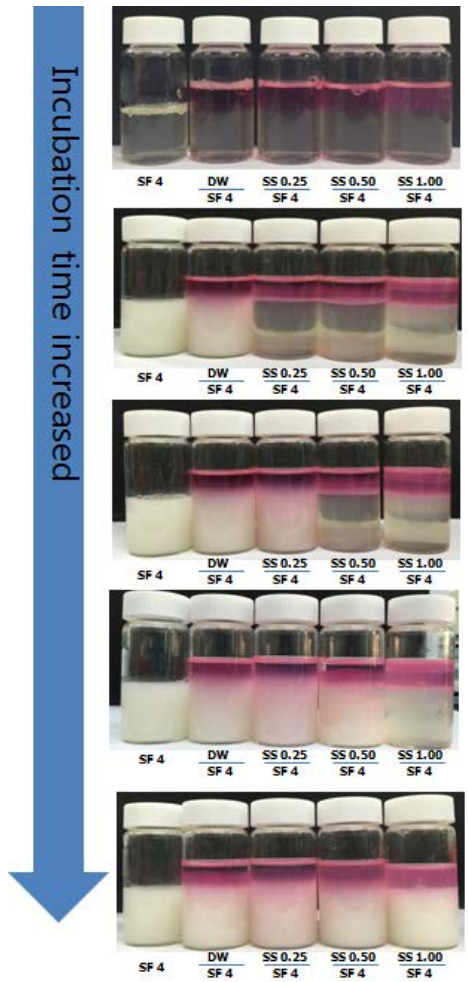

Figure 7. Images of SF-SS separation during SF gelation.

commercial azo dyes between phase-separated SF and SS layers were investigated, and the molecular weight of dyes and their chemical structures were found to be important in the diffusion behavior of silk proteins [80].

In this study, rhodamine B dye, which has a strong affinity for SF, was used to monitor the interface between the two proteins during the gelation of SF [79]. Regardless of the affinity difference between SS and SF, rhodamine B dye could not diffuse into the SF layer, indicating that the phase separation between silk proteins was maintained in a liquid state. Color separation was observed until the gelation of SF was completed; indicating that at least the interface between the two proteins was maintained during SF gelation. Furthermore, the interface between the two silk proteins might have a role as a barrier against the transfer of certain molecular weight substances.

Despite the phase separation between the two proteins, which remained macroscopically until the gelation of SF, the possibility of dilution or concentration differences between the two silk solutions was taken into account. To determine the protein transport between the SF and SS layers, the changes in the concentration of each layer before and after SF gelation were investigated. Figure 8 shows the concentrations of the SF and SS layers before and after the gelation experiment. When distilled water was on the upper layer, the protein concentration of the upper layer increased to 0.09 ± 0.02% (w/v), indicating that only a small amount of SF moved to the distilled water layer. This migration of SF into the distilled water

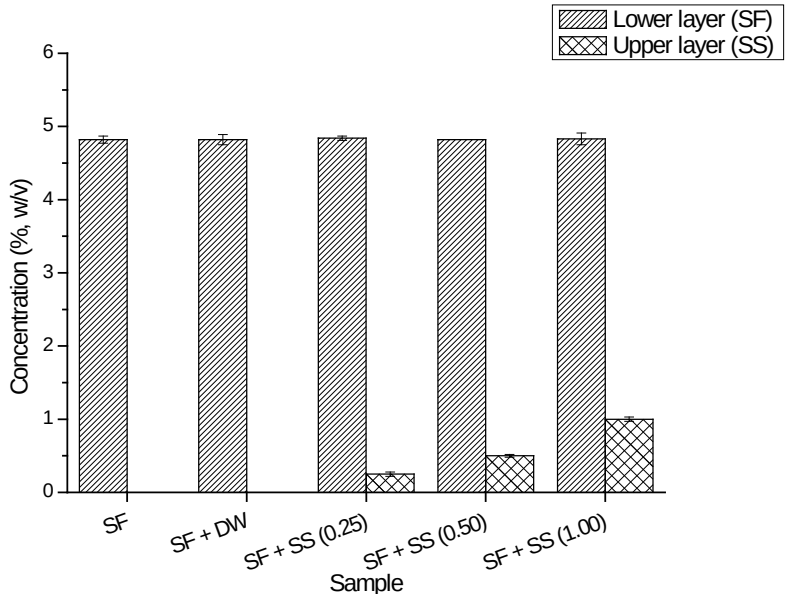

Figure 8. Concentration of each layer before (a) and after (b) gelation.

had similar effects on the dilution of the SF solution beneath it. When the SS was on the top layer, the concentration of SS solution also changed from 0.25 ± 0.03%, 0.50 ± 0.02%, and 1.00 ± 0.03% to 0.29 ± 0.07%, 0.57 ± 0.09%, and 1.10 ± 0.10%, respectively. Even though the concentration of the SS layer was slightly increased, this increase was negligible.

4.1.2. Retardation of gelation time of SF solution in the presence of phase separated SS solution

In the previous , photos showed the delay in SF solution gelation in the presence of a phase-separated SS layer. This means that the SS layer might play a significant role in the gelation kinetics of SF solution. Therefore, the gelation kinetics of SF solution in the presence of a phase-separated SS layer was investigated in more detail using an optical spectrometer.

As mentioned above, the transparent sol state SF solution becomes opaque when gelation has occurred [81]. To track the effect of phase-separated SS on the gelation behavior of SF, optical density changes at 550 nm were monitored. The SF gelation time was defined as the time from the beginning of incubation to the point when the plateau of optical density was reached [82]. For comparison, other polymers, such as bovine serum albumin (BSA) and synthetic polyethylene glycol (PEG 200K), were selected as controls for the experiment. Figure 9 shows the optical density

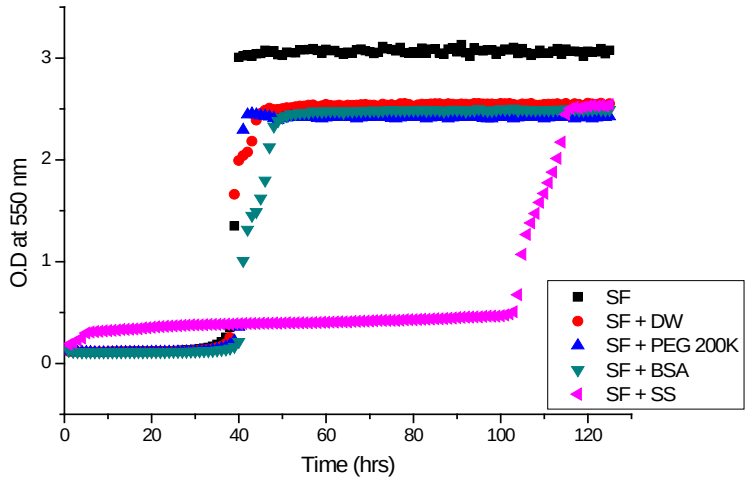

(a)

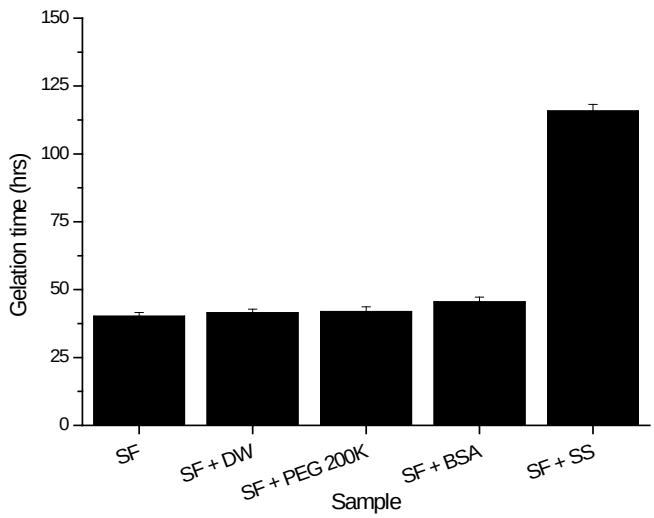

(b)

Figure 9. SF gelation delay with various polymers (1%) in the layer above SF (SF at 4%). (a) Representative optical density changes and (b) gelation time of various SF solutions.

changes and gelation time of regenerated SF solutions with various polymers in the phase-separated condition. The gelation time of the neat SF solution and SF solution separated with distilled water, the gelation time with BSA and PEG 200K was nearly 40 h. However, the gelation time of SF was delayed to 115 h in the presence of SS in the upper layer. This indicates that SS in a phase separation state can effectively retard the gelation behavior of SF solutions.

4.1.3. Effect of the phase-separated SS solution pH on the gelation kinetics of SF

The pH of protein solutions greatly affects the supramolecular structures of those proteins. Protein materials have isoelectric points with no net electrical charge state. If the pH of a protein solution is closer to its isoelectric point, the electrostatic repulsion of molecules is decreased, thereby allowing more opportunities for inter- or intramolecular interaction. SF exhibits conformational and morphological transitions from random coil and spherical micelles to β-sheet and nanofibrilar structures as the pH of a solution comes closer to the isoelectric point [27]. To find out the effect of the SS layer pH on the gelation kinetics of SF, an SF gelation experiment with phase-separated SS solution at various pH was carried out

(Figure 10). Regardless of the pH of the SS solution, it delayed the gelation of SF. This indicates that phase-separated SS with a weakly acidic or neutral pH, which is similar to the pH in silk glands, affects the SF gelation kinetics.

4.1.4. Effect of SF concentration on the gelation kinetics of SF with a phase-separated SS solution

The concentration of SF is known to affect gelation time. Generally, the gelation time of SF is inversely proportional to the SF concentration [83]. Figure 11 shows the gelation time with various concentrations of SF, with or without a phase-separation state of distilled water or SS. Phase separation with distilled water was used as a control. The gelation time of the SF aqueous solution without SS decreased with an increase in the SF concentration. While 8% SF formed a hydrogel within 45 h, 6%, 4%, and 2% SF took approximately 52, 59, and 62 h, respectively. In the case of phase-separation with distilled water, although the gelation was slowed, this delay was only about 2 h relative to SF solution alone. This might be due to a slight dilution effect, as shown in Figure 8. However, when 0.5% SS was phase-separated from SF, the gelation time was increased to 56 h, 61 h, 64 h, and 68 h for 8%, 6%, 4%, and 2% SF. These results indicate that phase-separated state SS has more of an effect than distilled water on the

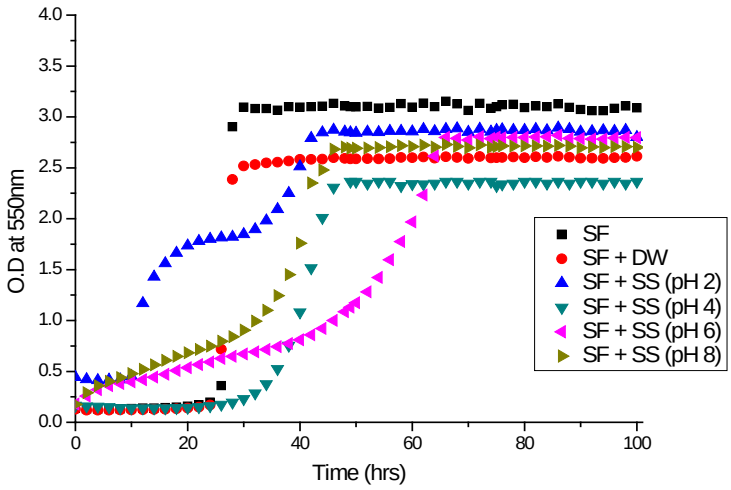

(a)

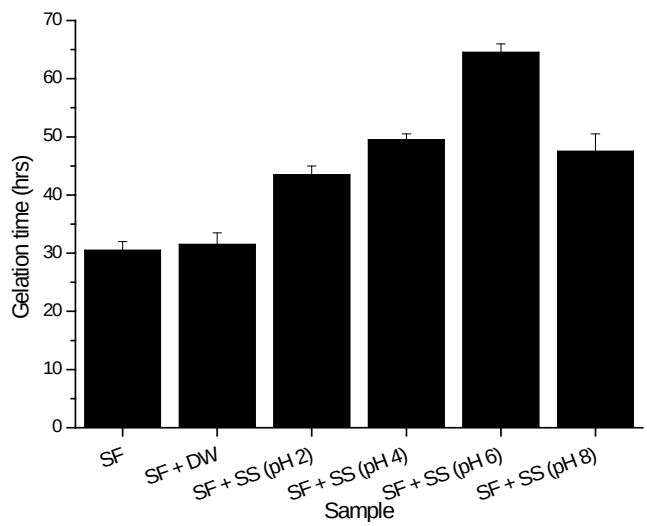

(b)

Figure 10. SF gelation delay with various pH values of sericin solution (0.5%, w/v) on top of SF (4%, w/v). (a) Representative optical density changes and (b) gelation time of various SF solutions.

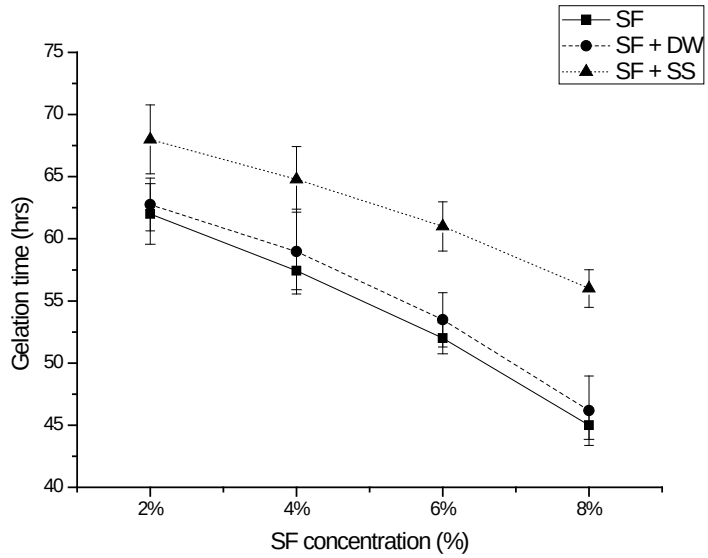

Figure 11. Effect of SS (0.5%, w/v) on the increase in gelation time at different SF concentrations.

gelation of SF. Even more interestingly, the delay was more significant when the concentration differences between SF and SS were greater.

4.1.5. Effect of the phase-separated SS concentration on the gelation kinetics of SF

To determine the effect of the SS concentration in the upper layer on the gelation of SF (4.0%, w/v), various SS concentrations (0%, 0.25%, 0.50%, 1.00%, w/v) were prepared and loaded onto the top of the SF solution. The optical density changes in the SF solution phase-separated from different concentration of SS are shown in Figure 12 (a). The relationships between the gelation time of SF and SS concentration at 50 ℃ is shown in Figure 12 (b). The SF gelation time increased with increasing SS concentrations. This indicates that the SS layer, although phase-separated, has a positive effect on slowing the gelation of an SF solution. However, these results cannot completely exclude the possibility that SF and SS mix when the concentration gradient is not high enough, because when SF and SS at the same concentrations are phase separated, the phase separation cannot be maintained. Interestingly, when SF and SS were mixed as a homogeneous solution, the gelation did not occur until 160 h. These results imply that SS can clearly delay the gelation time of SF only when they are phase separated.

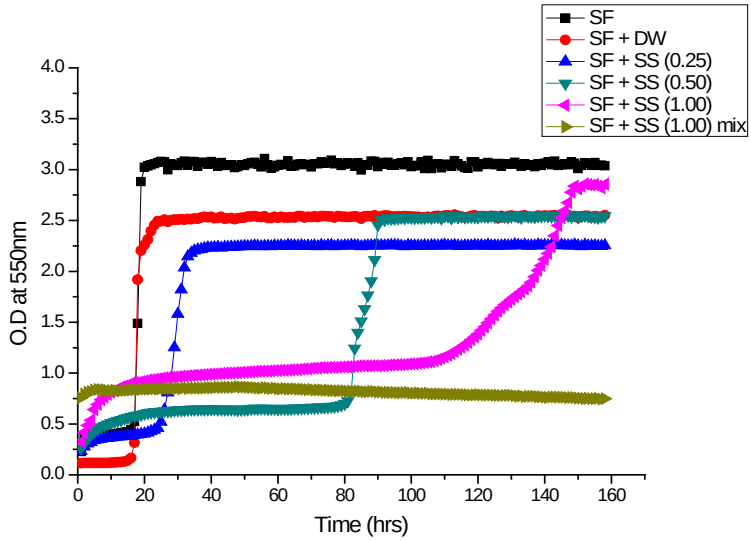

(a)

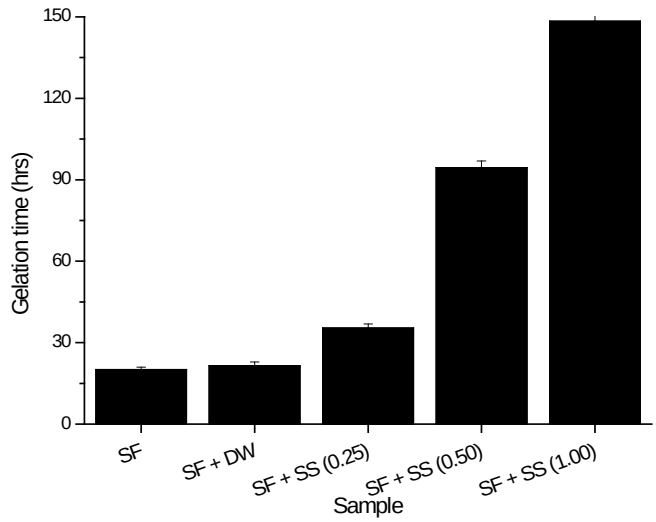

(b)

Figure 12. SF gelation delay with various concentrations of SS on top of SF (4%, w/v), (a) representative optical density changes and (b) gelation time of various SF solutions.

4.1.6. Effect of the macro phase separation condition on the β-sheet transition kinetics of SF

The mechanism of SF gelation is still unclear, but it is recognized that the sol-gel transition of SF results from the formation of β-sheets, which provides physical cross-links [84, 85]. Thioflavin T (ThT) is a benzo-thiazole extrinsic fluorescence dye that is widely used for the identification and quantification of amyloid β-fibrillation in real time [86]. It can be selectively associated with the β-sheet and the aggregated forms of the protein. Free ThT in an aqueous solution shows only weak fluorescence, with lower excitation and emission maxima at 350 and 440 nm, respectively. However, when ThT is added to samples containing β-sheet-rich deposits, it generates strong (red-shifted) fluorescence, with excitation and emission maxima at approximately 440 and 490 nm, respectively. Recently, a conformational transition in SF has been observed using this ThT fluorescence dye system [87-89].

To study the effect of SS concentration on the gelation behavior of SF, β-sheet transition kinetics were investigated by a fluorescence kinetics study using ThT dye. First, ThT fluorescence intensity of the SF solution was measured and is shown in Figure 13. While ThT fluorescence was not seen in the water solution, the intensity increased with the SF solution. This fluorescence intensity indicates that even if the initial conformation of the SF solution is mainly random coil, there is some β-sheet content. The intensity

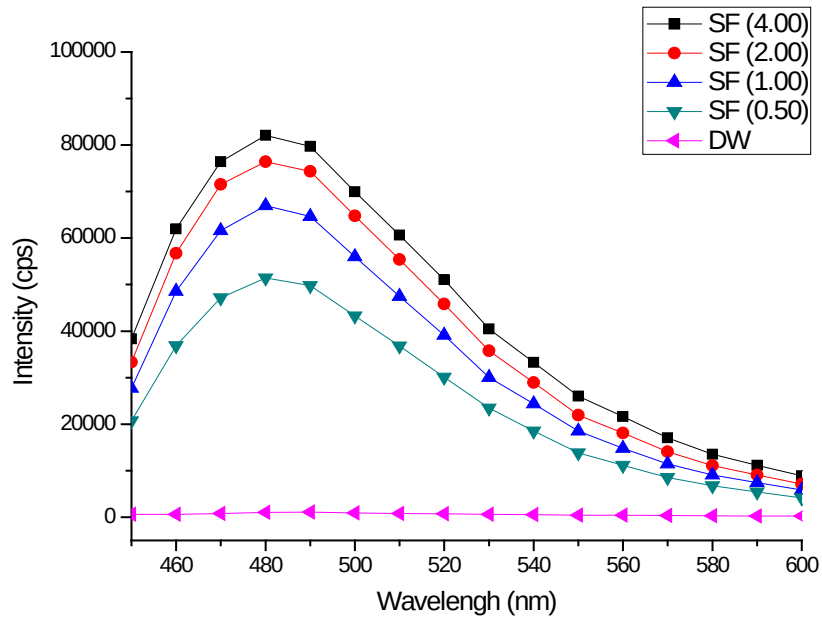

Figure 13. Fluorescence emission spectra of ThT in distilled water and in various concentrations of SF solution.

of fluorescence from 450 nm to 600 nm increased gradually as the concentration of the SF solution increased. This trend was due to the presence and amount of β−sheet structures in the SF solution. Dubey et al. [90] investigated the effect of incubation and metal ions on the conformational transition of SF using the ThT assay and found that fluorescence intensity increased with incubation time. However, this experiment was limited by the low concentration (1.0%, w/v) of SF solution used. Therefore, the relationship between the β−sheet conformational transition and gelation of SF was not explained. In this study, the ThT fluorescence kinetics of 4% and 8% (w/v) SF solution in the presence of various concentrations of SS (0%, 0.25%, 0.50%, and 1.0%, w/v) in the top layer were investigated. Figure 14 (a) shows the β−sheet transition kinetics of SF solution (4%, w/v) in the presence of phase−separated SS at different concentrations. This clearly indicates that the gelation of SF occurred with the conformational transition to β−sheets. In addition, the transition into a β−sheet structure was also retarded if the concentration of the SS layer increased.

Figure 14 (b) shows the same experiment using 8% SF solution. Compared to the 4% (w/v) SF, the transition time was less. However, the retardation effect of phase−separated SS on the β−sheet transition was maintained. From the β−sheet transition kinetics of SF solution with various concentrations of SS, the delay in SS gelation due to postponement of the β−sheet conformational

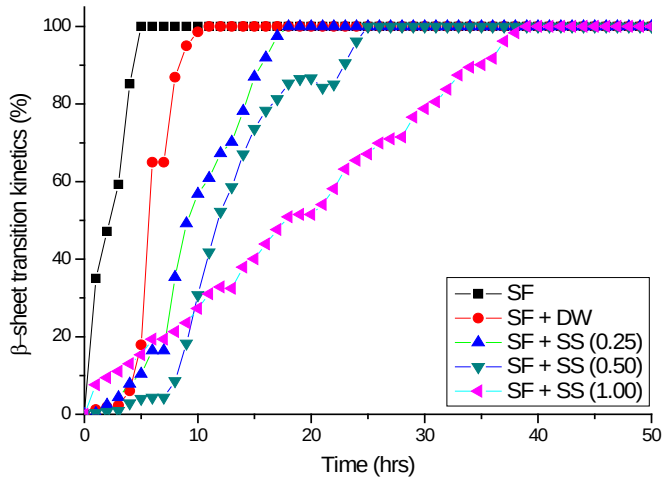

(a)

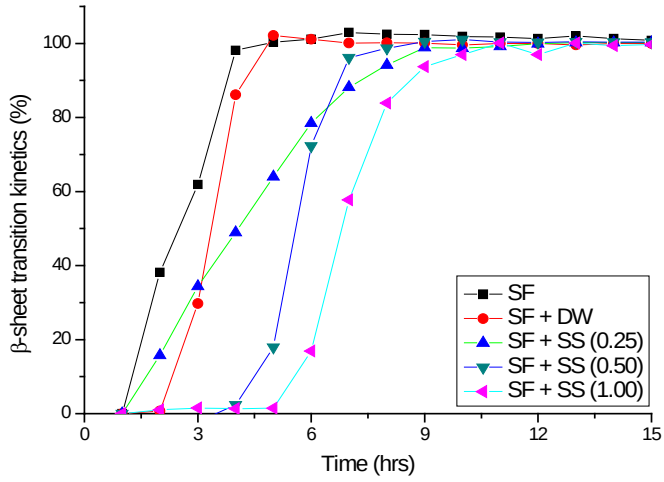

(b)

Figure 14. Relative β-sheet transition kinetics of SF based on ThT fluorescence intensity. (a) SF 4% (w/v) and (b) SF 8% (w/v).

transition of SF can be seen.

4.2. Characterization of an SF hydrogel prepared in the presence of phase-separated SS

4.2.1. Secondary structure of silk gland and fiber

Prior to investigating the secondary structure of the SF hydrogel prepared in a macro phase separation condition, we investigated the secondary structure of the middle gland in silkworm and silk fiber. FT-IR is a useful method to determine the secondary structure of proteins, as the characteristic spectral band of amide I is sensitive to the hydrogen-bonding pattern [91-94]. Consequently, the deconvolution of the amide I peak into its elementary contributions is customarily used for quantitative analysis of the protein secondary structure.

The secondary structure of SF in the middle gland of silkworms and in cocoon fiber was measured using ATR-FTIR spectroscopy. We examined the absorbance of amide I region, which has a wavenumber ranging between 1700 and 1600 cm^{-1}. Amide I results from the C=O stretching vibration of the amide group in the protein. For more detailed study of the secondary structure of SF, a quantitative analysis of the amide I band was performed using the Fourier self-deconvolution (FSD) fitting method. Figure 15 shows the FT-IR absorbance spectra from the silk gland SF and cocoon

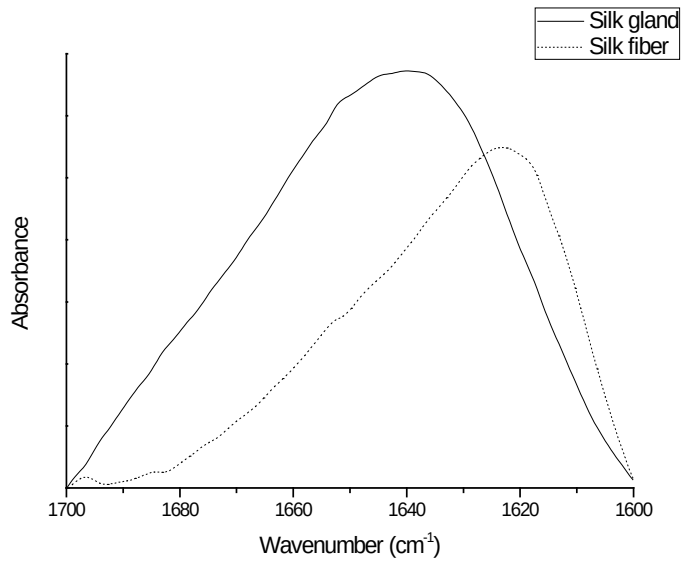

(a)

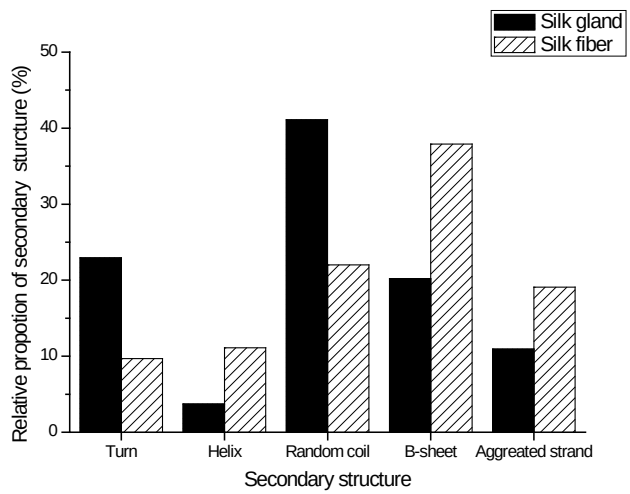

(b)

Figure 15. FT-IR spectra of the middle part of the silk gland and silk fiber (a) and their secondary structure compositions (b).

fiber, and the proportions of their secondary structure from the deconvoluted results (Figure 16). The silk gland showed a maximum amide I peak at 1643 cm^{-1}, which is characteristic of the random coil conformation [95]. The FT-IR absorbance spectra of the SF fiber exhibits an obvious peak at about 1620 cm^{-1}, corresponding to the β-sheet conformation. In the case of the silk gland, the proportion of random coils was the highest of all secondary structures, which was 42.1%, while silk fiber had the highest β-sheet proportion, which was 37.9%.

4.2.2. Secondary and crystalline structure of SF before gelation

There are various dissolution methods to prepare an aqueous SF solution. Chen et al. [96] investigated the rheology and secondary structure of various regenerated SF and determined that the LiBr-H_2O solvent system was better to study the conformational changes of SF than $CaCl_2$-ethanol-water and $Ca(NO_3)_2$-methanol-H_2O. LiBr-H_2O regenerated SF is predominantly a mixture of random coils and turns, which is similar to SF in the silk gland. In order to obtain initial structural information about SF solutions during the phase-separated experiments, SF solutions were collected from the bottom layer after incubation at 50 ℃ for 1 h. The collected SF solutions were lyophilized and subjected to ATR-FTIR and XRD analysis. Figure 17 shows the ATR-FTIR

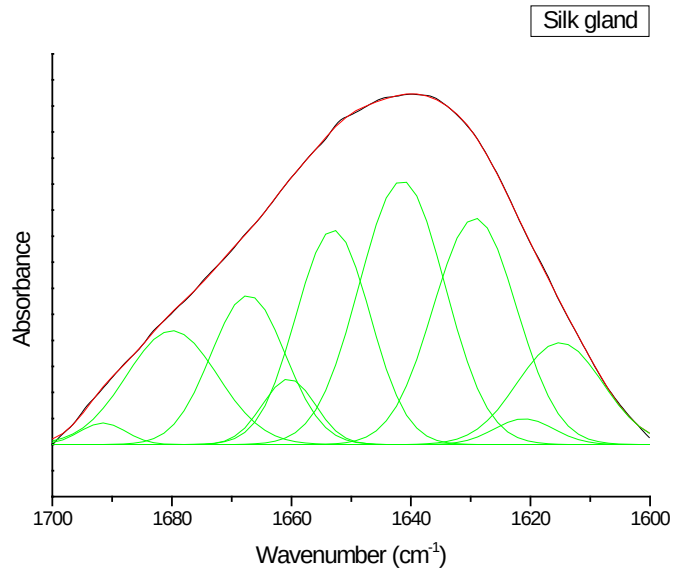

(a) Silk gland

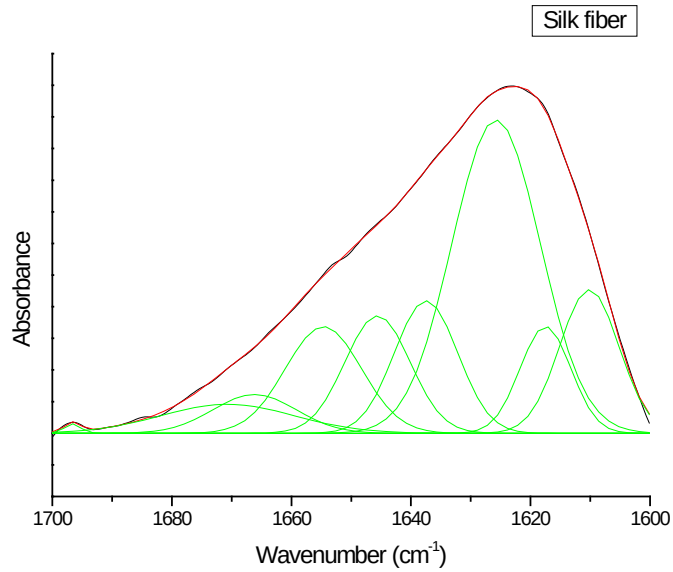

(b) Silk fiber

Figure 16. Deconvoluted FT-IR spectra of the middle part of the silk gland (a) and silk fiber (b).

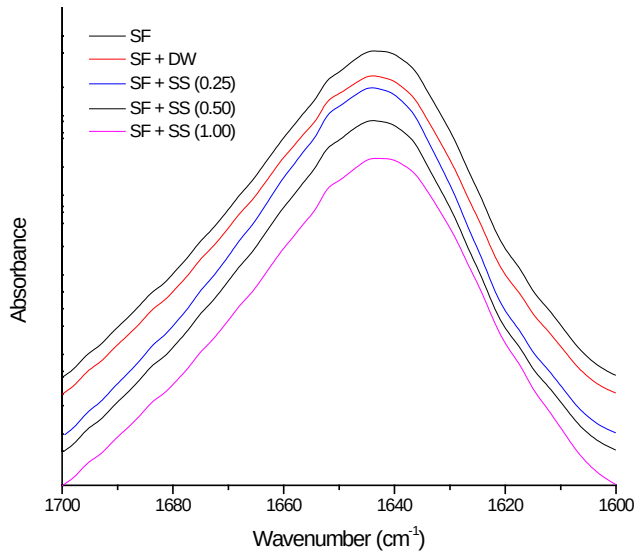

(a)

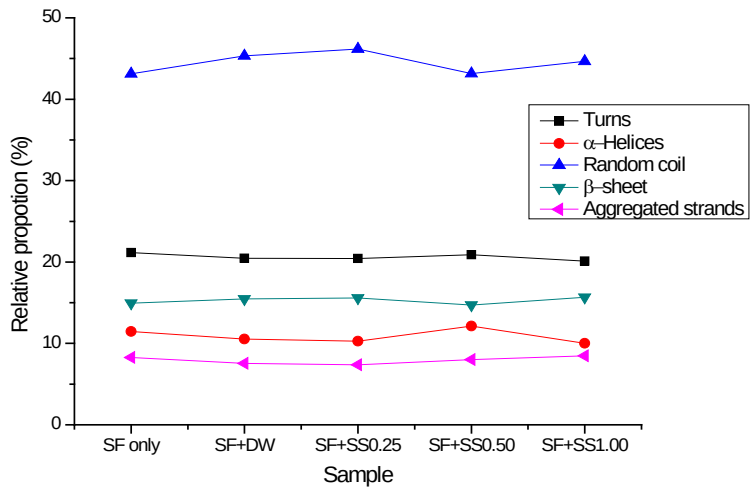

(b)

Figure 17. FT-IR spectra of SF phase separated from SS at different concentrations (a) and the SF secondary structure composition (b).

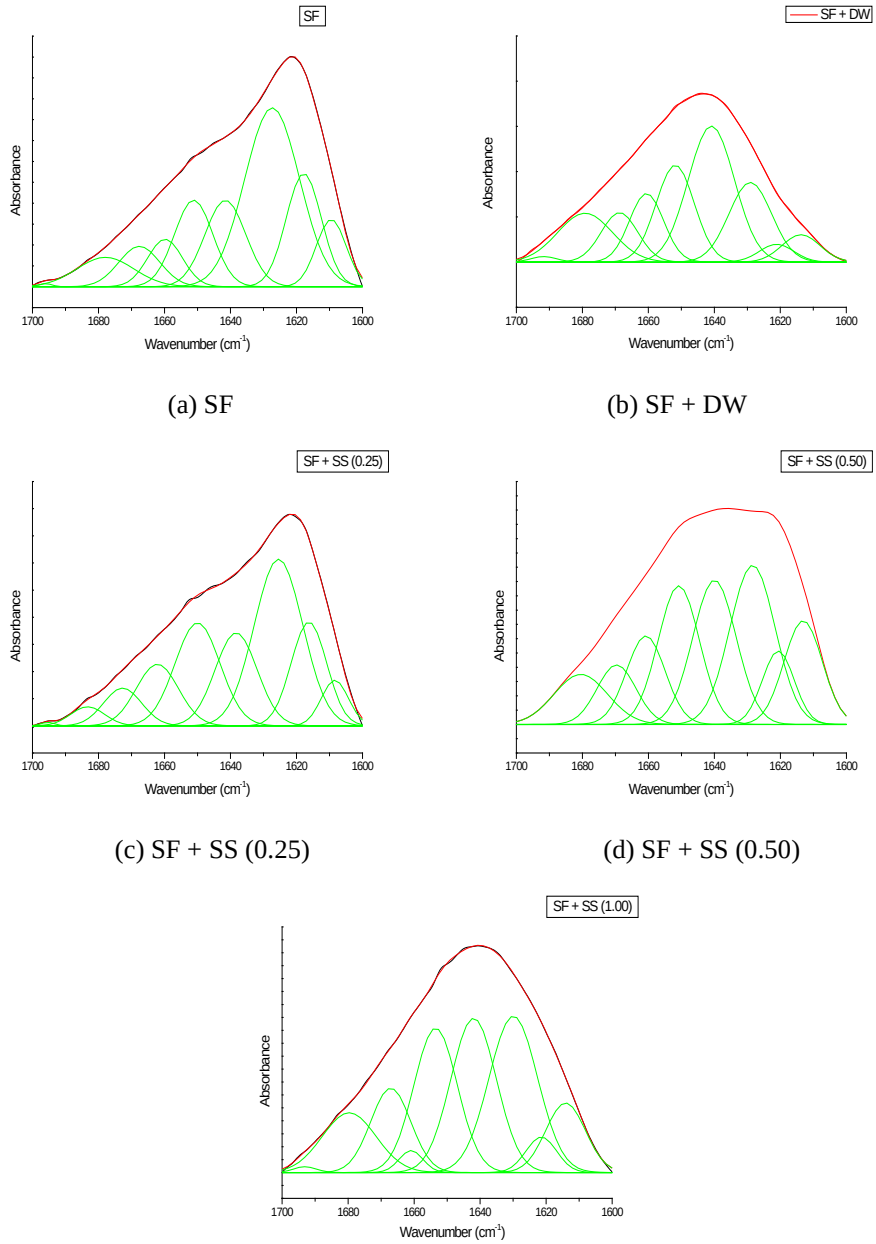

(a) SF

(b) SF + DW

(c) SF + SS (0.25)

(d) SF + SS (0.50)

(e) SF + SS (1.00)

Figure 18. Deconvoluted FT-IR spectra of SF phase separated from SS at different concentrations. (a) SF, (b) SF + DW, (c) SF + SS (0.25), (d) SF + SS (0.50), and (e) SF + SS (1.00)

absorbance spectra and secondary structures from the deconvoluted results (Figure 18) of lyophilized SF at the initial state of gelation in macro phase separation with various concentrations of SS. There was no significant difference between the samples, indicating that the SS concentration on the top layer did not have any effect on the SF conformation at the initial stage of SF gelation. As expected, the secondary structure composition of SF also exhibited no significant differences. The calculated crystallinity indices of SF solutions were also similar, ranging between 20–23% (Figure 19). These results indicate that the SS concentration on the top layer did not have any effect on either the secondary structure or crystallinity of the bottom SF layer at the initial stage of incubation.

The diffraction technique is the most effective method to clarify the crystal structure of SF, especially for Silk I and II. XRD curves of the lyophilized SF solutions are shown in Figure 20. All the samples showed an amorphous state, without any Silk I and Silk II crystalline structures.

Since the random coil–rich, amorphous regions of SF are water soluble and degradable, and thus prone to proteolytic enzymes, PBS buffer and α-chymotrypsin from human pancreas was used to dissolve and degrade the lyophilized SF. The SF mass following incubation for 1 day with PBS and α-chymotrypsin was quantified by weighing the SF residues after filtration and drying. More than

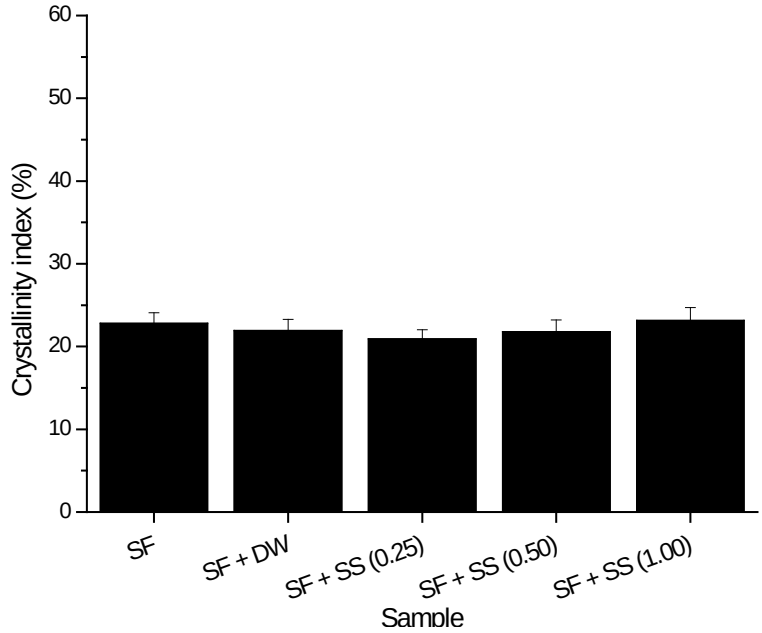

Figure 19. Effects of the SS concentration on the crystallinity index of the SF hydrogel prepared in phase separation conditions (n = 4).

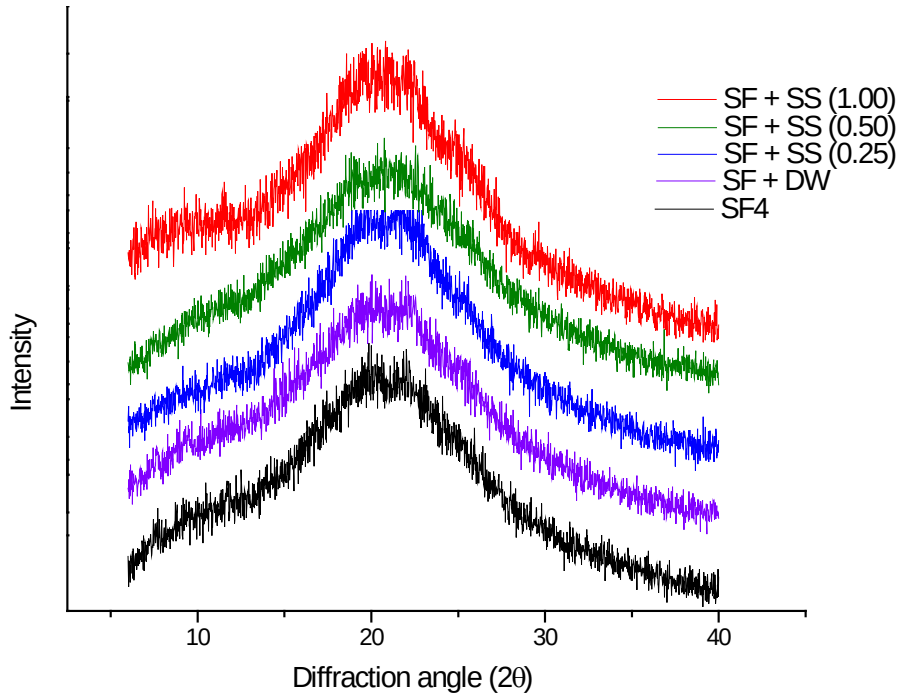

Figure 20. XRD patterns of SF phase separated from SS at various concentrations.

80% of the SF was dissolved by PBS and most of the SF was degraded by α-chymotrypsin (Figure 21). This also confirms that SF at the beginning of the incubation had a mainly random coil structure.

4.2.3. Secondary and crystalline structure of SF after gelation

In order to characterize the SF hydrogels prepared in the phase separation experiment, the SF hydrogels were lyophilized immediately after the gelation occurred. The SF gelation was considered complete when the maximum optical density of SF remained at a plateau for 5 h. Figure 22 (a) shows the ATR-FTIR absorbance spectra of the lyophilized SF hydrogels phase separated from SS at various concentrations. The peak position and shape of the spectra were similar between the neat SF hydrogel and the SF hydrogel prepared by phase separation with distilled water and 0.25% SS solution. The gelation time of these SF hydrogels did not show a significant difference. However, the SF hydrogel prepared by phase separation with 0.5% SS showed a broad absorbance spectra, ranging from 1620 cm^{-1} to 1650 cm^{-1}, and higher content of random coils and turn structures than β-sheets. The deconvoluted results of the FT-IR spectra (Figure 23) revealed that the SF hydrogel prepared by phase separation with 1.0% SS had more random coils and turn structures, with a low

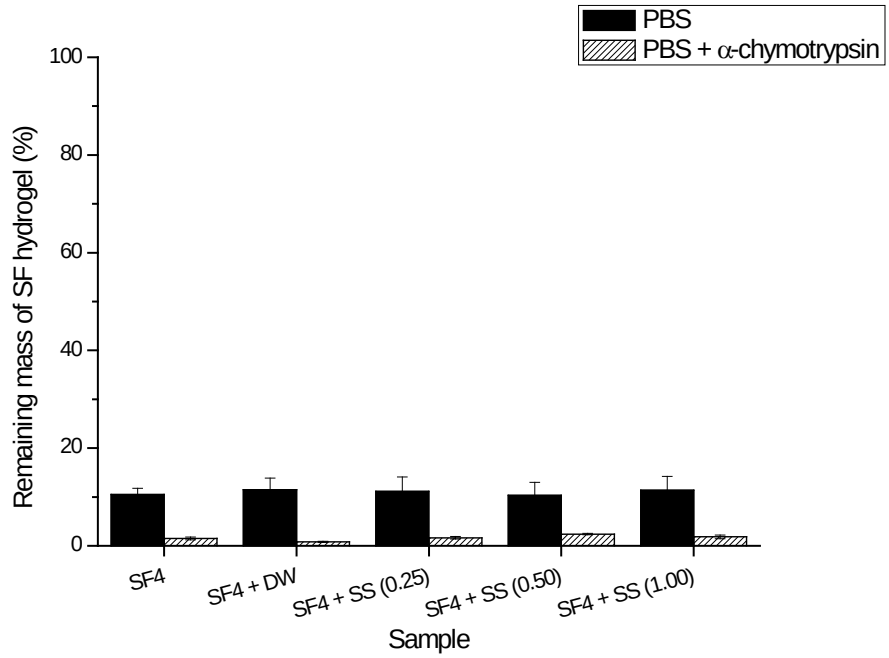

Figure 21. Dissolution and enzymatic degradation properties of SF phase separated from SS at various concentrations.

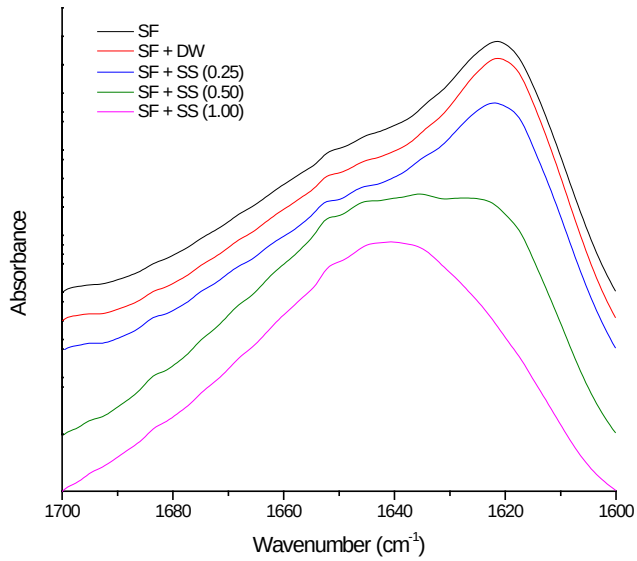

(a)

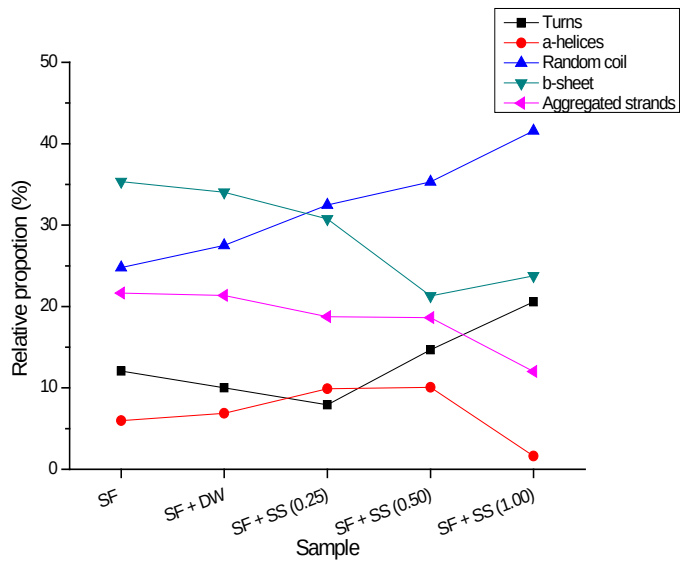

(b)

Figure 22. FT-IR spectra of SF phase separated from SS at various concentration (a) and SF secondary structure composition (b).

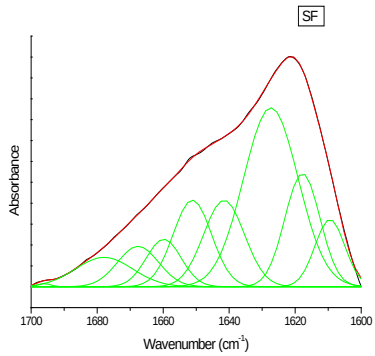

(a) SF

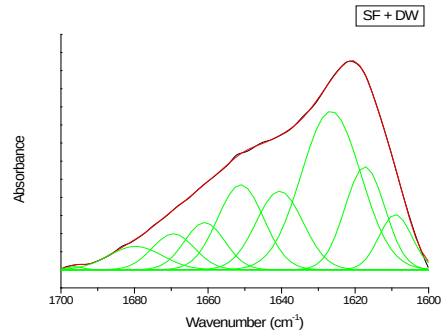

(b) SF + DW

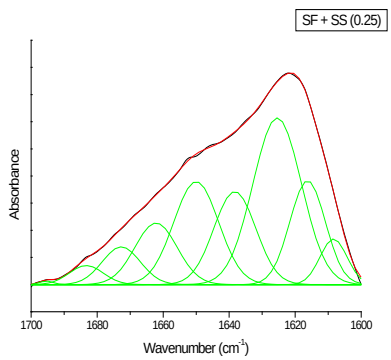

(c) SF + SS (0.25)

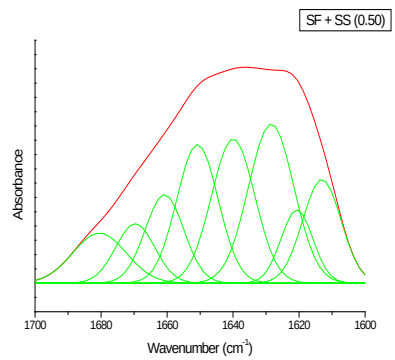

(d) SF + SS (0.50)

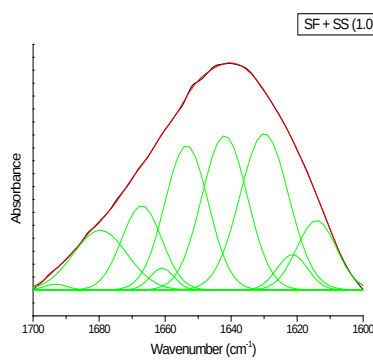

(e) SF + SS (1.00)

Figure 23. Deconvoluted FT-IR spectra of SF phase separated from SS at different concentrations. . (a) SF, (b) SF + DW, (c) SF + SS (0.25), (d) SF + SS (0.50), and (e) SF + SS (1.00)

content of aggregated strands and α-helix structures (Figure 22 (b)). The crystallinity index also varied with the concentration of SS; the crystallinity index of the SF hydrogel without phase separation was 61.7%, while that of the SF hydrogels prepared by phase separation with distilled water and 0.25% SS were 62.2% and 60.2%, respectively. The crystallinity indices decreased significantly to 49.4% and 40.1% as the SS concentration increased to 0.5% and 1.0% (Figure 24).

As mentioned before, the formation of SF hydrogels is generally understood to result from the development of β-sheets in the SF solution. However, the β-sheet content of SF hydrogels decreased as the concentration of the overlying SS increased. In addition, random coils and turn structures developed at the expense of β-sheets, α-helices, and aggregated strand structures at high SS concentration. Despite the unusual secondary structure composition, SF was still in a gel state. In order to further elucidate the structure of SF hydrogel, XRD analysis was performed.

XRD patterns of different SF hydrogels obtained from the phase separation experiments are shown in Figure 25. Based on previous studies, the typical Silk I peaks in XRD diffraction were expected to appear at 11.7°, 19.5°, 24.6°, and 28.7°, while the Silk II peaks were expected to appear at 9.2°, 18.9°, and 20.7° [97-99]. SF hydrogels without phase separation and SF hydrogel prepared by phase separation with distilled water and 0.25% SS solution were characterized by diffraction peaks at 2θ values of 9.2° and

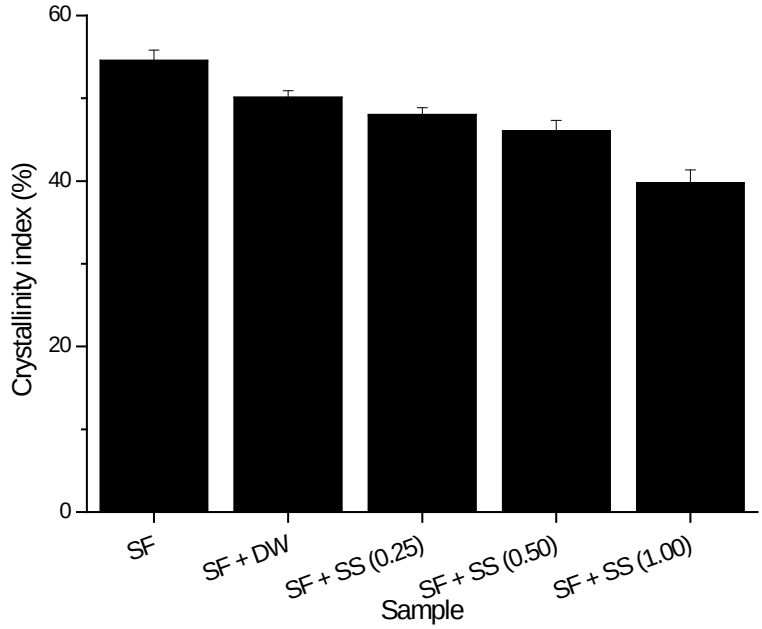

Figure 24. Effects of the SS concentration on the crystallinity index of the SF hydrogel prepared in phase separation conditions (n = 4).

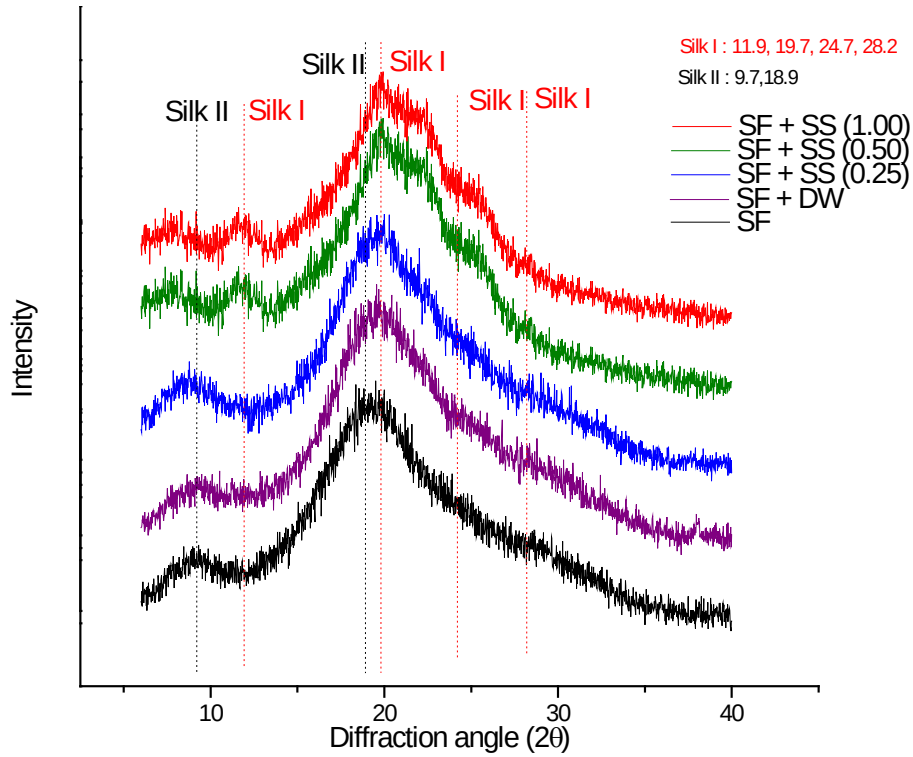

Figure 25. XRD patterns of SF phase separated from SS at various concentrations.

18.9° , indicating the formation of Silk II crystal structures. These peaks were almost the same as those of the β−sheet crystal structure of SF. This coincided with previous SF hydrogel results. However, in the case of the SF hydrogels prepared by phase separation with 0.5% and 1.0% SS, the diffraction peaks at 2θ values of 11.7° , 19.5° , 24.6° , and 28.7° were observed, indicating the typical Silk I structure in the SF hydrogels. Now, it was clear why the FT−IR results showed the unusual secondary structure composition of the SF hydrogels. According to previous studies, the Silk I structure is hard to detect with FT−IR. Mostly, it accompanies the increase in random coils and β−turn structures [100].

The Silk I structure is the typical structure of SF in the silk gland. The structural transformation from Silk I within the lumen of the gland to the oriented and water insoluble Silk II structure in the spun fiber is a well−recognized structural transition in SF. The reason that the highly concentrated SF solution is stable in the silk gland has been attributed to the silk I structure. The current results indicate that the Silk I structure can be developed in the presence of SS, even though they are phase separated. In other words, SS induces the Silk I structure in the middle gland. This is interesting behavior, because it is difficult to obtain the Silk I structure because of its metastability.

The compressive strength and modulus of SF hydrogels prepared in phase separation with different concentrations of SS are shown in

Figure 26. At the same SF concentrations, the mechanical properties of the SF hydrogel decreased with increasing concentrations of SS in the top layer. This also coincides with the secondary structure composition analysis by FT-IR. The increase in random coil structures might be responsible for the weak hydrogel strength. The degradation behavior of SF hydrogels was also significantly different from the initial state. The remaining mass of the lyophilized SF hydrogels in the PBS and α-chymotrypsin are shown in Figure 27. All SF hydrogels exhibiting either Silk I or Silk II structures were insoluble. However, the enzymatic degradation of SF hydrogels could be affected by the crystalline structure of SF hydrogels. It has been reported that α-chymotrypsin cannot degrade the Silk II crystalline region of SF [101], and thus, the degradation of SF hydrogel will be promoted only in the SF hydrogel having Silk I structure. In the case of pure SF hydrogels, an SF hydrogel prepared with phase separation with distilled water and 0.25% SS solution had greater stability against enzymatic degradation, indicating Silk II structure formation. On the other hand, SF hydrogels prepared with phase separated 0.50% and 1.0% SS were degraded with enzyme, indicating the existence of Silk I structures. This result supports the XRD data of SF hydrogels prepared with the phase-separated system.

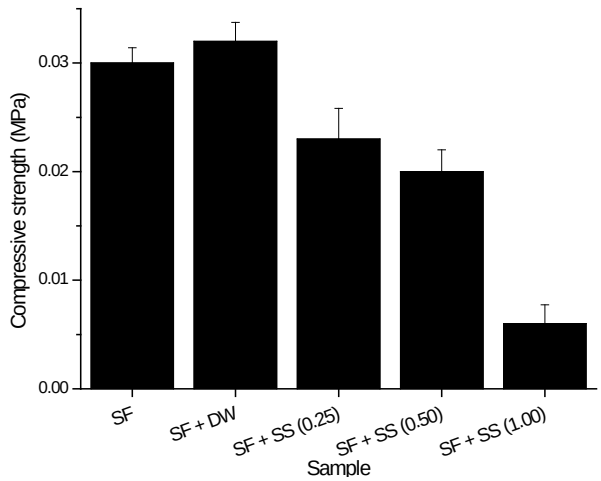

(a)

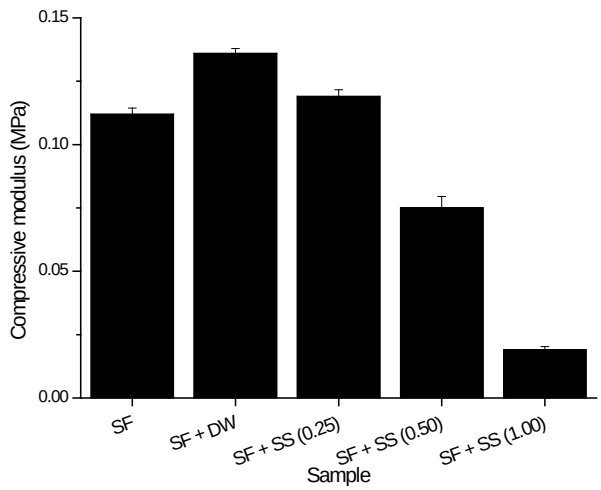

(b)

Figure 26. Mechanical properties of the SF hydrogel phase separated from SS at various concentrations. Compressive strength (a) and compressive modulus (b).

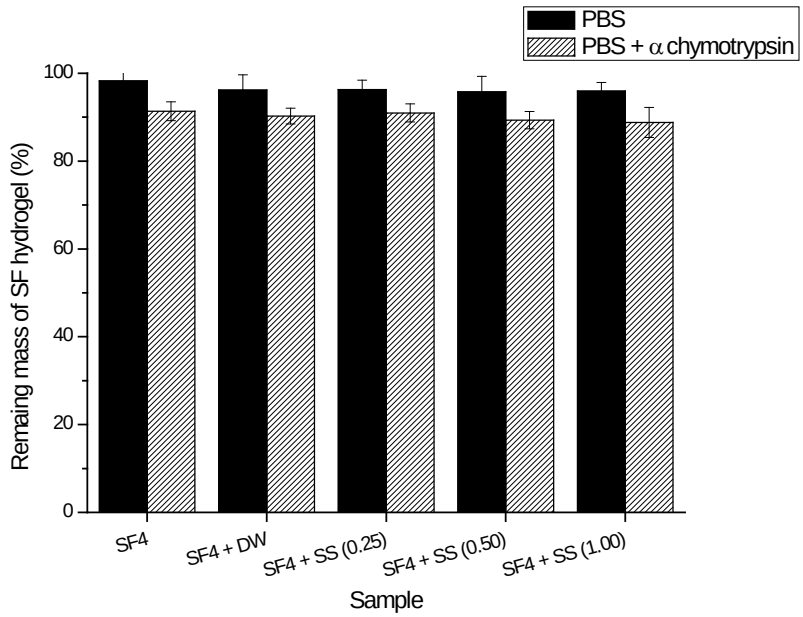

Figure 27. Dissolution and enzymatic degradation of SF phase separated with SS.

4.2.4. Secondary and crystalline structure of SF after aging

We obtained SF hydrogels that had the Silk I structure in macro phase separation conditions with aqueous SS solution. In the silkworm spinning process, Silk I structures are converted into Silk II structures. We further incubated the SF hydrogel prepared in phase separation with SS solutions for another 2 days with removal of upper SS layer and the resultant SF hydrogel was lyophilized. Figure 28 shows the FT-IR absorbance spectra and proportions of secondary structures in incubated SF hydrogels from deconvoluted results (Figure 29). These SF hydrogels all showed the β-sheet structure as the predominant secondary structure. The calculated crystallinity index of these SF hydrogels had similar values (Figure 30). Figure 31 shows the XRD diffraction of the incubated SF hydrogels. All SF hydrogels had similar β-sheet conformations with dominant Silk II crystalline structures, regardless of the preparation method. This indicates that further incubation of SF hydrogels allows Silk II structures to form.

4.2.5. Interaction between SF and SS in a phase-separated state

It can be concluded that SS in a macro phase separated state can stabilize the SF solution by preventing premature β-sheet

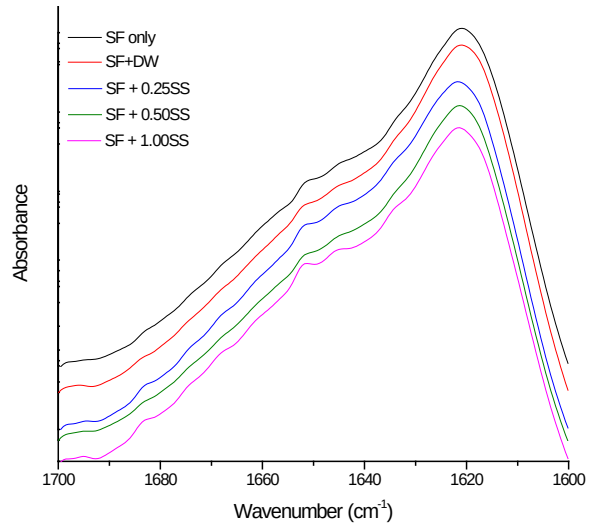

(a)

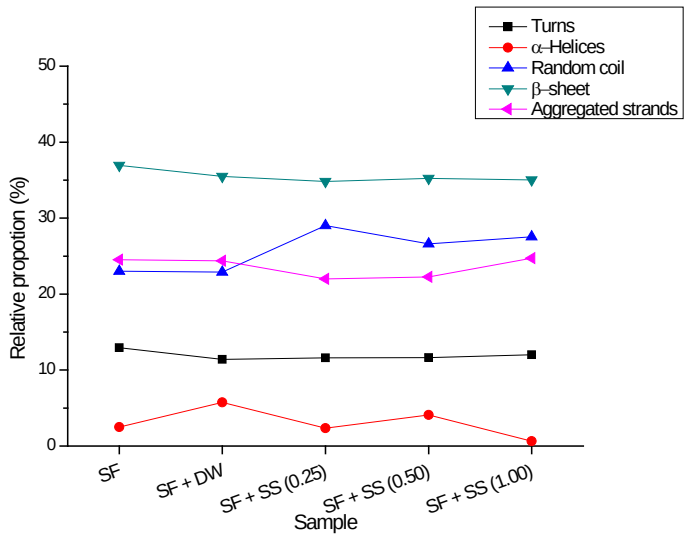

(b)

Figure 28. FT-IR spectra of SF phase separated from SS at various concentrations (a) and the SF secondary structure composition (b).

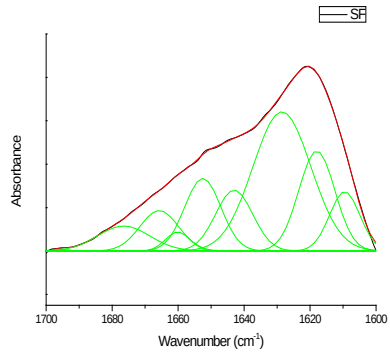

(a) SF

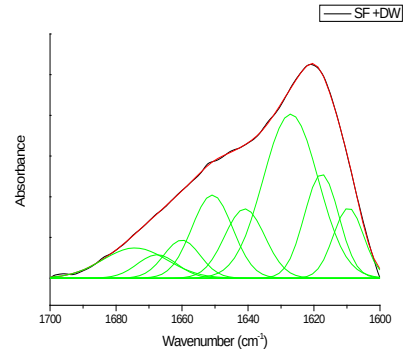

(b) SF + DW

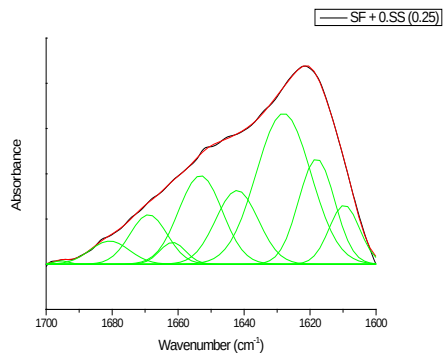

(c) SF + SS (0.25)

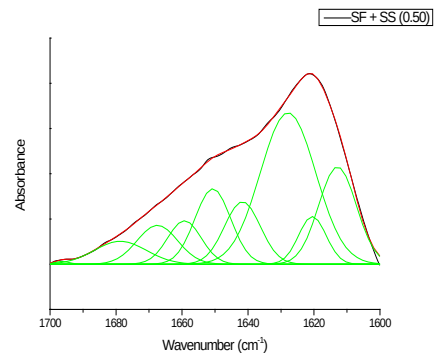

(d) SF + SS (0.50)

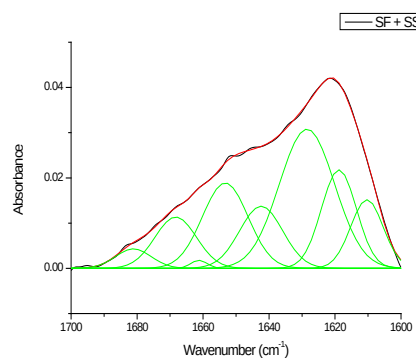

(e) SF + SS (1.00)

Figure 29. Deconvoluted FT-IR spectra of SF phase separated from SS at various concentrations. (a) SF, (b) SF + DW, (c) SF + SS (0.25), (d) SF + SS (0.50), and (e) SF + SS (1.00)

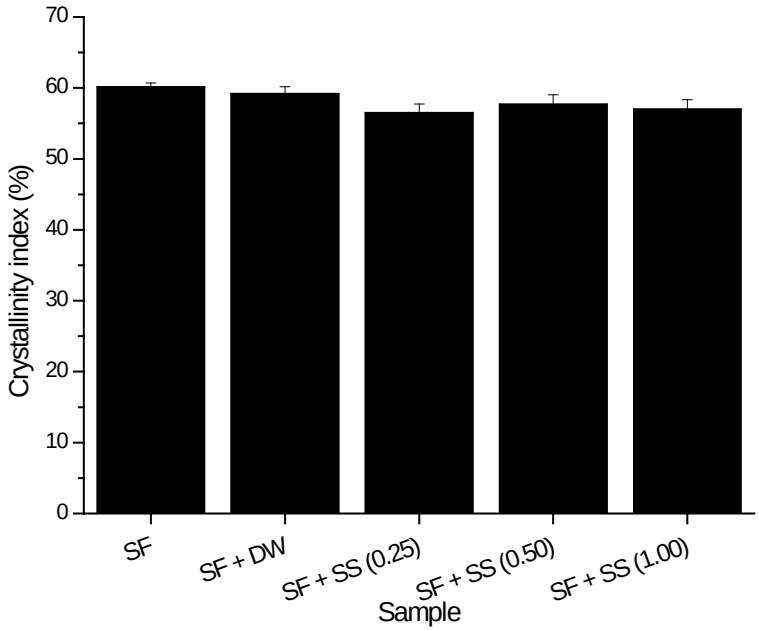

Figure 30. Effects of the SS concentration on the crystallinity index of an SF hydrogel prepared in phase separation conditions (n = 4).

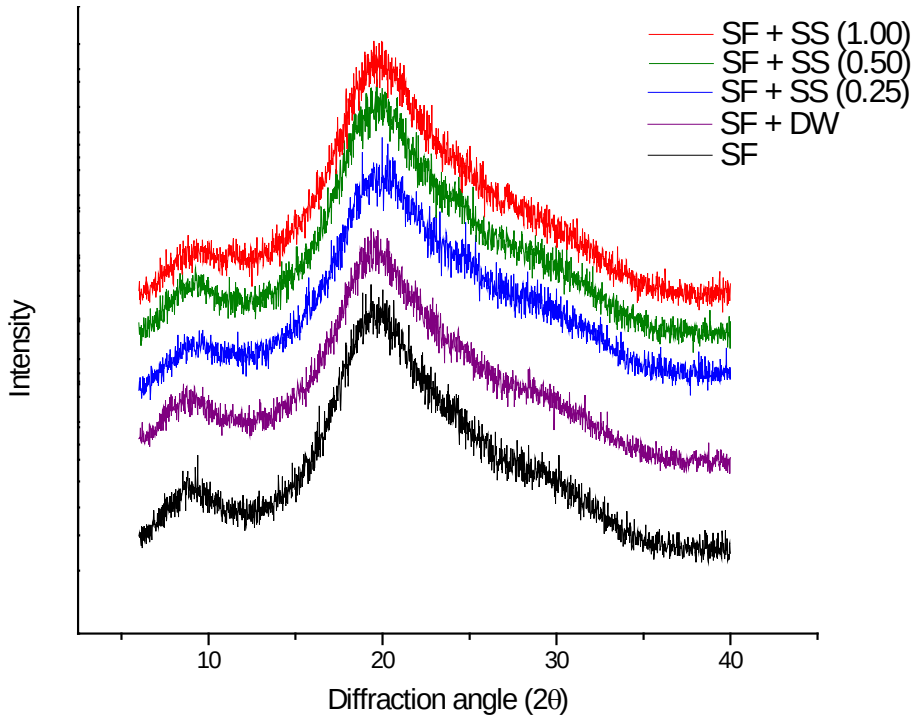

Figure 31. XRD patterns of SF phase separated SS at various concentrations.

formation over a certain SS concentration. This was observed by a delay in gelation, and by Silk I structure formation. So far, the role of SS during the process of silk spinning has not clear. Until now, its role was underestimated as simply working as lubricant. However, the current results indicate that SS can prevent premature crystallization and can induce Silk I structures in SF.

The concentration of SF in this study was far lower than the real concentration of SF in the silk gland. This was due to a sample preparation limitation. In the silk gland, the concentrations of SF and SS are approximately 24.3% (w/w) and 3.68% (w/w), respectively (Figure 32). However, greater than 1% SS solutions could not be prepared because of the gelation of SS during the dialysis. Therefore, the concentration of SF was set at a maximum of 8%, based on the concentration ratio between SF and SS in the silk gland. Although this experiment condition was different from the real situation in the silk gland, it should be noted that this is the first study to show the novel role of SS in the silk gland. The results clearly show that the presence of SS affects the structural transition of SF, even though it is phase separated. Moreover, SS induces a Silk I hydrogel from SF that resembles the crystal structure of SF in the middle silk gland.

The results clearly show that the presence of an SS layer induces the Silk I structure of SF hydrogels. We can deduce an interaction between SS and SF at the interface. Unfortunately, due to limited analysis techniques, it is difficult to identify the SS and SF

interaction at the interface. However, there are several reports that suggest some interaction between SS and SF. Lee [11] has reported retardation of SF crystallization in the presence of SS in films. Ki et al. [65] reported the effect of SS on the secondary structure of SF during wet spinning, and Hang et al. [67] suggested some interaction between SS and SF during co-axial electrospinning. These findings indicate that SS can affect the structural transition of SF at the interface. Based on current and former results, the following mechanism is suggested for the development of Silk I structures from SF in the presence of SS. It has been reported that the gelation of SF results from the conformational transition from random coil to β-sheet structures [102]. During this process, the hydrophobic part of SF, which consists of repeated sequences, will start to agglomerate in order to avoid an unfavorable aqueous environment. The process will continue until they find the most thermodynamically stable state by self-assembling into a β-sheet structure, which will act as a physical cross-linker in the SF hydrogel. However, the interaction between SF and SS at the interface may affect the self-assembly of SF. THt fluorescence developed only when beta-amyloid structures were formed. This suggests that SF at low concentration has alternating stacking of hydrophobic and repeated sequences, which resemble a β-amyloid structure. If one of the β-strands of SF interacts with another sequence of SS, which is also capable for β-strand formation, the whole SF structure could be affected. This type of intervention by structure can be observed in other self-

assembling peptides. The Stupp group has studied the self-assembly of peptide-amphiphiles and found that the β-sheet-stabilized self-assembly could only be found when the sequence was maintained [103]. Therefore, a slight disruption in the hydrogen-bonding pattern caused by SS may alter the structure of SF. Here, the alteration in SF structure resulted from the formation of Silk I instead of Silk II. The Silk I structure of SF was converted into a Silk II structure when the upper SS layer was removed. This also strongly supports the possibility of interaction between SF and SS. Since the SS was removed, there was no molecule to interfere with the self-assembly of SF. The proposed overall mechanism is presented in Figure 32.

4.3. Effect of metal ion in the phase separated SF and SS

4.3.1. Concentration of SF and SS in the middle division of silk gland

From the literature survey, it is clear that differences in the metal ion concentration in the silk gland significantly affect the conformational states of SF. However, the changes in metal concentration in SF cannot be explained without the outer SS layer. Since SF is surrounded by the SS layer, any metal ions must pass through the SS layer. To date, there have been no studies on

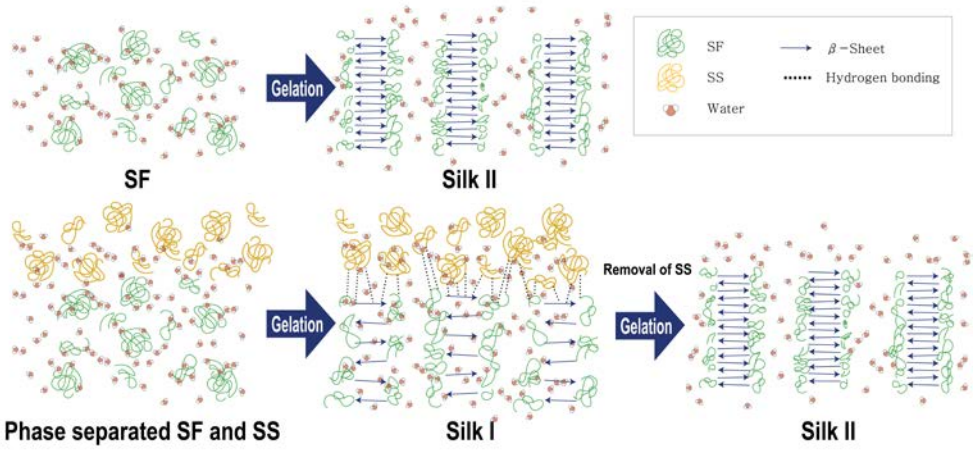

Figure 32. Schematic of the effect of phase separated SS on the conformational transition of SF.

differences in the metal concentration in SF solution in the presence of an SS layer. We checked the metal concentration changes before and after spinning. To determine the metal ion concentration to the total amount of silk protein in the silk gland, SF and SS metal concentrations were investigated. Figure 33 shows the composition of three parts of the middle division of the silkworm gland. From the posterior part of the middle gland to the anterior part of the middle gland, the concentrations of both SF and SS increased. The total silk protein concentration increased from 19.62% (w/w) in the posterior part of the middle gland to 29.4% in the anterior part of the middle gland. The concentration of SS increased gradually from 2.37% in the posterior part of the middle gland to 5.60% in the anterior part of the middle gland. This increase in SS concentration might be due to the secretion of s-1 or s-2 protein, which are synthesized and secreted in the middle and anterior parts of the middle gland, respectively [32].

4.3.2. Metal content in the Bombyx mori silk gland and silk fibers

Metal ions have an important role in the structural transition behavior of SF. Depending on the type of metal ion, SF can bind with these ions, and this often induces a conformational transition in SF from a random coil to a β-sheet structure. First, the metal concentrations in the silk gland and the fiber were investigated to show the overall changes in metal ion concentration during the

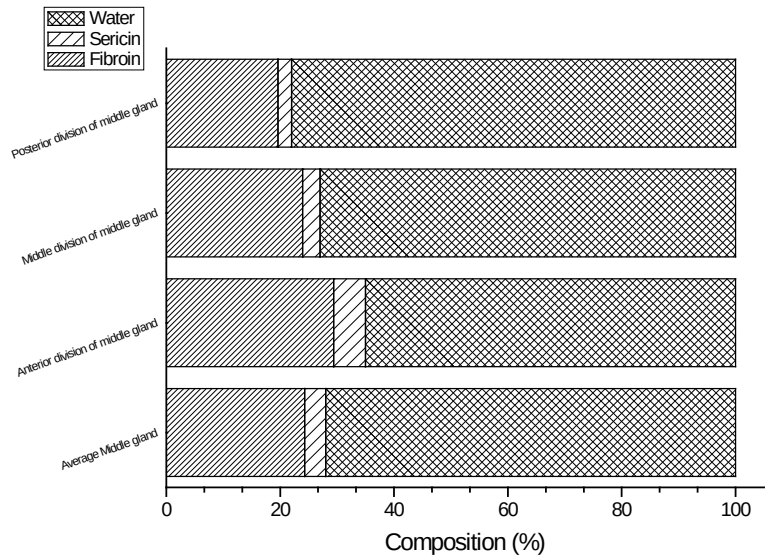

Figure 33. Composition of the middle division of the silk gland in silkworms.

spinning process.

To determine tiny amounts of metal species, an ion coupled plasma atomic emission spectrometer (ICP-AES), ICP mass spectrometer, and particle induced X-ray emission (PIXE) are frequently adopted. Among these instruments, ICP-AES was chosen for this study because it can analyze not only the transitional metal but also the alkaline and alkaline earth metals. In addition, due to the light atomic mass of Li and Na, detection of these metal species is difficult in both ICP-MS and PIXE analyses. For this reason, the metal element contents in the silk gland and fibers were investigated using ICP-AES.

Table 1 shows the concentration of metal ions in the silk gland and the fiber. K^+ and Ca^{2+} were the most abundant metal species in both the gland and fiber. Metal element contents in the silk gland were higher than that in the silk fiber, except for Cu^{2+} ions. These metal concentrations corroborate previous results [68]. These results were used as a reference in the following sections.

4.3.3. Metal ion diffusion behavior and its effect on SF gelation

If there is any change in metal concentration in the silk gland, the metal should be taken up or removed by the cells of the silk gland by either active or passive routes. However, the cells are not

Table.1 Comparison of metal element concentration (μg/g) in silk gland and *Bombyx mori* silk fiber.

Metal species	Silk gland	Silk fiber
Na^+	170.48 ± 3.45	106.96 ± 6.76
K^+	3807.63 ± 70.48	2795.73 ± 50.42
Li^+	4.73 ± 1.48	3.18 ± 1.54
Ca^{2+}	2704.70 ± 37.49	1724.08 ± 70.34
Cu^{2+}	147.68 ± 14.77	228.01 ± 10.64

indirect contact with SF. Any metal ion that is supplied or removed must pass through the SS layer. If the metal ion increases, it was secreted from the silk gland cells and passed through the SS layer to reach SF. Once the metal ion is released from the cell, it will diffuse along a concentration gradient. However, if the metal ion has a higher affinity for SS rather than SF, the metal will not diffuse properly and much higher amount of the metal ion will need to be released to promote the diffusion. Currently it is not certain whether the cells of the silk gland have such functionality and this is out of the scope of the current thesis. However, the binding affinity of specific metals for SF and SS can be investigated. In this study, the binding affinity of each metal ion (Li^+, Na^+, K^+, Ca^{2+}, and Cu^{2+}) with SF in the presence of SS layer was determined. For this, two different experimental designs were adopted. First, the diffusion of metal ions between distilled water and SF were investigated. Here, distilled water was carefully loaded onto the SF solution in order not to disturb the interface. Second, the diffusion of metal ions between SS and SF in a phase-separated system was tested, without using any barrier materials between the two protein solution layers. In each experiments, 4000 μg of metal ion was added only in one phase and the amount of metal ion that diffused was observed. The amount of each metal ion was fixed at 4000 μg, because concentrations above this amount induced the gelation of both SF and SS. The purpose of this study was to investigation the metal ion diffusion behavior between SF and SS in a liquid state. Therefore, the amount of each metal ion was fixed to 4000 μg to

prevent the gelation of each silk protein solution.

To determine the effect of the ion diffusion behavior between SF and SS on the gelation behavior of SF, various concentrations of metal ions (0, 1, 10, and 100 mM) were added into the SF or SS layer and the gelation kinetics of SF were investigated. In the case of the gelation experiment, for comparisons with other studies that measured the gelation of protein solutions with various metal ions, various concentrations of metal ions (0, 1, 10, and 100 mM) were added into the SF or SS layer.

4.3.3.1. Effect of Na^+

The alkali metals, represented by Na^+ and K^+, influenced the conformational transition of SF. Ruan et al. [104] investigated the effect of Na^+ ions on the conformational composition of SF. At low concentration of Na^+ (below 11.2 mg/g), there was no change in the conformational transition, but at concentrations above this, the amount of Silk II conformation increased. The concentration range that affected the conformational transition of SF was 11.8 to 37.5 mg/g. However, Na^+ ions in the middle silk gland and silk fiber existed only at 170 and 106 μg/g (Table 1), which is far less than our experimental result. Previous research did not determine the real effect of Na^+ on the SF conformational transition. In this study, I first examined the Na^+ diffusion behavior between the distilled water and SF. Figure 34 shows the amount of Na^+ ion that diffused

into the distilled water and blank SF solution from Na^+ containing SF solution and Na^+ containing distilled water, respectively. Since the amount of metal ion was fixed at 4000 μg, if the amount of ion reached to 2000 μg, it meant the system has reached to its equilibrium without any effect on SF or SS. In Figure 34 (a), the amount of Na^+ that diffused from the SF into the distilled water was only 515 μg (12.8% of the total Na^+). On the other hand, 1690 μg of Na^+ (42.25% of the total Na^+) diffused from the distilled water into SF solution (Figure 34 (b)). This indicates that the diffusion of Na^+ from SF to distilled water did not follow the concentration gradient, while in the opposite direction it reached equilibrium. SF molecules might have a binding affinity with Na^+ ions that limited the diffusion. Figure 35 shows the amount of Na^+ ion that diffused when the SF and SS layers were phase separated. From SF to SS, 1742 μg (43.5% of the total) of Na^+ ion diffused and only 682 μg diffused in the opposite direction. The inflow of Na^+ ions into SS was feasible, while the outflow of this ion from SS was suppressed. This result indicates that that SS layer acts as a barrier for Na^+ diffusion.

To investigate the effect of Na^+ concentration and diffusion behavior on the gelation kinetics of SF, the gelation behavior of SF was observed by a change in the optical density of the SF solution. Figure 36 shows the relative gelation kinetics and gelation time of SF containing various amounts of Na^+ ions in the absence or

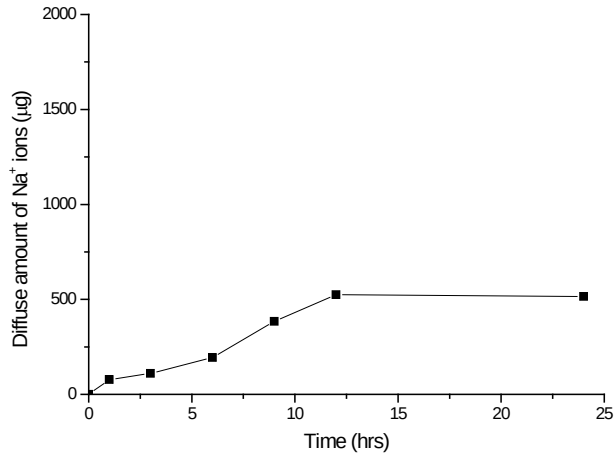

(a)

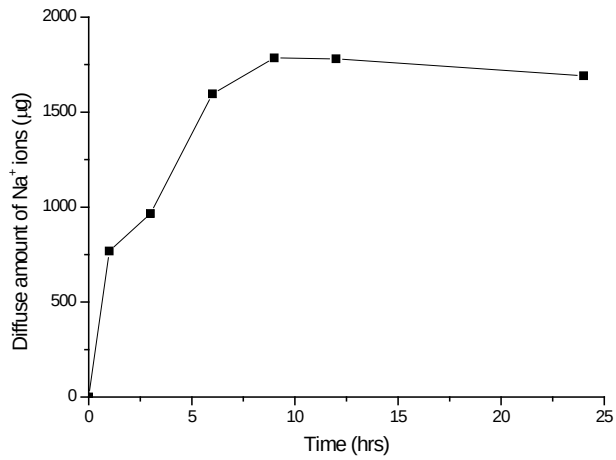

(b)

Figure 34. Amount of Na^+ that diffused into distilled water (a) and blank SF solution (b) from an Na^+-containing SF solution and Na^+-containing distilled water, respectively.

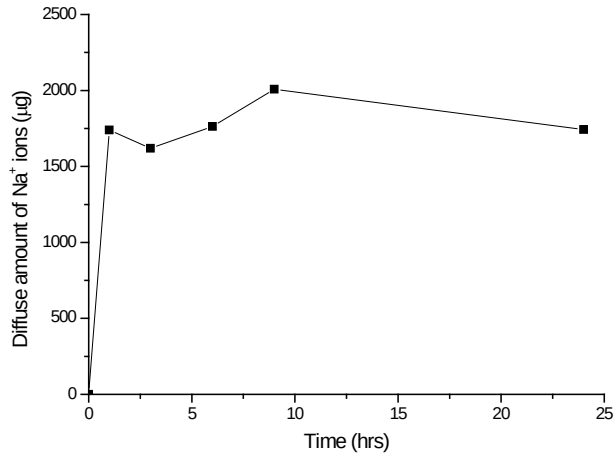

(a)

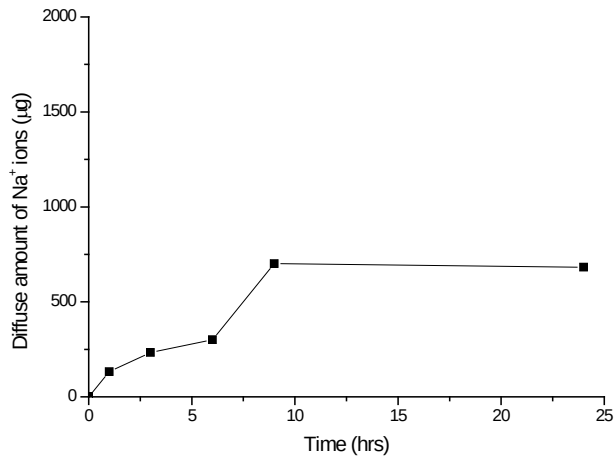

(b)

Figure 35. Amount of Na^+ that diffused into the SS solution (a) and blank SF solution (b) from an Na^+-containing SF solution and Na^+-containing SS solution, respectively.

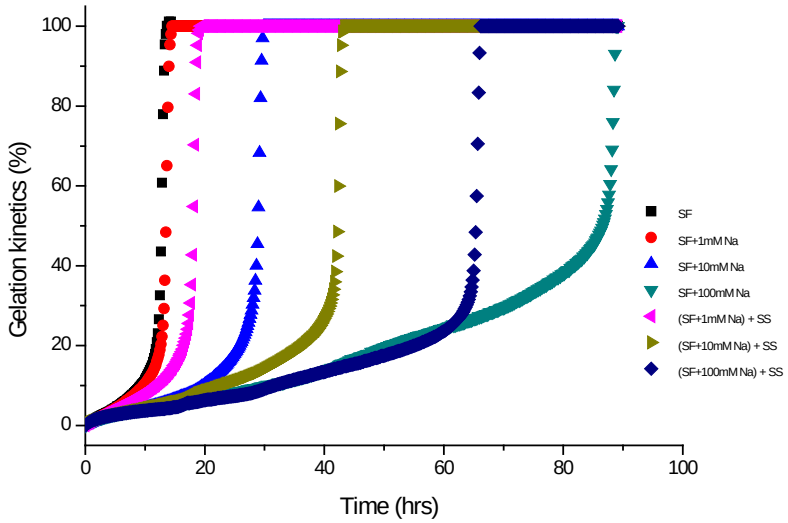

(a)

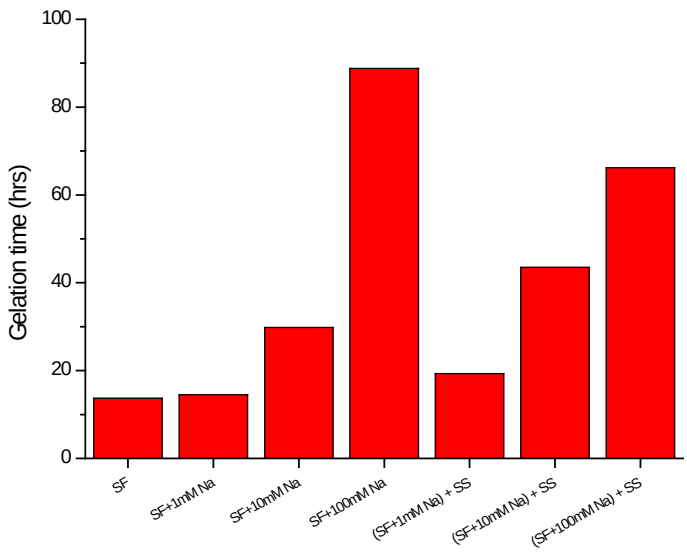

(b)

Figure 36. Relative gelation kinetics and gelation time of SF with various amounts of Na^+ ions in the presence or absence of phase-separated SS.

presence of phase-separated SS. A 1 mM concentration of Na^+ was found to have no significant effect on the gelation behavior of SF. The gelation time of SF without Na^+ and with 1 mM Na^+ was 13.6 and 14.5 h, respectively. However, when SS were presented, the same SF solution containing 1 mM Na^+ showed a delay in gelation by 19.33 h. This indicates that the gelation of SF was delayed in the presence of a phase-separated SS solution. The same tendency was observed when 10 mM Na^+ was added to the SF solution. An increase in Na^+ in the SF solution increased the gelation time up to 29.82 h, and it was even more increased (to 43.5 h) in the presence of a separated SS layer. However, when 100 mM Na^+ was added, the effect of the phase-separated SS layer was less significant. Without the SS layer on the top, the gelation time was 88.83 h, while it decreased to 66.16 h in the presence of the SS layer. The proportional increase in the gelation time of the SF solution with the increase in Na^+ concentration can be explained by the salting-in effect. As the amount of Na^+ increases, the protein-protein interactions will be reduced, which results in delayed self-assembly of SF molecules. In the presence of the SS layer, the Na^+ will diffuse from SF into SS and, thereby, the real concentration of Na^+ in the SF solution will be decreased. This will shorten the gelation time but the presence of the SS layer increased the gelation time even more. This indicates that the delay in SF gelation is much more affected by the presence of SS than the Na^+ concentration. However, when the Na^+ concentration was greater such as 100 mM, the SF gelation time in the presence of the SS

layer decreased. In this case, the effect of the Na^+ surpassed the effect of the SS layer.

Figure 37 shows the SF gelation kinetics and gelation time of the SF solution when Na^+ was added only in the upper SS layer. Since SS inhibits the diffusion of Na^+ into SF, there was a limited effect on the SF gelation time by Na^+ when the Na^+ concentration was less than 10 mM. However, when the Na^+ concentration reached 100 mM in the SS layer, Na^+ diffused into SF and delayed its gelation.

It can be concluded that the gelation time of SF can be increased in the presence of Na^+ and an SS layer, and that this increase is Na^+ concentration dependent. When the Na^+ concentration is low, the SS layer has a more significant effect, but when the Na^+ concentration is higher than some critical level, it is the dominant factor in the delay of SF gelation.

4.3.3.2. Effect of K^+

K^+ ions were the most abundant metal ions in both of the silk fibers and the middle part of the silk gland (Table 1). K^+ ions in the middle silk gland and silk fibers existed in concentrations of 3807 and 2795 μg/g, respectively. Figure 38 (a) and (b) show the amount of K^+ diffusion into distilled water and blank SF solution from a K^+−containing SF solution and K^+−containing distilled water,

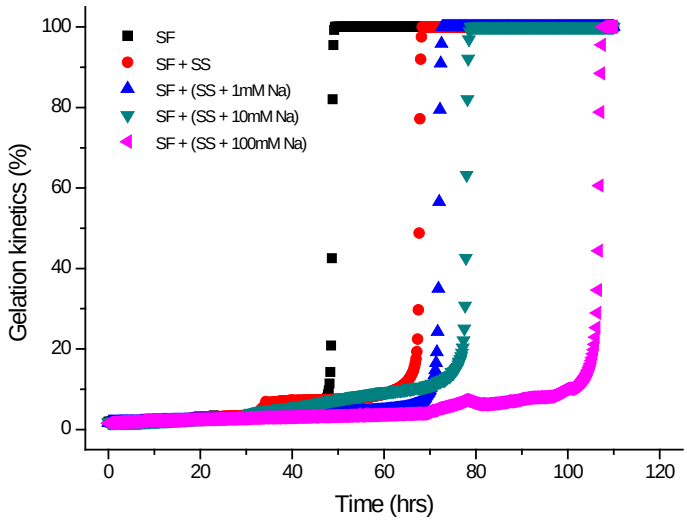

(a)

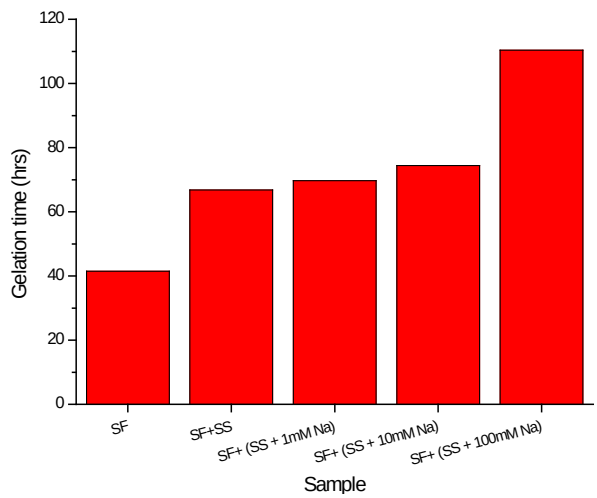

(b)

Figure 37. Relative gelation kinetics and gelation time of SF in the presence of phase-separated SS with various amounts of Na^+ ions.

respectively. The amount of K^+ that diffused from SF into distilled water was only 669 μg (16.7% of the total K^+), whereas the amount that diffused from distilled water into SF was 1867 μg (46.7% of the total K^+). Similar to Na^+, this also indicates that K^+ might have a binding affinity with SF molecules. Figure 39 shows the result of the experiment of phase-separated SF and SS. Here, SF had a higher binding affinity with K^+ ions, with only 630 μg of K^+ diffusing into the SS layer, while 1839 μg of K^+ entered the SF layers. From both ion diffusion experiments, it can be concluded that SF has a higher affinity for K^+ than SS.

The gelation kinetics and gelation time of SF containing various concentrations of K^+ ions in the absence or presence of phase-separated SS solutions are shown in Figure 40. The SF gelation time increased as the concentration of K^+ increased. The SF gelation time without K^+ ions was 12.6 h, while the SF gelation time increase to 15.3 h, 25.3 h, 111.3 h as the K^+ concentrations in the SF solution increased to 1 mM, 10 mM, and 100 mM, respectively. Unlike Na^+, the presence of the SS layer was not significant, only slightly increasing the gelation time from 15.3 h to 17.3 h when 1 mM K^+ was present in the SF solution. It is clear that K^+ increased the gelation time as its concentration increased. Although the diffusion of K^+ from SF is less significant than of Na^+, the real concentration in the SF layer would be less than the initial concentration in the presence of the SS layer. This would cause acceleration in the gelation time; however, the gelation time only

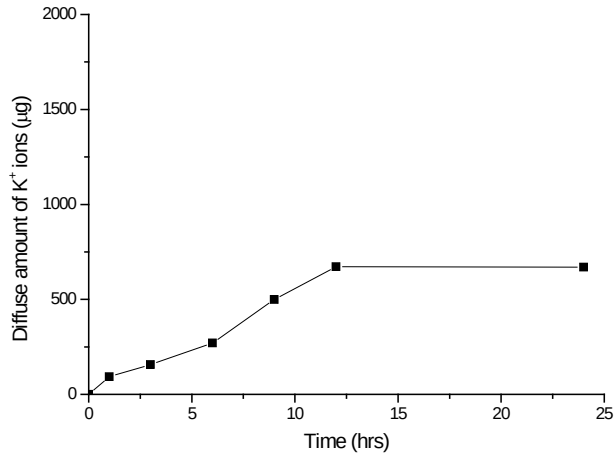

(a)

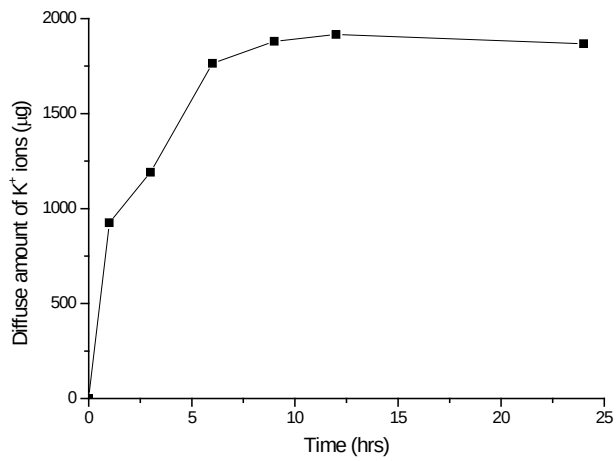

(b)

Figure 38. Amount of K^+ that diffused into distilled water (a) and blank SF solution (b) from a K^+-containing SF solution and K^+-containing distilled water, respectively.

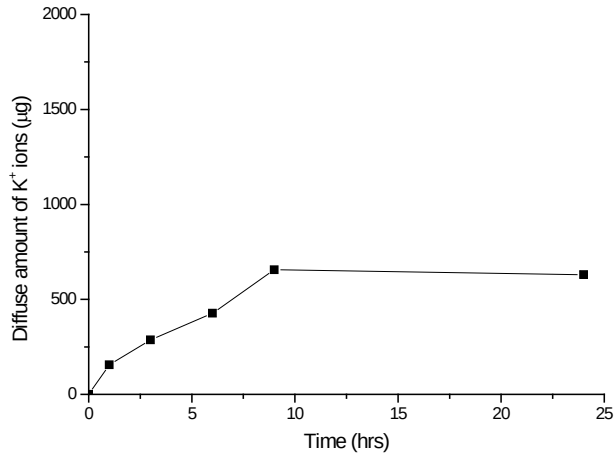

(a)

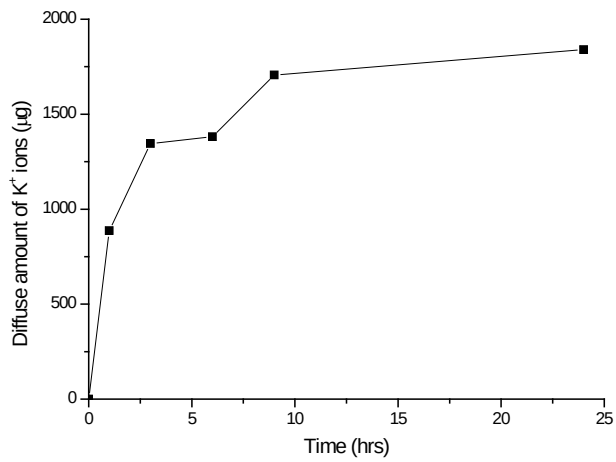

(b)

Figure 39. Amount of K^+ that diffused into SS solution (a) and blank SF solution (b) from a K^+-containing SF solution and K^+ containing SS solution, respectively.

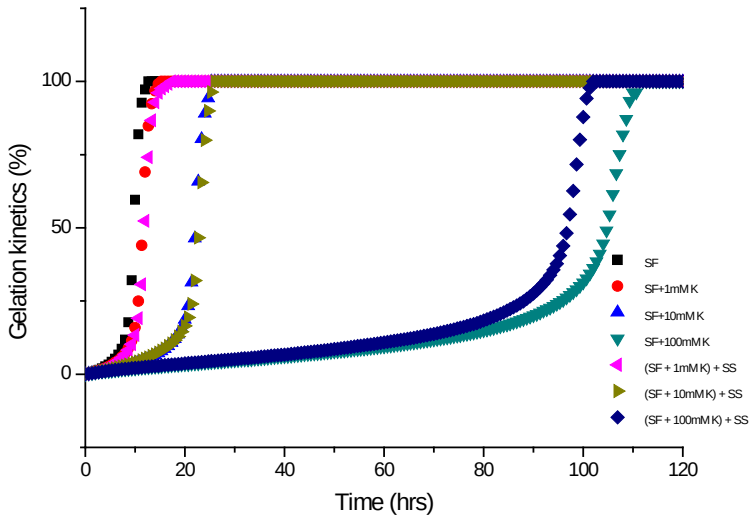

(a)

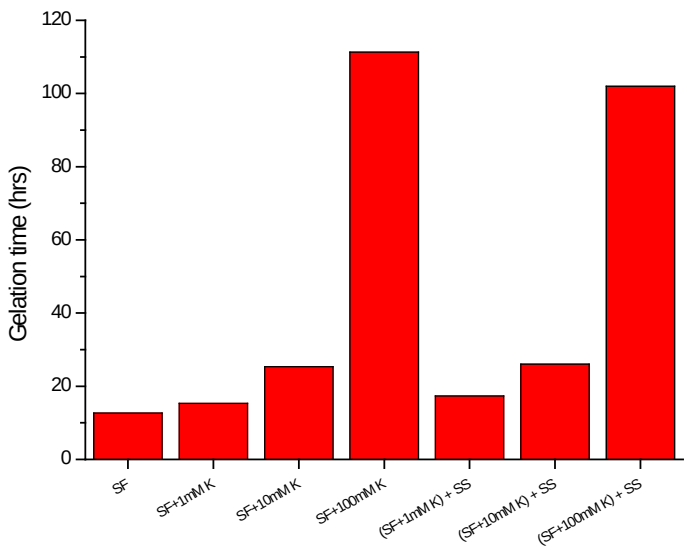

(b)

Figure 40. Relative gelation kinetics and gelation time of SF with various amounts of K^+ ions in the presence or absence of phase-separated SS.

slightly increased in the presence of the SS layer. This revealed that the presence of the SS layer increased the SF gelation time. The decreased gelation time at a 100 mM K^+ concentration can be explained by a high salting-in effect as in the case of Na^+. The effect of K^+ was more significant than the presence of the SS layer.

In the case of K^+ diffusion from SS to SF (Figure 41), the gelation time with K^+ ions increased as the K^+ concentration in the SS solution increased, except with 1 mM K^+ in the SS layer. In the case of 1 mM K^+ in the SS layer, there was no delaying effect compared to SS solution without K^+ ions. This can be explained by the real concentration of K^+ in SF. Even though a significant amount of K^+ diffuses into SF from SS (Figure 39, (b)), the real concentration of K^+ was not higher than the initial concentration of the SS layer. Therefore, the real concentration of K^+ in the SF solution was less than 1 mM, resulting in limited effects on the gelation delay.

Ruan et al. suggested that the K^+ ions can induce SF β-sheet formation, depending on its concentration [105]. The tyrosyl group of SF palindrome sequences such as VGYG and GYGV can be exposed to either hydrophilic or hydrophobic environments, depending on the concentration of K^+. At a low K^+ concentration, this sequence is exposed to a hydrophobic environment where α-helices are favored. With an increase in K^+ concentration, the sequence will be exposed to a hydrophilic environment, where hydrogen-bonding interactions with the phenolic hydroxyl group are possible. In this state, these sequences are available for

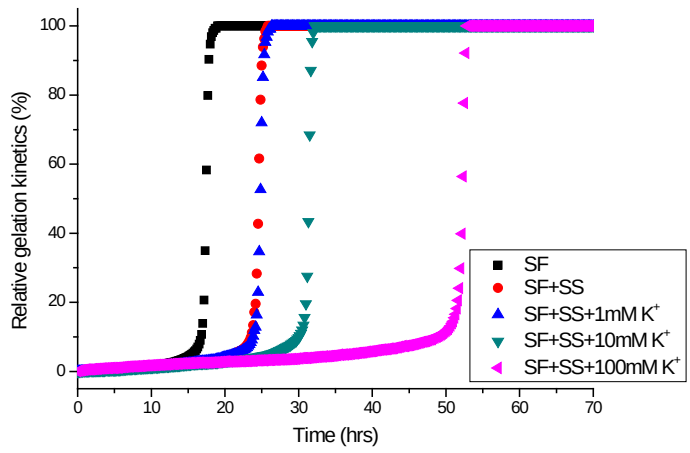

(a)

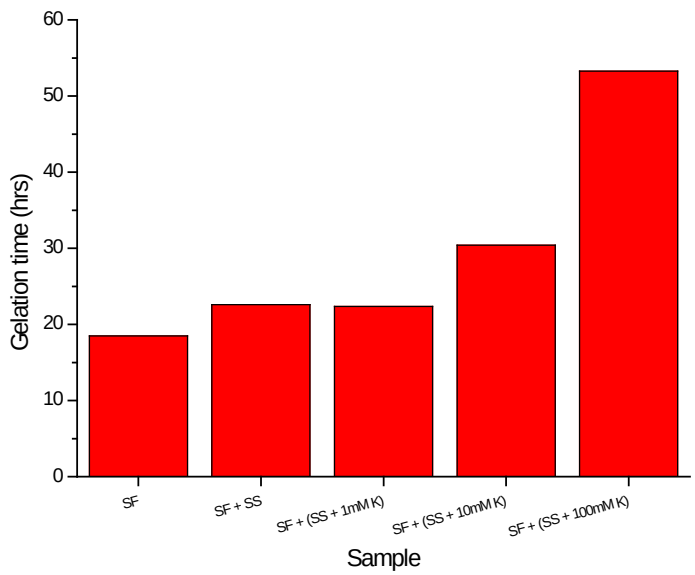

(b)

Figure 41. Relative gelation kinetics and gelation time of SF in the presence of phase-separated SS with various amounts of K^+ ions.

hydrogen bonding as a proton acceptor and can lead to β−sheet formation. However, further increases in K^+ will lead to a chaotropic effect, in which β−sheet formation is not favored. The K^+ concentrations that favored β−sheet formation were up to 3700 μg/g from the Ruan's study. However, in the current study, the concentration of K^+ was 977 μg/g which corresponding to the case of 1 mM K^+. Therefore, when the K^+ concentration was 1 mM, it was too low to induce β−sheet formation. At 10 mM K^+, it was too high for β−sheet formation. Therefore, no gelation acceleration effect could be found in this study.

4.3.3.3. Effect of Li^+

Li^+ is the lightest metal and the least dense element. Lithium salt has been used widely in the silk protein dissolving process. Since a LiBr/water solvent system was introduced by Weimarn, most researchers have regenerated aqueous silk solutions using this system [106]. It was interesting that, in addition to Na^+ and K^+ discussed above, trace amounts of Li^+ were also detected in the silk gland and fibers (Table 1). Figure 42 shows the amount of Li^+ ions that diffused into distilled water and blank SF solution from an Li^+−containing SF solution and Li^+−containing distilled water. It was found that 525 μg (13.1% of the total amount of Li^+ ions) and 1611 μg (40.3% of the total amount of Li^+ ions) diffused into distilled water and SF solution from SF and distilled water, respectively,

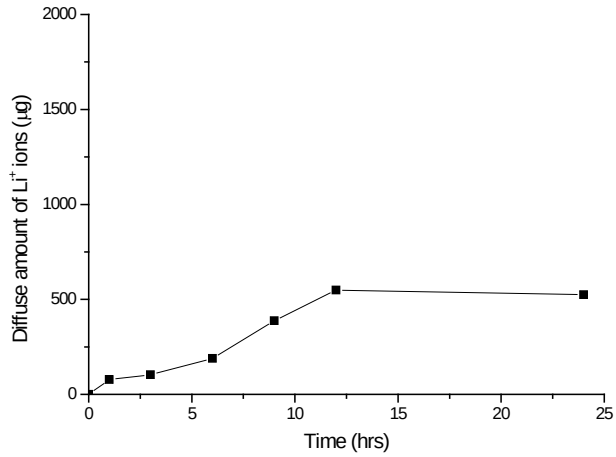

(a)

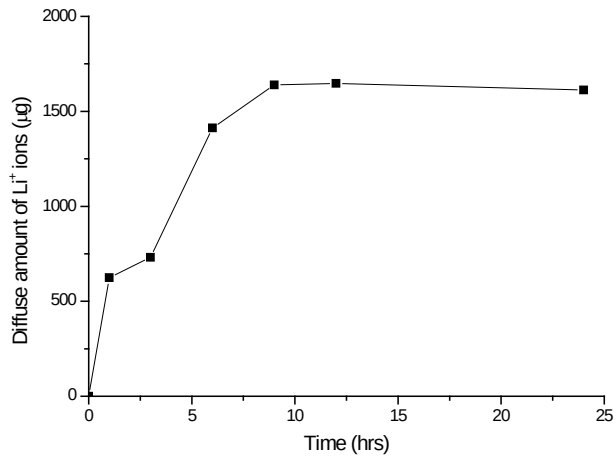

(b)

Figure 42. Amount of Li^+ that diffused into distilled water (a) and blank SF solution (b) from an Li^+-containing SF solution and Li^+-containing distilled water, respectively.

indicating binding of Li^+ with SF molecules, similar to Na^+ and K^+. In the macro phase-separated condition, the amount of diffused Li^+ ions was higher in the case of diffusion from the SS to SF solution (Figure 43). The amount of diffused Li^+ was less than that in the K^+ ion experiment, which means that the binding affinity of SF with Li^+ was less than that with K^+.

The gelation kinetics and gelation time of SF containing various amounts of Li^+ ion with or without phase-separated SS solution is shown in Figure 44. The gelation time of the SF solution increased as the concentration of Li^+ increased. In the case of 1 and 10 mM Li^+-containing SF solutions, significant gelation retardation was observed when the phase-separated SS solution was on top of the SF solution. This could be explained by a synergy stabilization effect of Li^+ ions and SS solution. This synergy effect was eliminated in the case of 100 mM Li^+ ions, because the Li^+ salting-in was affected more by the presence of the SS layer.

The gelation time of the SF solution in the presence of a phase-separated SS layer containing various amounts of Li^+ are shown in Figure 45. While the gelation time of SF and SF with a 1 and 10 mM Li^+-containing SS solution showed similar gelation times (41.72 h, 43.14 h, and 43.76 h, respectively), a 100 mM Li^+-containing SS solution slowed the gelation of SF significantly due to the salting-in effect.

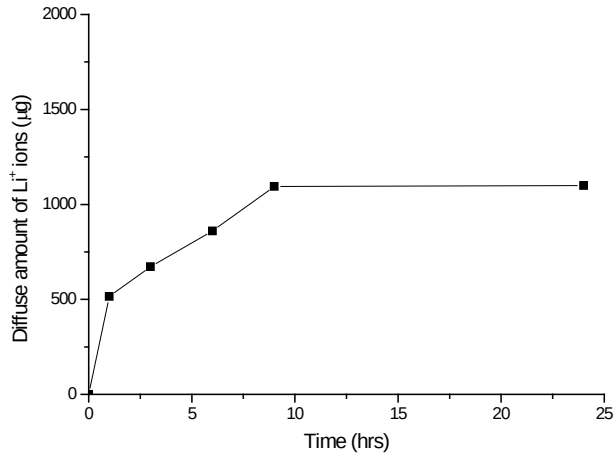

(a)

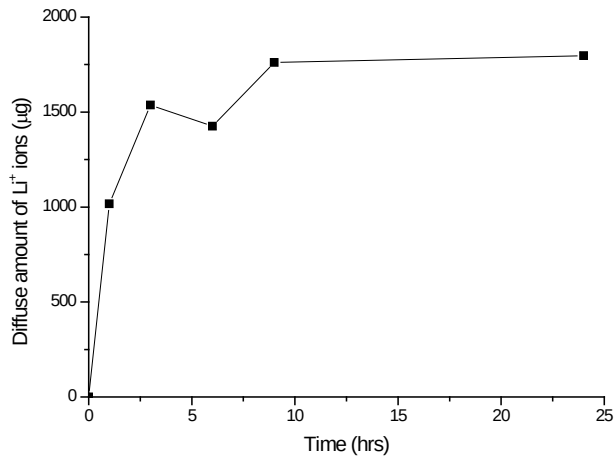

(b)

Figure 43. Amount of Li^+ that diffused into the SS solution (a) and blank SF solution (b) from an Li^+-containing SF solution and Li^+ containing SS solution, respectively.

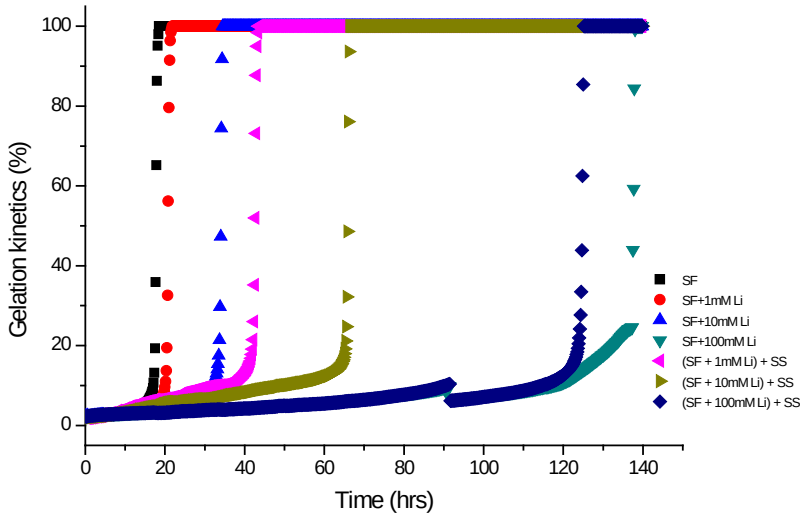

(a)

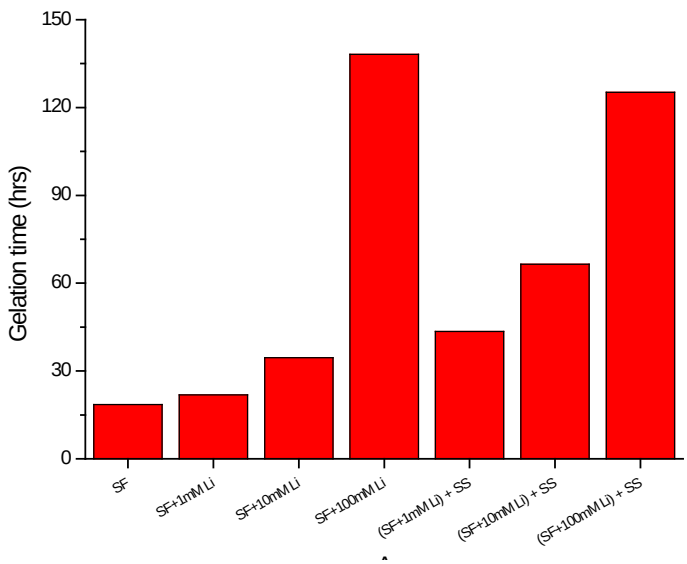

(b)

Figure 44. Relative gelation kinetics and gelation time of SF with various amounts of Li^+ ions in the presence or absence of phase-separated SS.

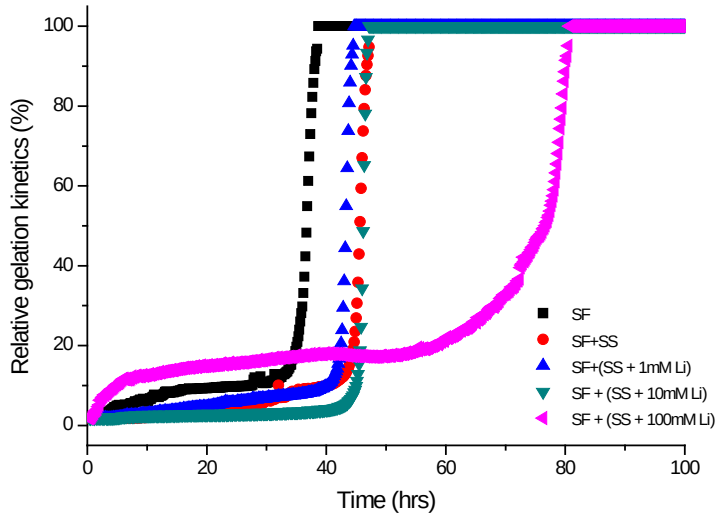

(a)

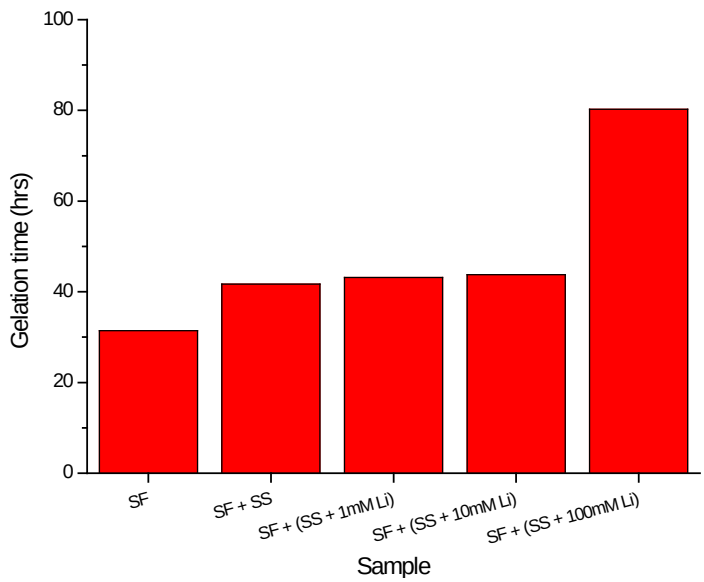

(b)

Figure 45. Relative gelation kinetics and gelation time of SF in the presence of phase-separated SS with various amounts of Li^+ ions.

4.3.3.4. Effect of Ca^{2+}

Alkaline earth metals are also known to affect the structural transition of many proteins. Since the alkaline earth metals are divalent ions, their interaction with proteins differs from those of alkaline monovalent metal ions. Ca^{2+} is the second most abundant metal ion species in silk glands (2704 μg/g) and fiber (1724 μg/g) (Table 1.). The interaction between SF and Ca^{2+} ions has been studied by many researchers. Zhou et al. investigated the influence of Ca^{2+} ions and pH on the conformational transition of SF using Raman spectroscopy and ^{13}C cross polarization magic angle spinning (CP/MAS) solid state NMR. [107]. At low pH and with a certain amount of Ca^{2+} ions, the formation of β-sheet structures was induced. Higher amount of calcium ions prevented the formation of β-sheet structures because of strong electrostatic interaction between molecular chains.

Figure 46 shows amount of Ca^{2+} ion that diffused into distilled water and blank SF solution from a Ca^{2+}-containing SF solution and Ca^{2+}-containing distilled water. The amount of Ca^{2+} that diffused from SF to distilled water was only 332 μg (8.3% of the total Ca^{2+}), while 1652 μg of Ca^{2+} (41.3% of the total Ca^{2+}) diffused into SF solution from the distilled water. In a macro phase separation between SF and SS, more Ca^{2+} diffused from SS to SF than in the opposite direction (Figure 47). Similar to K^+ and Li^+, SF has a higher affinity with Ca^{2+} than SS. Yang et al. investigated the binding ability of SS by monitoring the formation of turbid calcium

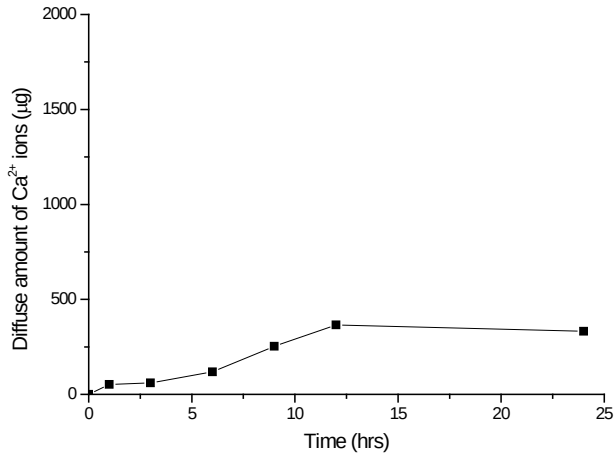

(a)

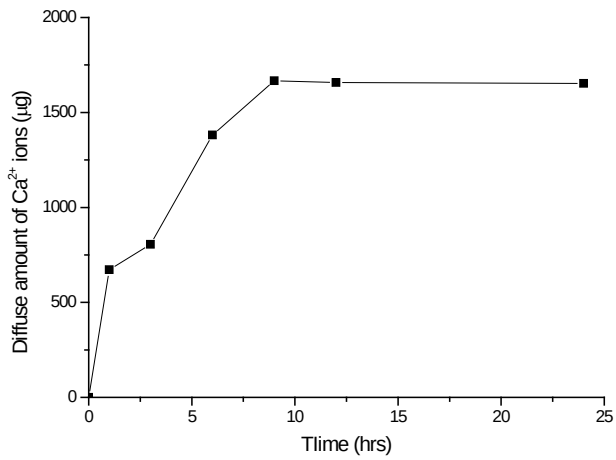

(b)

Figure 46. Amount of Ca^{2+} that diffused into distilled water (a) and blank SF solution (b) from a Ca^{2+}-containing SF solution and Ca^{2+} containing distilled water, respectively.

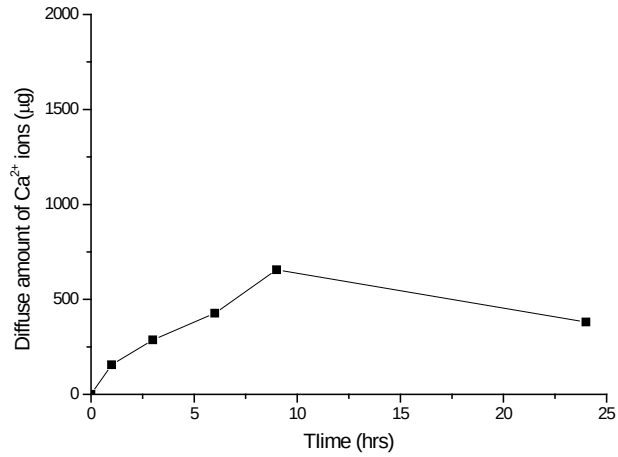

(a)

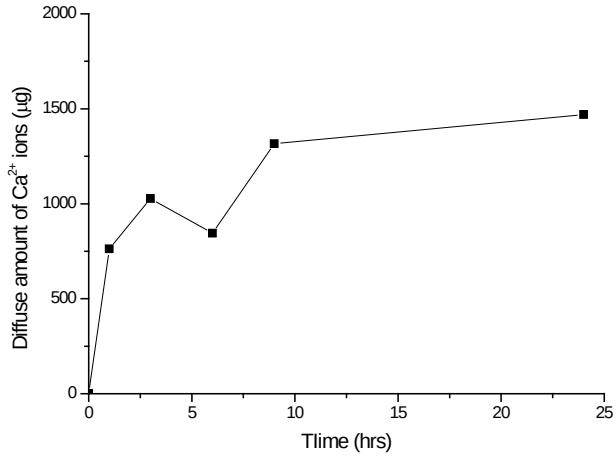

(b)

Figure 47. Amount of Ca^{2+} that diffused into SS solution (a) and blank SF solution (b) from a Ca^{2+}-containing SF solution and a Ca^{2+}-containing SS solution, respectively.

carbonate precipitates [78]. We tested the calcium binding ability of SF and SS using this method. Figure 48 shows the calcium binding ability of 0.5% and 1.0% (w/v) SF and SS solutions, respectively. The rate of calcium carbonate formation was slower in the case of the SF than the SS solution, indicating that the calcium binding affinity of SF was much stronger. This Ca^{2+} binding ability supports the Ca^{2+} ion diffusion behavior between SF and SS. Figure 49 shows the relative gelation kinetics and gelation time of the SF solution containing various amounts of Ca^{2+} ions in the presence of a phase-separated SS solution. The gelation time of the SF solution increased as the amount of Ca^{2+} increased. Interestingly, the 100 mM Ca^{2+} ion-containing SF solution did not undergo gelation even after 200 h. During the sol-gel transition of SF, the interaction of Ca^{2+} with SF residues hindered the conformational transition of SF into β-sheet structures [90]. SF formed predominantly β-sheet structures at the end, but, due to the interactions with Ca^{2+}, the helical intermediates remained intact even in the final conformation. The incomplete gelation of 100 mM Ca^{2+} ions might be a results of the helical intermediates. Moreover, among the five metal species that were investigated in this study, Ca^{2+} had the strongest gelation delaying effect at a 1 mM metal ion concentration. A 1 mM concentration of Ca^{2+} (converted to 1001 μg of Ca^{2+} in grams of SF) was half the amount of Ca^{2+} ions in the silk gland. This indicates that even small amounts of Ca^{2+} were sufficient for the stabilization of SF molecules; therefore, gelation of SF was delayed. When Ca^{2+} was only in the SS layer, Ca^{2+} ions also retarded the

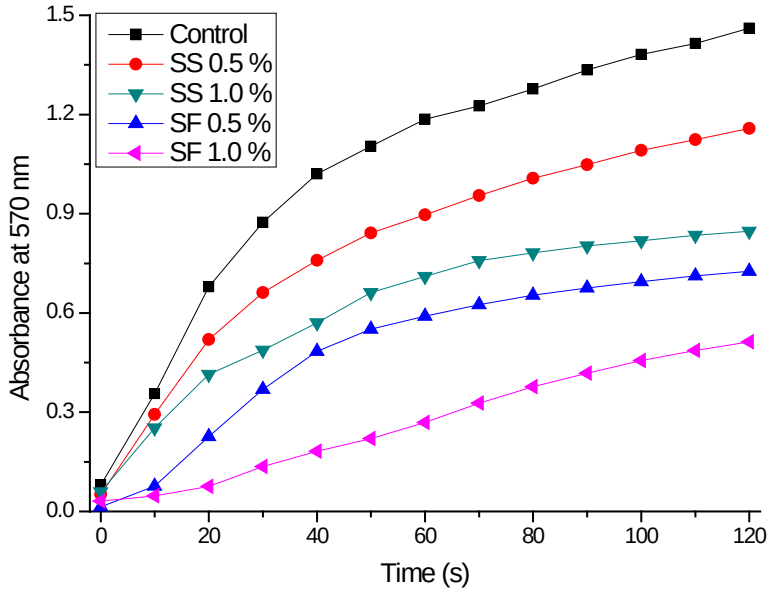

Figure 48. The Ca^{2+} binding ability of SF and SS described by the absorbance of the mixture at 570 nm. Distilled water was used as a control.

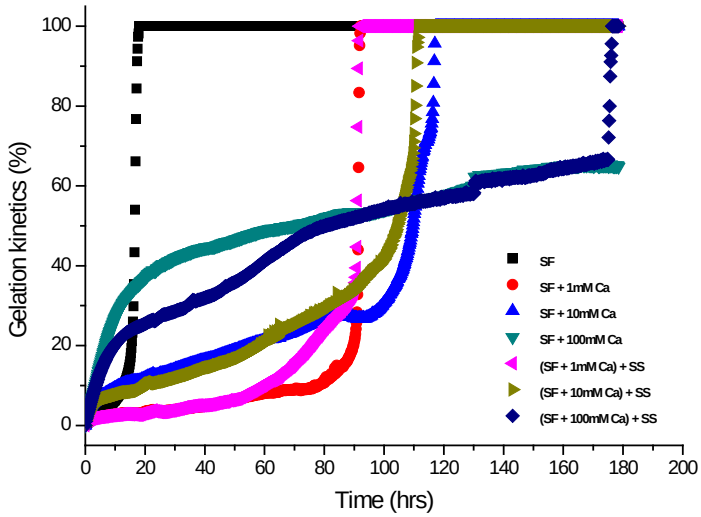

(a)

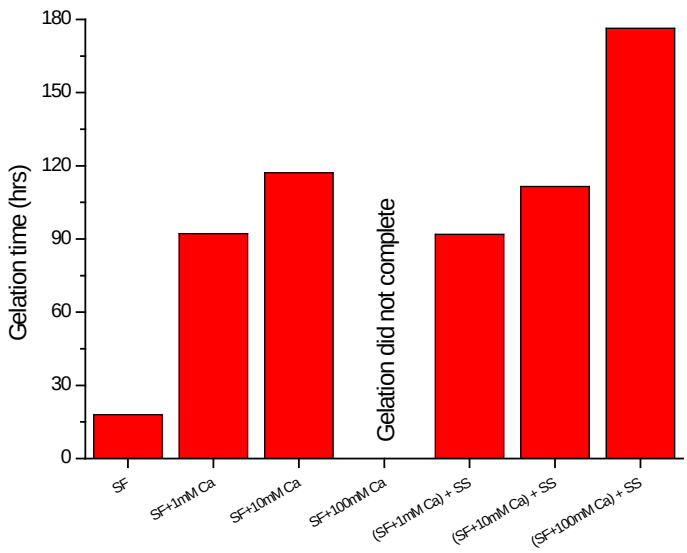

(b)

Figure 49. Relative gelation kinetics and gelation time of SF with various amounts of Ca^{2+} ions in the presence or absence of phase-separated SS.

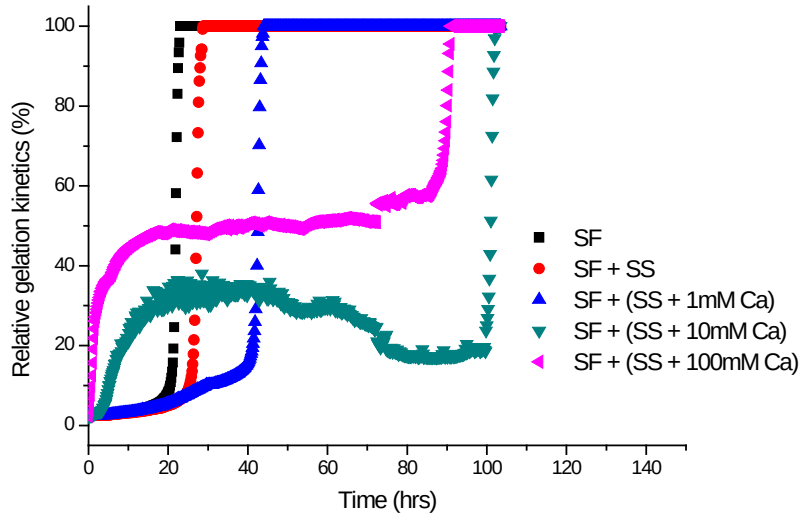

(a)

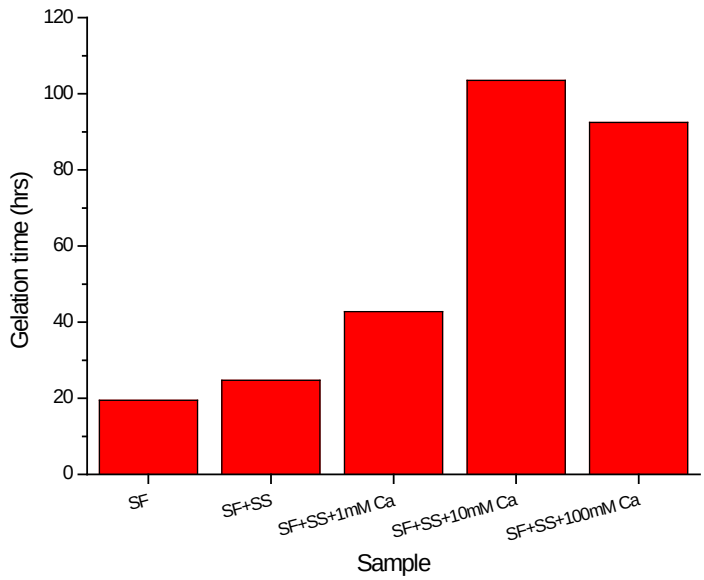

(b)

Figure 50. Relative gelation kinetics and gelation time of SF in the presence of phase-separated SS with various amounts of Ca^{2+} ions.

gelation of SF solution (Figure 50).

4.3.3.4. Effect of Cu^{2+}

Cu^{2+} is the most common transition metal ion, and it has been shown to affect the conformational transition of fibrous protein such as scrapie prion (PrPsc) and the aggregation of amyloid-β peptides [108-111]. Cu^{2+} ions have been reported to induce SF β-sheets by forming coordination complexes with histidine residues. Zong et al. [112] investigated the effect of Cu^{2+} ions on the secondary structure of *Bombyx mori* regenerated SF in dilute solution by CD and found that a small amount of Cu^{2+} induced the conformational transition from random coils to β-sheets. This powerful effect may have resulted from the strong coordination ability of Cu^{2+}, which can be observed with other protein materials. Cu^{2+} coordinated the regenerated SF differently depending on pH and concentration of Cu^{2+}. As the pH decreased in the regenerated SF solution, Cu(II) coordination atoms in SF could change from four nitrogens (Cu-4N) to two nitrogens and two oxygens (Cu-2N2O) as well as to one nitrogen and three oxygens (Cu-1N3O). At neutral and basic pH values, the hydrophilic domain peptide sequence AHGGYSGY in SF may form a 1:1 complex with Cu(II) by coordination via the imidazole Nπ atom of His, together with two deprotonated main-chain amide nitrogens in the two glycine peptides and one oxygen from the hydroxyl group of serine or from water. However, under weakly acidic conditions (pH 5.2-4.0), the

Cu(II)−amide linkages may be broken due to the protonation of amide nitrogen. The Cu^{2+} binding site of His changes from Nπ to Nτ to share a Cu(II) ion between two His residues in peptide chains. This intermolecular His(Nτ)−Cu(II)−His(Nτ) bridge may induce β−sheet formation and gelation.

Silk gland and fibers had trace amounts of Cu^{2+} ions (Table 1). The middle part of the silk gland had 147.7 μg and the silk cocoon fibers had 228.0 μg of Cu^{2+} ions. Figure 51 shows the Cu^{2+} ion diffusion into distilled water and blank SF solution from a Cu^{2+}−containing SF solution and Cu^{2+}−containing distilled water, respectively. Cu^{2+} did not diffuse into the distilled water from the SF solution, whereas only 114 μg of Cu^{2+} (8.3% of the total Cu^{2+}) diffused into the distilled water. In the opposite case, 2027 μg of Cu^{2+} (50.7% of the total Cu^{2+}) diffused into the SF solution. This ion diffusion trend continued in the macro phase separation with SS, where only 228 μg of Cu^{2+} (5.7% of the total Cu^{2+}) diffused from SF to SS, while 2366 μg of Cu^{2+} (59.2% of the total Cu^{2+}) diffused from SS to SF (Figure 52). These experimental results strongly suggest that SF has a higher binding affinity with Cu^{2+} than does SS. To investigate the relative Cu^{2+} binding affinity of SF and SS, a Cu^{2+} adsorption experiment using SF and SS beads was carried out. Figure 53 shows the Cu^{2+} adsorption capacity of SF and SS bead types. This clearly shows that SF has a higher adsorption capacity against Cu^{2+} than SS.

The gelation time of the SF solution containing various amounts of

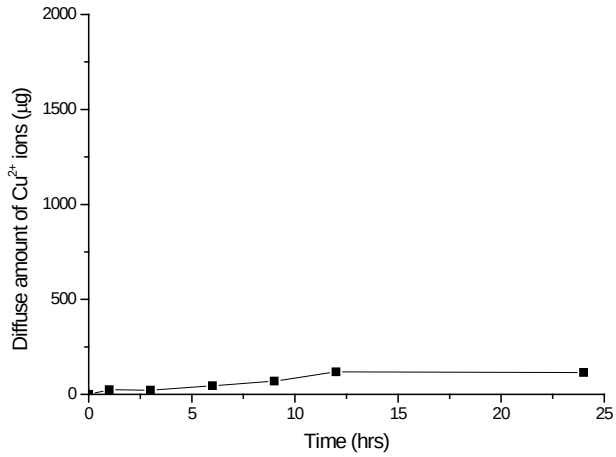

(a)

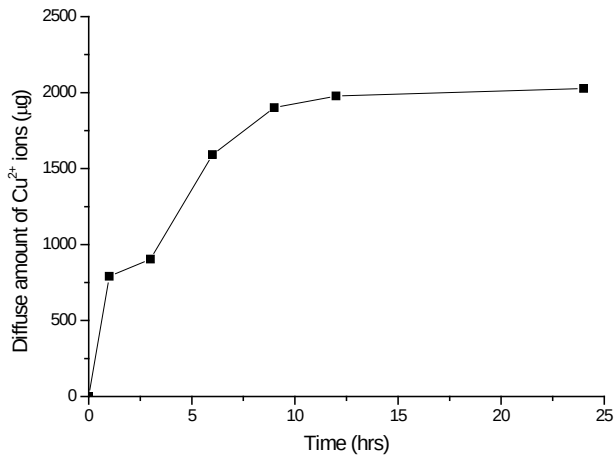

(b)

Figure 51. Amount of Cu^{2+} that diffused into distilled water (a) and blank SF solution (b) from a Cu^{2+}-containing SF solution and Cu^{2+}-containing distilled water, respectively.

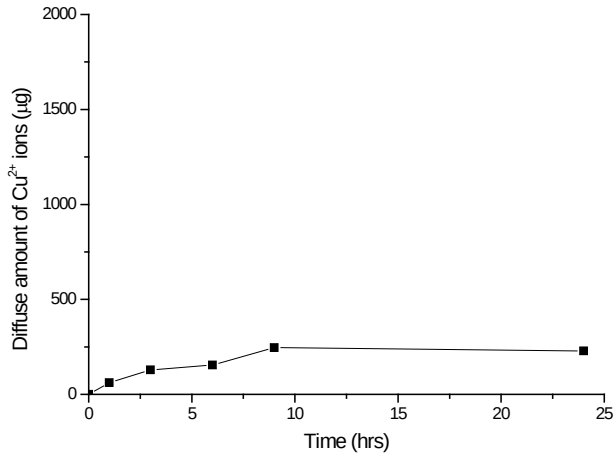

(a)

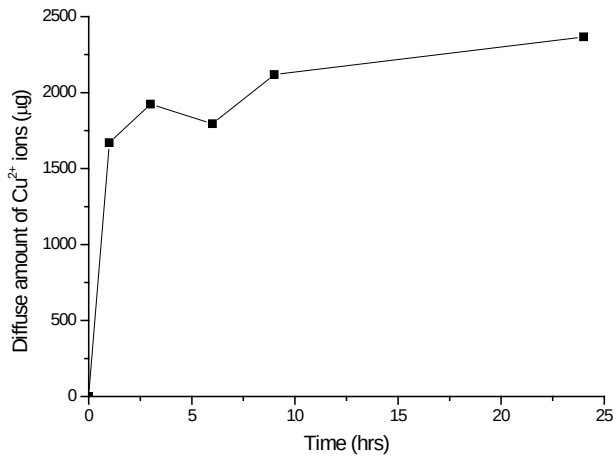

(b)

Figure 52. Amount of Cu^{2+} that diffused into SS solution (a) and blank SF solution (b) from a Cu^{2+}-containing SF solution and Cu^{2+}-containing SS solution, respectively.

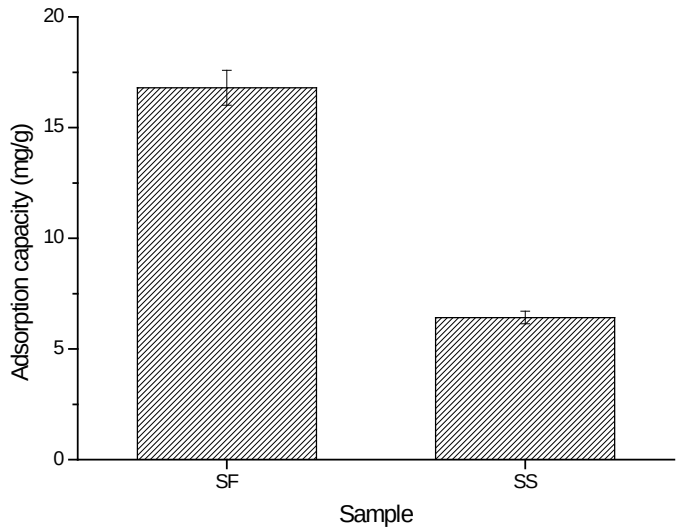

Figure 53. Cu^{2+} adsorption capacity of SF and SS beads. Adsorption experiment carried out in a 100 ppm Cu^{2+} solution with the dose of beads fixed at 1g/L.

Cu^{2+} ions in the presence or absence of phase-separated SS solution are shown in Figure 54. Interestingly, unlike the other ions, which delayed the gelation of SF, Cu^{2+} ions accelerated the gelation of SF. The gelation time of SF solution decreased as the concentration of Cu^{2+} increased to 10 mM, and, over this concentration, the gelation time increased again up to 100 mM Cu^{2+} ion-containing SF solutions. However, in any case, the SF solution containing Cu^{2+} ions had shorter gelation times compared to SF solutions without Cu^{2+} ions. The effect of the SS layer was not significant relative to the strong binding of Cu^{2+} in the SF solution. In the case of Cu^{2+} diffusion from SS solutions, the gelation time of the SF solution decreased because of the tendency of Cu^{2+} to diffuse into SF solution (Figure 55).

4.3.4 Diffusion behavior of metal ions and their effects on the gelation time of SF

Many researchers have focused on the conformational transition of SF with different types of metal ion in different concentration ranges. It is clear that most metal ions with appropriate microenvironments can affect the conformational transition from Silk I to Silk II structures. However, *Bombyx mori* silk is surrounded by an SS layer in their middle glands. The SS is always located at the sheath part of the silk protein and flows together with SF in the spinning duct during the formation of silk fibers. This

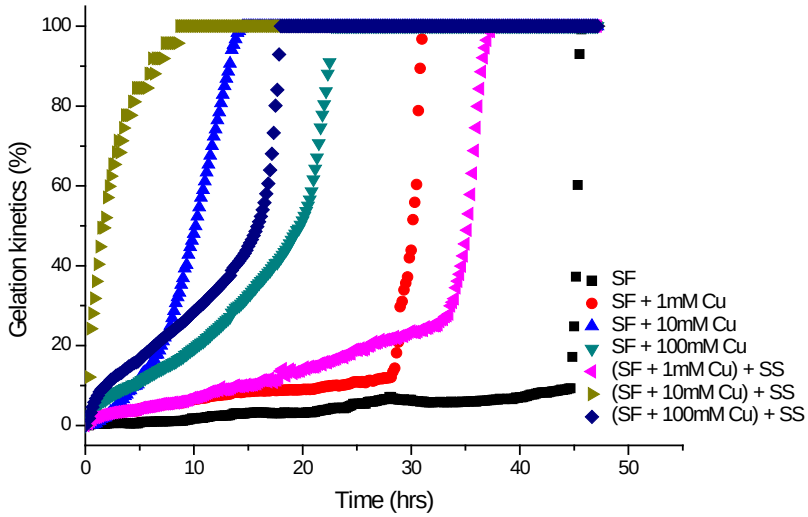

(a)

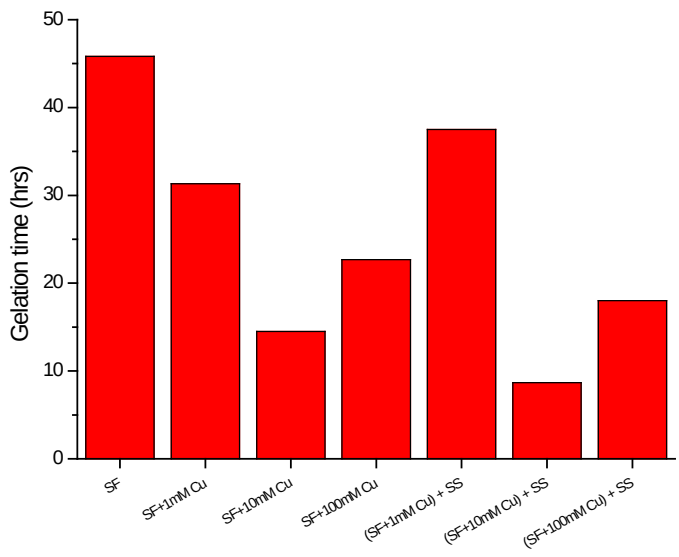

(b)

Figure 54. Relative gelation kinetics and gelation time of SF with various amounts of Cu^{2+} ions in the presence or absence of phase-separated SS.

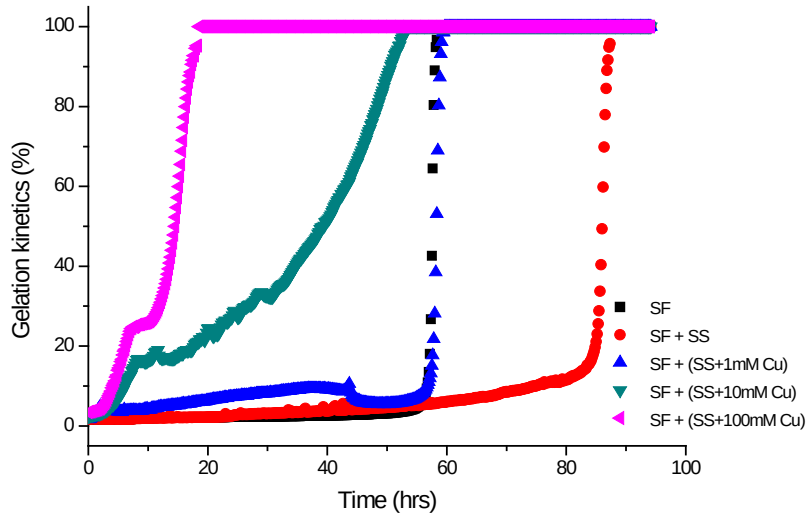

(a)

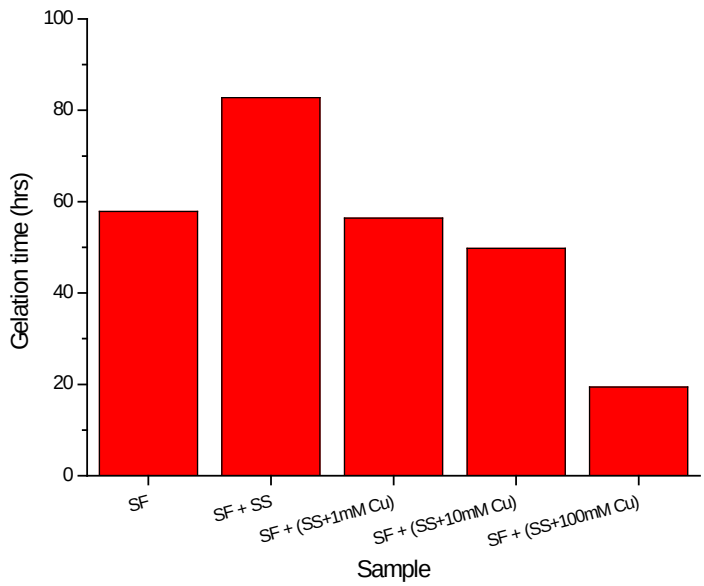

(b)

Figure 55. Relative gelation kinetics and gelation time of SF in the presence of phase-separated SS with various amounts of Cu^{2+} ions.

means that there is a possibility of ion migration between the SF and SS. However, there has been no research on such ion transfers or diffusion potential. Investigations on the effect of metal ion species and their kinetics between phase-separated proteins have been limited by the ability to monitor the transfer of metal ions. In this study, to investigate the metal ion transfer between phase-separated SF and SS layers, a different method was used. First, the metal transfer from or into the SF solution was compared with that of distilled water. This showed the fundamental binding ability of SF with various metal ions. Second, an in vitro macro phase separation between SF and SS was established, mimicking the environment in the silk gland. The concentration of SF was 4% (w/v) and that of SS was 1% (w/v).

Figures 56 and 57 show the concentration changes between phase-separated SF and SS during the ion diffusion experiments from SF to SS and from SS to SF, respectively. In both cases, the concentration of SF decreased to about 0.1% and that of SS increased to about 0.1%. This concentration variation was similar to that seen in a previous experiment, where the gelation time of SF was observed with phase-separated SS without any ions. Therefore, in the ion diffusion experiment, the change in ion concentration was only determined by the diffusion of ions by to the concentration gradient. If an ion did not have any affinity with the protein in the initial layer, the final amount of migrated ion from the initial layer would be close to 2000 μg. When the final amount of

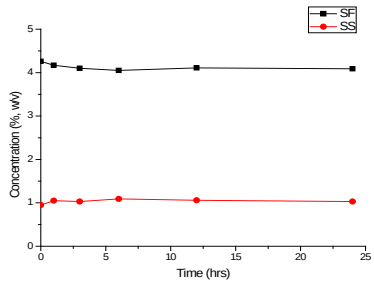

(a)

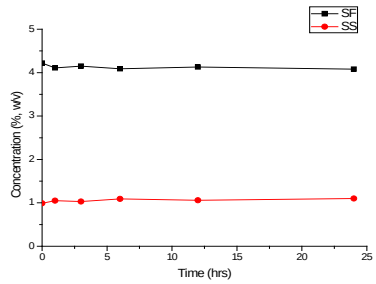

(b)

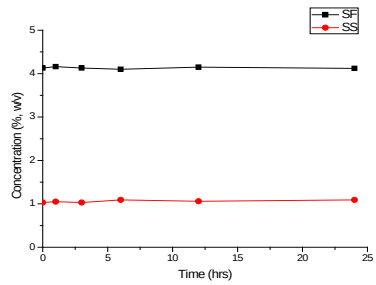

(c)

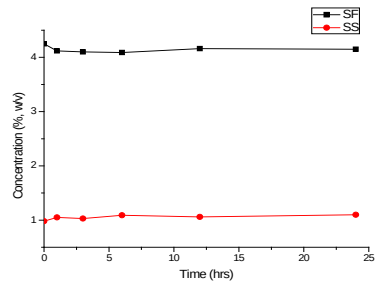

(d)

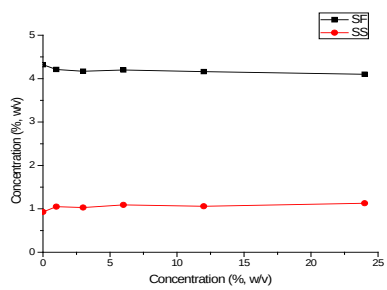

(e)

Figure 56. Concentrations in each layer during metal ion diffusion from SF to SS. (a) Na^+ ,(b) K^+, (c) Li^+, (d) Ca^{2+}, and (e) Cu^{2+}.

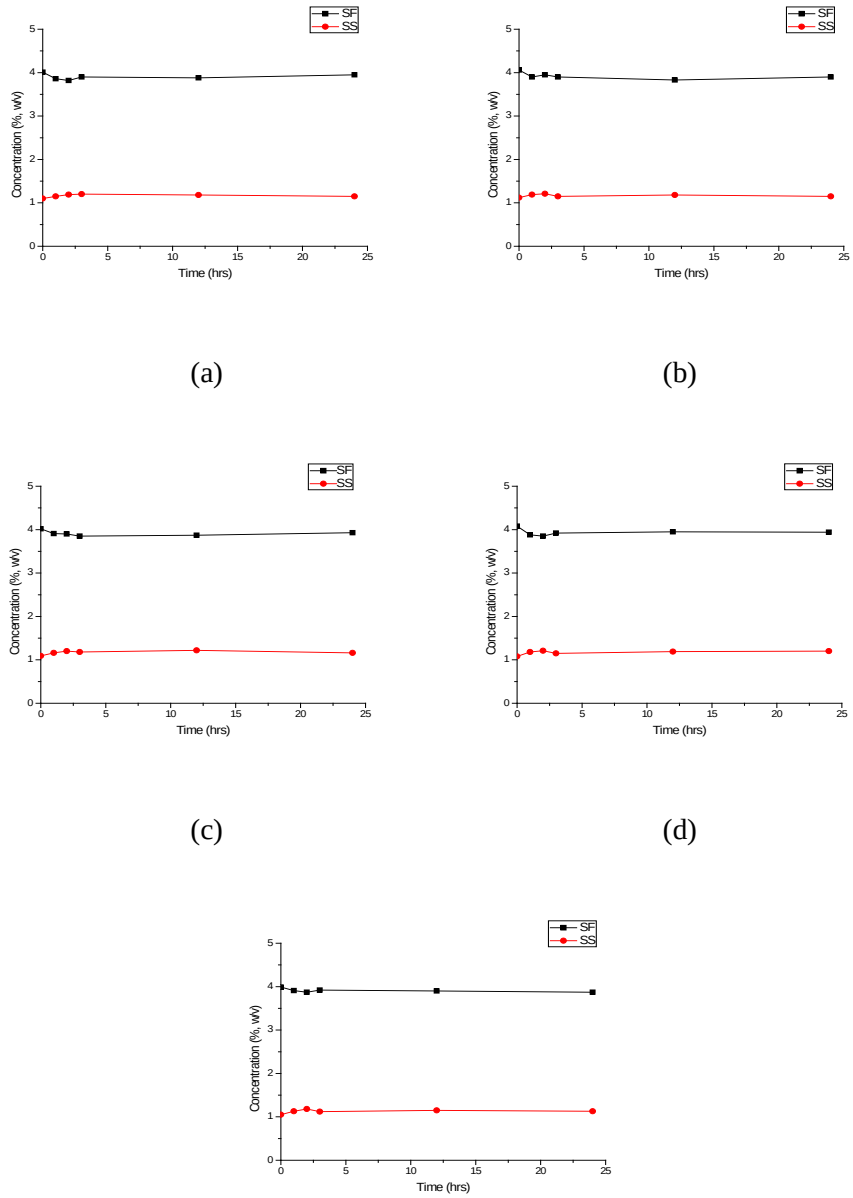

Figure 57. Concentrations in each layer during metal ion diffusion from SS to SF. (a) Na^{+} , (b) K^{+}, (c) Li^{+}, (d) Ca^{2+}, and (e) Cu^{2+}.

migrated ion from the initial layer was far low than 2000 μg, the ion had a high affinity with the protein in the initial layer.

SF and distilled water maintained the phase separation until the gelation of SF was completed (data not shown). Figure 58 (a) shows the amount of metal ions that diffused from the SF layer to the distilled water. For all metal ion species, less than 20% of the total ions moved to the distilled water layer. This result indicates that the metal ion diffusion from SF to phase-separated water was not only dependent on the concentration gradient, but also by the differences in metal binding affinities between the phase-separated solutions. There were interactions between SF and metal ions, and these interactions inhibited the movement of metal ions to the phase-separated water layer. In a comparison of the amounts of diffused metal ions, Cu^{2+} ion was the least diffusible ion, meaning that it there were stronger interactions between SF molecules and Cu^{2+} ions than SF with other ions.

Figure 58 (b) shows the amount of diffusion of each metal species from distilled water into the SF solution. In contrast with the ion transfer from the SF, the metal ion transfer from distilled water to the SF layer depended on the concentration gradient only. More than 40% of the total ions moved to the SF layer in the cases of all metal species. Comparing the total amount of diffused ions, Cu^{2+} was the only ion with more than 2,000 μg diffused into the SF layer. This result demonstrates, once again, the interaction between

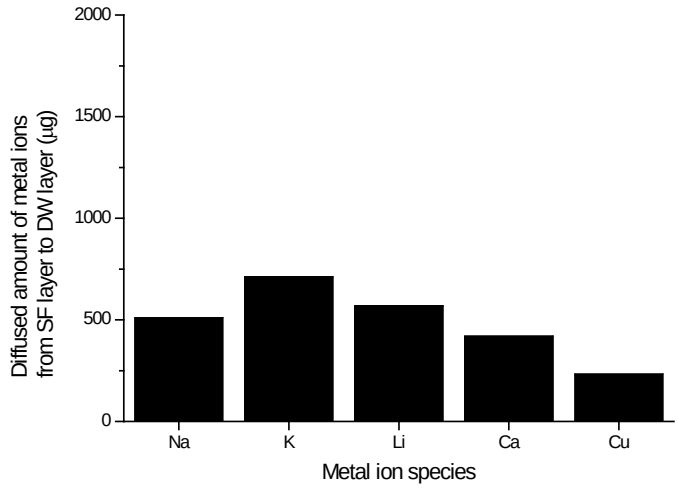

(a)

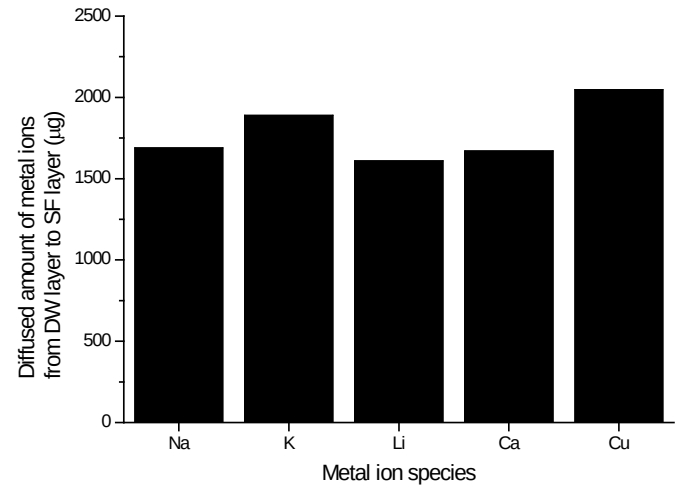

(b)

Figure 58. Amount of metal ions that diffused between SF and the distilled water layer with metal ions in each layer. (a) Metal ion added into SF and (b) metal ion added into distilled water.

SF and Cu^{2+}.

The middle gland of silkworms serves as a reservoir of silk protein during the spinning process. We designed a static macro phase separation system with SF and SS that mimicked the middle gland of silkworms. Figure 59 shows the amount of metal ions that diffused between phase-separated SF and SS. Most ions preferentially bound with SF, except for Na^{+} ions. From SS to SF, Na^{+} ion diffusion to SF was difficult because of the high bind affinity between Na^{+} and SS molecules. It is unclear why Na^{+} has a higher binding affinity to SS, but the high content of carboxyl-bearing amino acids in SS might be responsible. Conversely, Cu^{2+} ions bound preferentially with SF molecules. This finding was supported by the Cu^{2+} adsorption experiments using SF and SS beads.

The time of SF gelation during metal transfer was also investigated (Figures 60 and 61). Overall, the increased ion concentration and the presence of an SS layer delayed the gelation of SF solutions, except with Cu^{2+} ions. Alkaline metal ions such as Na^{+}, K^{+}, and Li^{+} retarded the gelation of SF. However, these ions did not have a significant affect in the concentration range of metal ions in the actual silk gland and fibers. Ca^{2+} ions retarded the gelation of SF solutions greatly. The gelation time of SF solutions in the case of 1 mM Ca^{2+} was four-fold longer than that of SF solutions without Ca^{2+} ions, even though the concentration was just half the amount of Ca^{2+} in the silk gland.

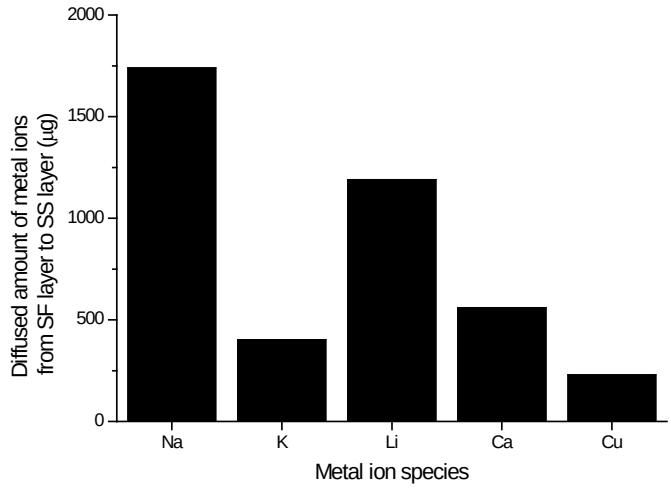

(a)

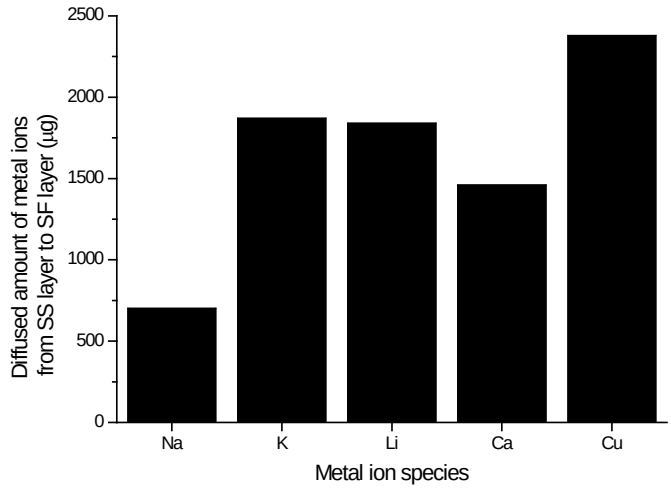

(b)

Figure 59. Amount of metal ions that diffused between the SF and SS layers with metal ion in each layer. (a) Metal ion added into SF and (b) metal ion added into SS.

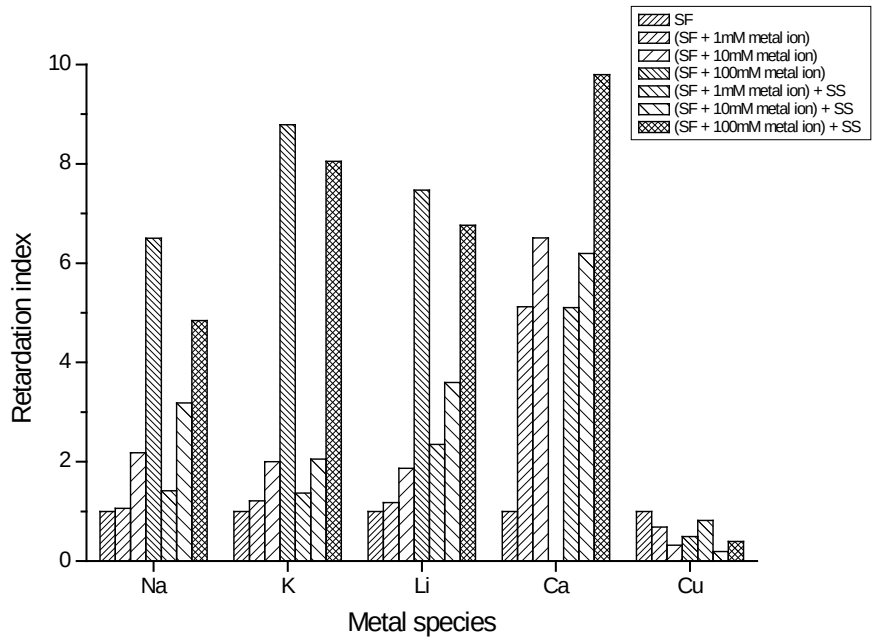

Figure 60. Effects of metal ions in the SF layer on the gelation time of SF, described by a gelation retardation index.

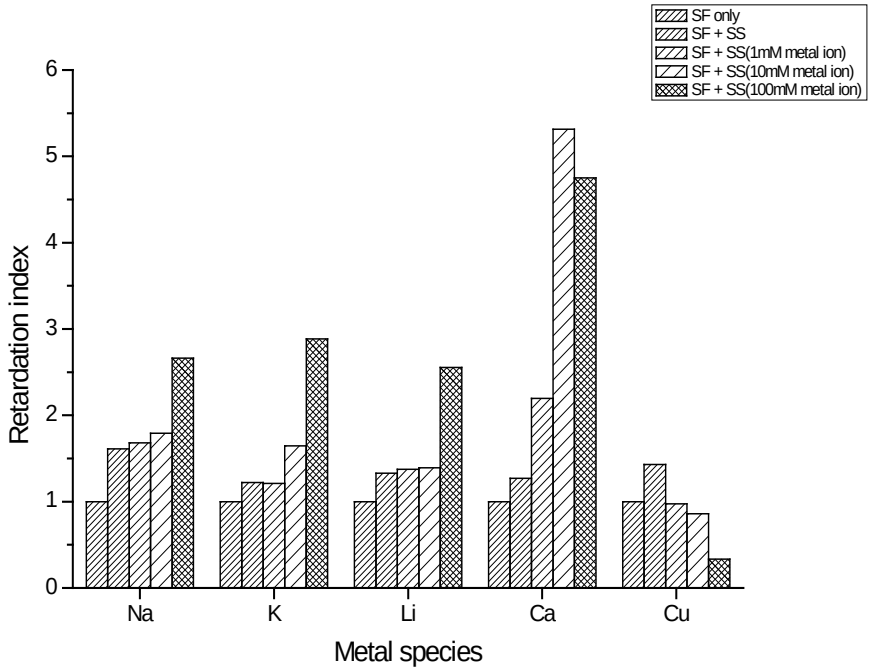

Figure 61. Effects of metal ions in the SS layer on the gelation time of SF, described by a gelation retardation index.

In the case of Cu^{2+} ions, the SF gelation time decreased relative to that of SF without Cu^{2+} ions. This gelation acceleration effect might have been caused by the strong binding affinity between SF and Cu^{2+}. Zouh et al. investigated the effect of Cu^{2+} on the conformational transition of SF using Raman spectroscopy and found that Cu^{2+} induced a conformational transition from random coils to β−sheets [113]. Taken together, these findings indicate that Cu^{2+} could play a role in the spinning process of SF. From silk gland to silk fiber, only the concentration of Cu^{2+} ions increased, while the concentrations of Na^{+}, K^{+}, Li^{+}, and Ca^{2+} ions decreased. The formation of silk fibers is carried out with a conformational transition from random coils to the β−sheets. For such a conformational transition to occur, Cu^{2+} ions that promote the β−sheet transition might increase. In comparing the Cu^{2+}−binding affinity between SF and SS, these SF conformational transitions could occur by diffusion of Cu^{2+} ions from the SS layer during the formation of silk fibers.

5. Conclusion

In this study, a phase-separated SF and SS solution layer was constructed that mimicked the state in the middle silk gland. Two effects of the SS solution layer on the SF solution layer were investigated: the gelation time and hydrogel structure of SF and the ion partition between the two layers.

The phase-separated SS slowed the gelation of SF, and this became more significant as the SS concentration and the concentration ratio of SF/SS increased. From the Tht fluorescence intensity kinetics, the gelation delay resulted from the slow β-sheet structure development in the SF layer. Interestingly, the X-ray diffraction pattern of the SF hydrogel exhibited a typical Silk I structure. These results suggest that SS, even though it was phase separated, could prevent premature crystallization of SF and induce a Silk I hydrogel structure, resembling the original state in the middle silk gland.

Ion partitioning between the SF and SS layers was investigated with Li^+, Na^+, K^+, Ca^{2+}, and Cu^{2+}. Additionally, the gelation times of the SF layer in the presence of different ion concentrations was determined. Depending on the metal ion species, different diffusion behaviors were observed. Most metal ions diffused towards the SF layer, except for Na^+, which diffused into the SS layer. The metal species and amount of diffused metal ion affected the gelation kinetics of SF as well. Overall, increased ion concentrations and the

presence of the SS layer delayed the gelation of the SF solution, except with Cu^{2+} ions. Ca^{2+} ions had the strongest retardation effect, while Cu^{2+} accelerated the gelation of SF.

In conclusion, the SS layer that surrounds the SF layer can affect the structural conformation of SF in the middle silk gland, stabilizing the SF before spinning. This is the first report indicating that the SS layer in the middle silk gland may have more important roles than has previously been recognized.

Bibliography

[1] T. Tanaka, M. Kobayashi, S. I. Inoue, H. Tsuda, J. Magoshi, Biospinning: Change of water contents in drawn silk, *Journal of Polymer Science Part B: Polymer Physics*. **41**, 274-280 (2003).

[2] A.E. Thurber, F.G. Omenetto, D.L. Kaplan, In vivo bioresponses to silk proteins, *Biomaterials*. **71**, 145-157 (2015).

[3] A. B. Li, J. A. Kluge, N. A. Guziewicz, F. G. Omenetto, D. L. Kaplan, Silk-based stabilization of biomacromolecules, *Journal of Controlled Release*. **219,** 416-430 (2015).

[4] B. Panilaitis, G. H. Altman, J. Chen, H. J. Jin, V. Karageorgiou, D. L. Kaplan, Macrophage responses to silk, *Biomaterials*. **24**, 3079-3085 (2003).

[5] S, Bisch Knaden, T. Daimon, T. Shimada, B. S. Hansson, S. Sachse, Anatomical and functional analysis of domestication effects on the olfactory system of the silk moth Bombyx mori, *Proceedings of the Royal Society of London B: Biological Sciences*. **281**, 2013-2582 (2014).

[6] P. Aramwit, T. Siritientong, S. Kanokpanont, T. Srichana, Formulation and characterization of silk sericin-PVA scaffold

crosslinked with genipin, *International Journal of Biological Macromolecules*. **47**, 668-675 (2010).

[7] W. Wei, Y. Zhang, Y. Zhao, J. Luo, H. Shao, X. Hu, Bio-inspired capillary dry spinning of regenerated silk fibroin aqueous solution, *Materials Science and Engineering: C*. **31**, 1602-1608 (2011).

[8] L. J. Domigan, M. Andersson, K. A. Alberti, M. Chesler, Q. Xu, J. Johansson, A. Rising, D. L. Kaplan, Carbonic anhydrase generates a pH gradient in *Bombyx mori* silk glands, *Insect Biochemistry and Molecular Biology*. **65**, 100-106 (2015).

[9] H. Chang, T. Cheng, Y. Wu, W. Hu, R. Long, C. Liu, P. Zhoa, Q. Xia, Transcriptomic Analysis of the Anterior Silk Gland in the Domestic Silkworm (Bombyx mori) - Insight into the Mechanism of Silk Formation and Spinning, *Plos One*. **10**, 0139424 (2015).

[10] H. J. Jin, D. L. Kaplan, Mechanism of silk processing in insects and spiders, *Nature.* **424**, 1057-1061 (2003).

[11] K. H. Lee, Silk sericin retards the crystallization of silk fibroin, *Macromolecular Rapid Communications*. **25**, 1792-1796 (2004).

[12] L. D. Koh, Y. Cheng, C. P. Teng, Y W. Khin, X. J. Loh, S. Y. Tee, Structures, mechanical properties and applications of silk

fibroin materials, *Progress in Polymer Science*. **46**, 86-110 (2015).

[13] Z. Shao, F. Vollrath, Materials: Surprising strength of silkworm silk, *Nature*. **418**, 741-741 (2002).

[14] G. H. Altman, F. Diaz, C. Jakuba, T. Calabro, R. L. Horan, J. Chen, H. Lu, J. Richmond, D. L. Kaplan, Silk-based biomaterials, *Biomaterials*. **24**, 401-416 (2003).

[15] F. Vollrath, D. Porter, Silks as ancient models for modern polymers, *Polymer*. **50**, 5623-5632 (2009).

[16] C. S. Ki, Y. H. Park, H. J. Jin, Silk protein as a fascinating biomedical polymer: Structural fundamentals and applications, *Macromolecular research*. **17**, 935-942 (2009).

[17] F. Takei, Y. Kikuchi, A. Kikuchi, S. Mizuno, K. Shimura, Further evidence for importance of the subunit combination of silk fibroin in its efficient secretion from the posterior silk gland cells, *The Journal of Cell Biology*. **105**, 175-180 (1987).

[18] M. S. Zafar, D. J. Belton, B. Hanby, D. L. Kaplan, C. C. Perry, Functional Material Features of Bombyx mori Silk Light versus Heavy Chain Proteins, *Biomacromolecules*. **16**, 606-614 (2015).

[19] K. Tanaka, N. Kajiyama, K. Ishikura, S. Waga, A. Kikuchi, K.

Ohtomo, T. Takaqi, S. Mizuno, Determination of the site of disulfide linkage between heavy and light chains of silk fibroin produced by Bombyx mori, *Biochimica et Biophysica Acta(BBA) – Protein Structure and Molecular Enzymology*. **1432**, 92-103 (1999).

[20] F. Oyama, S. Mizuno, K. Shimura, Studies on immunological properties of fibroin heavy and light chains, *Journal of Biochemistry*. **96**, 1689-1694 (1984).

[21] K. Tanaka, K. Mori, S. Mizuno, Immunological identification of the major disulfide-linked light component of silk fibroin, *Journal of Biochemistry*. **114**, 1-4 (1993).

[22] C. Z. Zhou, F. Confalonieri, M. Jacquet, R. Perasso, Z. G. Li, J. Janin, Silk fibroin: structural implications of a remarkable amino acid sequence, *Proteins*. **44**, 119-122 (2001).

[23] S. W. Ha, H. S. Gracz, A. E. Tonelli, S. M. Hudson, Structural Study of Irregular Amino Acid Sequences in the Heavy Chain of Bombyx mori Silk Fibroin, *Biomacromolecules.* **6**, 2563-2569 (2005).

[24] C. L. Craig, C. Riekel, Comparative architecture of silks, fibrous proteins and their encoding genes in insects and spiders, *Comparative Biochemistry and Physiology Part B: Biochemistry and*

Molecular Biology. **133**, 493-507 (2002).

[25] J. Ming, M. Li, Y. Han, Y. Chen, H. Li, B. Zuo, Novel two-step method to form silk fibroin fibrous hydrogel, *Materials Science and Engineering: C*. **59**, 185-192 (2016).

[26] T. Lefèvre, M-E. Rousseau, M. PézoletK, Protein Secondary Structure and Orientation in Silk as Revealed by Raman Spectromicroscopy, *Biophysical Journal*. **92**, 2885-2895, (1993)

[27] P. Chen, H. S. Kim, C. Y. Park, H. S. Kim, I. J. Chin, H. J. Jin, pH-Triggered transition of silk fibroin from spherical micelles to nanofibrils in water, *Macromolecular Research*. **16**, 539-543 (2008).

[28] C .Z. Zhou, F. Confalonieri, N. Medina, Y. Zivanovic, C. Esnault, T. Yang, M Jacquet, J Janin, M. Duguet, R Perasso, Z, G, Li, Fine organization of Bombyx mori fibroin heavy chain gene, *Nucleic Acids Research*. **28**, 2413-2419 (2000).

[29] K. Kodama, The Preparation and Physico-chemical Properties of Sericin, *Biochemical journal*. **20**, 1208-1222 (1926).

[30] Z. Wang, Y. Zhang, J. Zhang, L. Huang, J. Liu, Y. Li, G. Zhang, S. C. Kundu, L. Wang, Exploring natural silk protein sericin for regenerative medicine: an injectable, photoluminescent, cell-

adhesive 3D hydrogel, *Scientific Reports*. **4**, 7064 (2014).

[31] T. Gamo, T. Inokuchi, H. Laufer, Polypeptides of fibroin and sericin secreted from the different sections of the silk gland in Bombyx mori, *Insect Biochemistry*. **7**, 285-295 (1977).

[32] Y. Takasu, H. Yamada, K. Tsubouchi, Isolation of three main sericin components from the cocoon of the silkworm, Bombyx mori, *Bioscience Biotechnology and Biochemistry*. **66**, 2715-2718 (2002).

[33] P. Aramwit, S. Damrongsakkul, S. Kanokpanont, T. Srichana, Properties and antityrosinase activity of sericin from various extraction methods, *Biotechnology and Applied Biochemistry*. **55**, 91-98 (2010).

[34] Y. Q. Zhang, Applications of natural silk protein sericin in biomaterials, *Biotechnology Advances*. **20**, 91-100 (2002).

[35] H. Oh, J. Y. Lee, M. K. Kim, I. C. Um, K. H. Lee, Refining hot-water extracted silk sericin by ethanol-induced precipitation, *International Journal of biological macromolecules*. **48**, 32-37 (2011).

[36] H. Yun, H. Oh, M. K. Kim, H. W. Kwak, J. Y. Lee, I. C. Um, S. K. Vootal, K. H. Lee, Extraction conditions of Antheraea mylitta sericin

with high yields and minimum molecular weight degradation, *International Journal of biological macromolecules*, **52**, 59-65 (2013).

[37] R. Dash, S. K. Ghosh, D. L. Kaplan, S. C. Kundu, Purification and biochemical characterization of a 70 kDa sericin from tropical tasar silkworm, Antheraea mylitta, *Comparative Biochemistry and Physiology Part B: Biochemistry and Molecular Biology,* **147**, 129-134 (2007).

[38] R. Valluzzi, SP. Gido, W. Muller , D. L. Kaplan, Orientation of silk III at the air-water interface. *International Journal of biological macromolecules*, **24**, 237-242 (1999).

[39] T. Yamane, K. Umemura, Y. Nakazawa, T. Asakura, Molecular Dynamics Simulation of Conformational Change of Poly(Ala-Gly) from Silk I to Silk II in Relation to Fiber Formation Mechanism of *Bombyx mori* Silk Fibroin. *Macromolucules*, **36**, 6766-6772 (2003).

[40] S. J. He, R. Valluzzi, S. P. Gido, Silk I structure in Bombyx mori silk foams, *International Journal of Biological Macromolecules*. **24**, 187-195 (1999).

[41] B. Lotz, F. Colonna Cesari, The chemical structure and the crystalline structures of Bombyx mori silk fibroin, *Biochimiestry.* **61**,

205-214 (1979).

[42] B. Lotz, H. D. Keith, Crystal structure of poly(l-Ala-Gly)II: A model for silk I, *Journal of Molecular Biology*. **61**, 201-215 (1971).

[43] B. Lotz, A. Brack, G. Spach, Beta structure of periodic copolypeptides of L-alanine and glycine. Their relevance to the structure of silks, *Journal of Molecular Biology*. **87**, 193-203 (1974).

[44] J. Magoshi, M. Mizuide, Y. Magoshi, K. Takahashi, M. Kubo, S. Nakamura, Physical properties and structure of silk. VI. Conformational changes in silk fibroin induced by immersion in water at 2 to 130℃, *Journal of Polymer Science: Polymer Physics Edition*. **17**, 515-520 (1979).

[45] R. E. Marsh, R. B. Corey, L. Pauling, An investigation of the structure of silk fibroin, *Biochimica et Biophysica Acta*. **16**, 1-34, (1955).

[46] Y. Takahashi, M. Gehoh, K. Yuzuriha, Structure refinement and diffuse streak scattering of silk (Bombyx mori), *International Journal of Biological Macromolecules*. 24, 127-138 (1999).

[47] M. Demura, T. Asakura, T. Kuroo, Immobilization of biocatalysts with *Bombyx mori* silk fibroin by several kinds of

physical treatment and its application to glucose sensors, *Biosensors.* **4** 361-372 (1989).

[48] Q. Lu, X. Hu, X. Wang, J. A. Kluge, S. Lu, P. Cebe, D. L. Kaplan, Water-insoluble silk films with silk I structure, *Acta Biomaterialia*. **6**, 1380-1387 (2010).

[49] J. Ming, B. Zuo, Silk I structure formation through silk fibroin self-assembly, *Journal of Applied Polymer Science*. **125**, 2148-2154 (2012).

[50] C. Zhang, D. Song, Q. Lu, X. Hu, D.L. Kaplan, H. Zhu, Flexibility regeneration of silk fibroin in vitro, *Biomacromolecules*. **13**, 2148-2153 (2012).

[51]O. Kratky, E. Schauenstein, A. Sekora, A New Type of Lattice with Large Periods in Silk, *Nature*. **165**, 527-528 (1950).

[52] E. S. Sashina, A. M. Bochek, N. P. Novoselov, D. A. Kirichenko, Structure and solubility of natural silk fibroin, *Russian Journal of Applied Chemistry.* **79**, 869-876 (2006).

[53] S. Sohn, H. H. Strey, S. P. Gido, Phase Behavior and Hydration of Silk Fibroin, *Biomacromolecules.* **5**, 751-757 (2004).

[54] A. Percot, P. Colomban, C. Paris, H.M. Dinh, M. Wojcieszak, B.

Mauchamp, Water dependent structural changes of silk from *Bombyx mori* gland to fibre as evidenced by Raman and IR spectroscopies, *Vibrational Spectroscopy*. 73, 79-89 (2014).

[55] S. Inoue, H. Tsuda, T. Tanaka, M. Kobayashi, Y. Magoshi, J. Magoshi, Nanostructure of Natural Fibrous Protein: In Vitro Nanofabric Formation of *Samia cynthia ricini* Wild Silk Fibroin by Self-Assembling, *Nano Letter*. 3, 1329-1332 (2003).

[56] J. D. van Beek, L. Beaulieu, H. Schäfer, M. Demura, T. Asakura, B. H. Meier, Solid-state NMR determination of the secondary structure of *Samia cynthia ricini* silk, *Nature*. 405, 1077-1079 (2000).

[57] G. Li, P. Zhou, Z. Shao, X. Xie, X. Chen, H. Wang, L. Chunyu, T. Yu, The natural silk spinning process. A nucleation-dependent aggregation mechanism?, *European Journal of Biochemistry,* 268, 6600-6606 (2001).

[58] Z. Gong, L. Huang, Y. Yang, X. Chen, Z. Shao, Two distinct beta-sheet fibrils from silk protein, *Chemical Communications,* 48, 7506-7508 (2009).

[59] S. Matsuura, T. Morimoto, S. Nagata, Y. Tashiro, Studies on the posterior silk gland of the silkworm, Bombyx mori. II. Cytolytic

processes in posterior silk gland cells during metamorphosis from larva to pupa, *The Journal of Cell Biology*. **38**, 589-603 (1968).

[60] P. Zhang, Y. Aso, K. Yamamoto, Y. Banno, Y. Wang, K. Tsuchida, Proteome analysis of silk gland proteins from the silkworm, Bombyx mori, *Proteomics*. **6**, 2586-2599 (2006).

[61] H. Akai, The structure and ultrastructure of the silk gland, *Experientia*. **39**, 443-449 (1983).

[62] F. Sehnal, H. Akai, Insect silk glands: their types, development and function, and effects of environmental factors and morphogenetic hormones on them, *International Journal of Insect Morphology and Embryology*. **19**, 79-132 (1990).

[63] R. Valluzzi, S. J. He, S. P. Gido, D. L. Kaplan, Bombyx mori silk fibroin liquid crystallinity and crystallization at aqueous fibroin-organic solvent interfaces, International Journal of Biol*ogical Macromolecules*. **24**, 227-236 (1999).

[64] B. Lotz, A. Gonthier-Vassal, A. Brack, J. Magoshi, Twisted single crystals of Bombyx mori silk fibroin and related model polypeptides with beta structure. A correlation with the twist of the beta sheets in globular proteins, *Journal of Molecular Biology*. **156**, 345-357 (1982).

[65] C. S. Ki, J. W. Kim, H. J. Oh, K. H. Lee, Y. H. Park, The effect of residual silk sericin on the structure and mechanical property of regenerated silk filament, *International Journal of Biological Macromolecules*. **41**, 346-353 (2007).

[66] C.S. Ki, I.C. Um, Y.H. Park, Acceleration effect of sericin on shear-induced β-transition of silk fibroin, *Polymer*. **50**, 4618-4625 (2009).

[67] Y. Hang, Y. Zhang, Y. Jin, H. Shao, X. Hu, Preparation of regenerated silk fibroin/silk sericin fibers by coaxial electrospinning, *International Journal of Biological Macromolecules*. **51**(5), 980-986 (2012).

[68] H. Oh, M. K. Kim, J. Y. Lee, K. H. Lee, The Role of Silk Sericin during the Spinning Process of Silk Fiber(I) -The Effect of Silk Sericin on the Crystallization and Gelation of Silk Fibroin-, *Textile Science and Engineering*. **46**, 289-294 (2009)

[69] N. Singh, D. Das, A. Singh, M. L. Mohan, Prion protein and metal interaction: physiological and pathological implications, *Current Issues Molecular Biology*. **12**, 99-107 (2010).

[70] P. Faller, C. Hureau, O. Berthoumieu, Role of Metal Ions in the Self-assembly of the Alzheimer's Amyloid-β Peptide, *Inorganic*

Chemistry. **52**, 12193-12206 (2013).

[71] L. Zhou, X. Chen, Z. Shao, Y. Huang, D. P. Knight, Effect of metallic ions on silk formation in the Mulberry silkworm, Bombyx mori, *The Journal of Physical Chemistry B*. **109**, 16937-16945 (2005).

[72] A. Ochi, K. S. Hossain, J. Magoshi, N. Nemoto, Rheology and dynamic light scattering of silk fibroin solution extracted from the middle division of *Bombyx mori* silkworm, *Biomacromolecules*. **3**, 1187-1196 (2002).

[73] X. Wang, P. Zhao, Y. Li, Q. Yi, S. Ma, K. Xie, H. Chen, Q. Xia, Modifying the Mechanical Properties of Silk Fiber by Genetically Disrupting the Ionic Environment for Silk Formation, *Biomacromolecules.* **16**, 3119-3125 (2015).

[74] X. Hu, D. Kaplan, P. Cebe, Determining Beta-Sheet Crystallinity in Fibrous Proteins by Thermal Analysis and Infrared Spectroscopy, *Macromolecules.* **39**, 6161-6170 (2006).

[75] H. Zhang, L. Deng, M. Yang, S. Min, L. Yang, L. Zhu, Enhancing Effect of Glycerol on the Tensile Properties of Bombyx mori Cocoon Sericin Films, *International Journal of Molecular Sciences.* **12**, 3170-3181 (2011).

[76] Y.N. Jo, D.G. Bae, I.C. Um, The Effect of Extraction Conditions and Film Side on the Molecular Conformation of Silk Sericin Film, *International Journal of Industrial Entomology*, **26**, 113-118, (2013)

[77] Y.N. Jo, I.C. Um, Effects of solvent on the solution properties, structural characteristics and properties of silk sericin, *International Journal of Biological Macromolecules*. **78**, 287-295 (2015).

[78] M. Yang, G. Zhou, Y. Shuai, J. Wang, L. Zhua, C. Mao, Ca^{2+}-induced self-assembly of Bombyx mori silk sericin into a nanofibrous network-like protein matrix for directing controlled nucleation of hydroxylapatite nano-needles, *Journal of Materials Chemistry B*, **3**, 2455-2462 (2015)

[80] H. W. Kwak, K. H. Lee, Monitoring of phase separation between silk fibroin and sericin using various dye system, *International Journal of Industrial Entomology*, **30**, 1-5 (2015)

[81] X. Wang, J. Kluge, G. G. Leisk, D. L. Kaplan, Sonication-Induced Gelation of Silk Fibroin for Cell Encapsulation, *Biomaterials*, **29**, 1054-1064 (2009)

[82] X. Wang, B. Partlow, J. Liu, Z. Zheng, B. Su, Y. Wang, D. L. Kapln, Injectable silk-polyethylene glycol hydrogels, *Acta Biomaterialia*. **12**, 51-61 (2015).

[83] S. Nagarkar, T. Nicolai, C. Chassenieux, A. Lele, Structure and gelation mechanism of silk hydrogels, *Physical Chemistry Chemical Physics.* **12** 3834-3844 (2010).

[84] A. Matsumoto, J. Chen, A. L. Collette, U. J. Kim, G. H. Altman, P. Cebe, D. L. Kaplan, Mechanisms of silk fibroin sol-gel transitions, *The Journal of Physical Chemistry B.* **110**, 21630-21638 (2006).

[85] P. Dubey, L. Nawale, D. Sarkar, A. Nisal, A. Prabhune, Sophorolipid assisted tunable and rapid gelation of silk fibroin to form porous biomedical scaffolds, *RSC Advances.* **5**, 33955-33962 (2015).

[86] Y. Hou, P. Li, H. Zhou, X. Zhu, H. Chen, J. Lee, H. Chen, Evaluation of β-Amyloid Peptides Fibrillation Induced by Nanomaterials Based on Molecular Dynamics and Surface Plasmon Resonance, *Journal of Nanoscience and Nanotechnology.* **15**, 1110-1116 (2015).

[87] T. Jiang, G. R. Zhou, Y. H. Zhang, P. C. Sun, Q. M. Du, P. Zhou, Influence of curcumin on the Al(III)-induced conformation transition of silk fibroin and resulting potential therapy for neurodegenerative diseases, *RSC Advances.* **2**, 9106-9113 (2012).

[88] T. Yao, T. Jiang, D. Pan, Z. X. Xu, P. Zhou, Effect of Al(III) and

curcumin on silk fibroin conformation and aggregation morphology, *RSC Advances*. **4**, 40273-40280 (2014).

[89] J. Wang, S. Zhang, T. Xing, B. Kundu, M. Li, S. C. Kundu, S. Lu., Ion-induced fabrication of silk fibroin nanoparticles from Chinese oak *tasar Antheraea pernyi*, *International Journal of Biological Macromolecules*. **79**, 316-325 (2015).

[90] P. Dubey, S. Murab, S. Karmakar, P. K. Chowdhury, S. Ghosh, Modulation of Self-Assembly Process of Fibroin: An Insight for Regulating the Conformation of Silk Biomaterials, *Biomacromolecules*. **16**, 3936-3944, (2015).

[91] P. I. Haris, F. Severcan, FTIR spectroscopic characterization of protein structure in aqueous and non-aqueous media, *Journal of Molecular Catalysis B: Enzymatic*. **7,** 207-221 (1999).

[92] D. M. Byler, H. Susi, Examination of the secondary structure of proteins by deconvolved FTIR spectra, *Biopolymers*. **25,** 469-487 (1986).

[93] H. Y. Kweon, Y. H. Park, Structural and conformational changes of regenerated Antheraea pernyi silk fibroin films treated with methanol solution, *Journal of Applied Polymer Science*. **73**, 2887-2894 (1999).

[94] Q. N. Wei, A. M. Huang, L. Ma, Z. Huang, X. Huang, P. P. Qiang, Z. P. Gong, L. Zhang, Structure regulation of silk fibroin films for controlled drug release, *Journal of Applied Polymer Science.* **125,** 477-484 (2012).

[95] Q. Peng, H. Shao, X. Hu, Y. Zhang, Role of humidity on the structures and properties of regenerated silk fibers, *Progress in Natural Science: Materials International.* **25**, 430-436 (2015).

[96] X. Chen, D. P. Knight, Z. Shao, F. Vollrath, Regenerated Bombyx silk solutions studied with rheometry and FTIR, *Polymer*. **42,** 9969-9974 (2001).

[97] F. Han, S. Liu, X. Liu, Y. Pei, S. Bai, H. Zhao, Q. Lu, F. Ma, D. L. Kaplan, H. Zhu, Woven silk fabric-reinforced silk nanofibrous scaffolds for regenerating load-bearing soft tissues, *Acta Biomateria.* **10**, 921-930 (2014).

[98] S. Bai, W. Zhang, Q. Lu, Q. Ma, D. L. Kaplan, H. Zhu, Silk nanofiber hydrogels with tunable modulus to regulate nerve stem cell fate, *Journal of Materials Chemistry B*. **2**, 6590-6600 (2014).

[99] Q. Lu, X. Wang, S. Lu, M. Li, D. L. Kaplan, H. Zhu, Nanofibrous architecture of silk fibroin scaffolds prepared with a mild self-assembly process, *Biomaterials*. **32**, 1059-1067 (2011).

[100] Q. Lu, H. Zhu, C. Zhang, F. Zhang, B. Zhang, D. L. Kaplan, Silk Self-Assembly Mechanisms and Control-From Thermodynamics to Kinetics, *Biomacromolecules*. **13**, 826-832 (2012).

[101] K. Shang, J. Rnjak-Kovacina, Y. Lin, R. S. Hayden, T. Hu, D. L. Kaplan, Accelerated in vitro Degradation of Optically Clear Low β-sheet Silk Films by Enzyme-Mediated Pretreatment, *JAMA Ophthalmology*, **131**, 676-693 (2013).

[102] Z. H. Ayub, M. Arai, K. Hirabayashi, Mechanism of the Gelation of Fibroin Solution, *Bioscience, Biotechnology, and Biochemistry*, **57**, 1910-1912 (1993)

[103] P. A. Korevaar, C .J. Newcomb, E. W. Meijer, S. I. Stupp, Pathway Selection in Peptide Amphiphile Assembly, *Journal of the american chemical society*, **136**, 8540-8543 (2014)

[104] Q. X. Ruan, P. Zhou, Sodium ion effect on silk fibroin conformation characterized by solid-state NMR and generalized 2D NMR-NMR correlation, *Journal of Molecular Structure.* **883**, 85-90 (2008).

[105] Q. X. Ruan, P. Zhou, B. W. Hu, D. Ji, An investigation into the effect of potassium ions on the folding of silk fibroin studied by generalized two-dimensional NMR-NMR correlation and Raman

spectroscopy, *Febs Journal*. **275**, 219-232 (2008).

[106] V. Weimarn, Alexander, Water-Soluble Silk: an α-Protein, Determination of the Configuration of Silk SF Dissolved in Aqueous Solutions of Lithium Bromide, *Colloid Chemistry*, **4**, 363. (1932)

[107] P. Zhou, X. Xie, D. P. Knight, X. H. Zong, F. Deng, W-H. Yao, Effects of pH and Calcium Ions on the Conformational Transitions in Silk Fibroin Using 2D Raman Correlation Spectroscopy and ^{13}C Solid-State NMR, *Biochemistry*, **43**, 11302-11311 (2004)

[108] R. M. Whittal, H. L. Ball, F. E. Cohen, A. L. Burlingame, S. B. Prusiner, M. A. Baldwin, Copper binding to octarepeat peptides of the prion protein monitored by mass spectrometry, *Protein Science*, **9**, 332-343 (2000)

[109] J. Stöckel, J. Safar, A. C. Wallace, F. E. Cohen, S. B. Prusiner, Prion Protein Selectively Binds Copper(II) Ions, *Biochemistry*, **37**, 7185-7193 (1998)

[110] C. J. Sarell, C. D. Syme, S. E. J. Rigby, J. H. Viles, Copper(II) Binding to Amyloid-β Fibrils of Alzheimer's Disease Reveals a Picomolar Affinity: Stoichiometry and Coordination Geometry Are Independent of Aβ Oligomeric Form, *Biochemistry*, **48**, 4388-4402

(2009)

[111] V. A. Streltsov, S. J. Titmuss, V. C. Epa, K. J. Barnham, C. L. Masters, J. N. Varghese, The Structure of the Amyloid-β Peptide High-Affinity Copper II Binding Site in Alzheimer Disease, *Biophysical Journal*, **95**, 3447-3456 (2008)

[112] X-H. Zong, P. Zhou, Z-Z. Shao, S-M. Chen, X. Chen, B-W. Hu, F. Deng, W-H. Yao, Effect of pH and copper(II) on the conformation transitions of silk fibroin based on EPR, NMR, and Raman spectroscopy, *Biochemistry*, **43**, 11932-11941 (2004)

[113] L. Zhou, X. Chen, Z Shao, P. Zhou, D. P. Knight, F. Vollrath, Copper in the silk formation process of Bombyx mori silkworm, *FEBS Letters*, **554**, 337-341 (2003)

국문 초록

실크섬유의 방사과정은 합성섬유의 방사공정에 비하여 다양한 측면에서 이점을 가지고 있다. 하지만 실크 방사과정은 아직까지 명확하게 밝혀져 있지 않다.

지금까지 실크방사과정에 관한 연구결과들은 대부분 피브로인 단백질 자체에만 국한하여 연구가 진행되었다. 누에가 생산하는 실크섬유는 피브로인과 세리신 이라는 두 가지 단백질로 구성되어 있다. 세리신은 누에의 중부 실샘에서 합성되어 피브로인 단백질을 상분리 상태로 감싸져 있는 형태로 존재한다. 지금까지 세리신은 실크 방사과정에서 큰 관심을 받지 못했다. 하지만 최근 들어 세리신이 피브로인의 구조전이에 관여한다는 연구결과가 보고되었다.

따라서 본 연구의 목적은 상분리된 세리신이 피브로인의 겔화 과정에 있어 피브로인의 구조전이에 미치는 영향을 알아보는 것이다. 또한 상분리된 세리신의 존재가 금속이온 분배 및 피브로인의 겔화 시간에 미치는 영향에 대해 알아보는 것이다.

실험을 위하여 피브로인과 세리신의 상분리 상태에서 피브로인의 겔화 시간을 관찰하였으며 생성된 피브로인 하이드로겔의 특성을 분석하였다. 피브로인의 겔화 시간은 상분리된 세리신의 농도가 증가할수록 지연되는 경향을 보였으며 이러한 겔화 지연 현상은 피브로인의 베타 시트로의 구조전이가 상분리된 세리신의 존재 하에서 지연되기 때문에 발생하는 것으로 확인되었다. 또한 X 선 회절 분석을 통하여 0.5% 및 1.0%의 세리신 존재 하에 형성된 피브로인 하이드로겔의 경우 전형적인 실크 I 구조를 나타내는 것을 발견하였다. 이러한 결과는 상분리된 상태에서도

세리신이 피브로인의 구조전이를 지연시킬 수 있으며 실크 I 구조를 갖는 하이드로겔 형성을 촉진시킨다는 것을 의미한다.

이온 분배 실험의 경우 Na^+ 를 제외한 대부분의 이온이 피브로인과의 친화도가 높았으며 이동한 금속이온의 종류 및 그 양이 피브로인의 겔화 시간에 영향을 주는 것으로 밝혀졌다. 피브로인으로 이동한 대부분의 금속이온은 겔화 시간을 지연시켰으며 그 중 Ca^{2+} 이온은 그 지연 효과가 가장 큰 것으로 밝혀졌다. 또한 모든 실험에서 상분리된 세리신 존재 시에 피브로인의 겔화 시간이 지연됨을 확인하였다.

결과적으로 본 연구에서는 상분리된 세리신이 피브로인의 구조전이에 미치는 영향을 살펴보았으며 위 실험결과들을 종합하여 볼 때, 상분리된 세리신이 피브로인의 실크 I 구조를 유도하여 피브로인의 구조적 안정화에 크게 기여함을 확인하였다.

색인어 : 실크 피브로인, 실크 세리신, 실크 I 구조, 겔화, 금속 이온

학번 : 2010-21192